estec

European Space Research
and Technology Centre
Keplerlaan 1
2201 AZ Noordwijk
The Netherlands
T +31 (0)71 565 6565
F +31 (0)71 565 6040
www.esa.int

DOCUMENT

POLARIS IceGrav Antarctic Campaign 2011: ESA Processed Data Inventory

Prepared by	**David Bekaert**
Reference	**IPD-ESA-TN-250**
Issue	**1**
Revision	**2**
Date of Issue	**28.03.2012**
Status	**Final**
Document Type	**Technical Note**
Distribution	

European Space Agency
Agence spatiale européenne

TABLE OF CONTENTS:

DISCLAIMER:

Neither ESA nor any other party involved in creating this report and its associated data shall be liable for any direct, incidental, consequential, indirect or punitive damages arising out of Users' access to, or use of, them. ESA and all other party involved do not guarantee the accuracy of information provided and make no warranties, expressed or implied, that the processing tools are free of errors, or are consistent with any particular standard of merchantability. We should be grateful if users could notify us of any errors or inaccuracies they may find. Please note that users use the processed data at their own risk, see terms and conditions outlined on the ESA Earthnet Online website.

COPYRIGHTS:

1 INTRODUCTION

This report contains the data inventory of the processed data of the 2011 IceGrav Antarctic campaign, and is in addition to the "IceGrav Campaign Report and Data Inventory" [1], referred to as Campaign report. Data files of the acquired tracks, as outlined in table 4 on p14 of the Campaign report, were provided to ESA in level 0c format, meaning the data is delivered in complex format and has been range compressed. The campaign dataset includes data acquired with 85, 30 and 6 MHz transmit bandwidth and at multiple polarisations (HH, HV, VH and VV).
As the transmitted chirp bandwidths are different for the multiple operational modes, so will be the respective range resolutions. A bandwidth of 85, 30 and 6 MHz, translates respectively to a vertical ("range") resolution in ice of 0.98; 2.78 and 13.88 m.
The obtained azimuth resolution is also dependant on the bandwidth, because of the approach chosen for along-track focusing, which sets the integration time such that no range cell migration occurs. In other words, the processed Doppler bandwidth is limited to an integration time that results in a range cell migration not larger than half of the range resolution. Last but not least, a Hamming window was applied during processing to suppress side lobes, resulting in a slightly degraded azimuth resolution. Figure 1 gives the estimated azimuth resolution varying with depth, for the three bandwidths, assuming a aircraft height of 3300 m above the ice surface and before multi-looking. The respective multi-looking factors might vary and are listed in the tables.

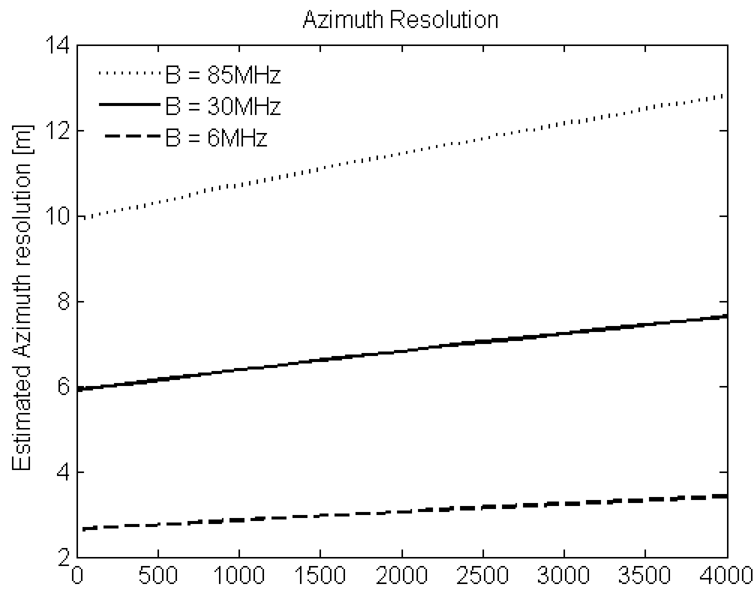

Figure 1: Estimated azimuth resolution in the ice for each operated bandwidth of the multi-channel dataset (Jutulstraumen glacier) as obtained for the reference aircraft height of 3300 m above ice, a flight speed of 86 m/s and applying a Hamming taper with a factor of 0.54.

The along track focussing requires the retrieval of the altitude over the ice. The data tracks which have a combination of the 85/30 or 85/6 MHz bandwidths have the same altitude over the ice, as both were acquired at the same instant. The sounding window of the 85 MHz dataset was chosen such that it includes the ice surface, allowing us to retrieve the altitude over the ice as the first received intensity peak. For the other data tracks, in absence of the 85 MHz bandwidth, we used the bandwidth dataset at hand.

An overview of the available data, with the corresponding polarisations and operated bandwidth, is provided in Table 1 for the Adelaide dataset, in Table 2 for the Coastal flight dataset, in Table 3 for the Multi-aperture dataset and in Table 4 for the IceGrav dataset. Processing of the raw data was performed using the tools as outlined in the first POLARIS Proof of Concept report [3]. The processed data is available as a multi-looked intensity product, with the number of looks documented in the tables.

The POLARIS antenna was erroneously configured while acquiring the Multi-channel dataset, with a transmit "null" in boresight direction, as shown in the right plot of Figure 2. This "null" (effectively a deep drop of gain) is directed in the nadir, in absence of airplane roll. More information about this is contained in Section 7.4 on p19 of the Campaign report. All other datasets where acquired correctly, with the main beam pointing towards 0°, as shown in the left plot of Figure 2.

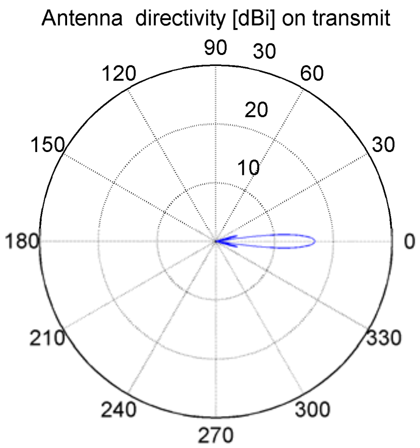

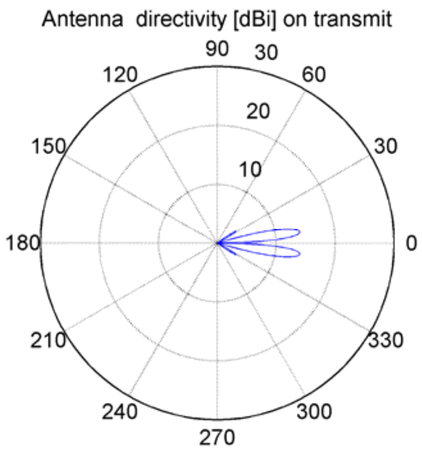

Figure 2: (Left) transmit directivity of the POLARIS antenna during the Adelaide, Coastal flight and IceGrav dataset acquisitions, (Right) transmit directivity during the Multi-channel dataset acquisition.

POLARIS was operated together with the HiCARS radar (High Capability Radar Sounder), during part of the IceGrav data acquisition. This resulted in Radio Frequency Interference of the signal, affecting the V polarisations (see p16 of the Campaign report). The RFI in the HH seems not to be caused by HiCARS, but may originate from other on-board instruments. For the HH and HV polarisations, a correction (interpolation of RFI affected lines by neighbouring lines) has been carried out. An example of this for the HH polarisation is provided in Figure 48 of Chapter 6, were the highlighted regions only indicate the most clear changes visible from print.

File name convention:

Same file name convention is used as for the raw data [1], with an extra indication of the processed data by the suffix "_out".

p<YYMMDD>_m<HHMMSS>_<scene_or_cal>_<Lvl>_<type><pol><digit><processed>

<YYMMDD>	date of acquisition (year, month, day)
<HHMMSS>	UTC time (hour, minute, second)
<scene_or_cal>	alphanumeric string with a descriptive name for the dataset.
<Lvl>	data product level
<type>	<s> and <d> for the combination shallow and deep sounding. With s and d respectively indicating the shallow and the deep data files. <f> for deep sounding (not in combination with shallow sounding).
<pol>	polarisations on transmit and receive. Possible combinations are <hh>, <hv>, <vh> or <vv>
<digit>	Represents the summing of the different channels:

digit	Summing of channels:
0	1+2+3+4
1	1
2	2
3	3
4	4
a	2+3
b	1+4

<processed>	not specified for raw data. <_AL_out> for ESA ALong track processed data

Roadmap:

Chapter 2 gives more information about the data format and how to read the data. The processed data and the obtained results are contained in Chapter 3 through 6, for respectively the Adelaide, Coastal flight, Multi-aperture, and IceGrav datasets. Results do not change significantly between different polarisations. For this reason, this report shows only a single polarization as a representative example. All images have an aspect ratio of 40 to 1 m (depth with respect to along track distance). In addition, Chapter 4 gives an example of the internal ice layering (Figure 13). Please note that not all tracks are visualized for the IceGrav dataset in this report. However, images of all processed data (including the full IceGrav dataset) are provided with the processed data.

Dataset	Track	0c	Polarization	Bandwidth (MHz)	multi-look factor
p110226_m165455	HC1aHC1HC2HC2a	p110226_m165455_HC1aHC1HC2HC2a_0c_fvv0	VV	6	64
p110226_m170353	HC1aHC1partial	p110226_m170353_HC1aHC1partial_0c_fvh0	VH	30	64
		p110226_m170353_HC1aHC1partial_0c_fhh0	HH	30	64
		p110226_m170353_HC1aHC1partial_0c_fvv0	VV	30	64
		p110226_m170353_HC1aHC1partial_0c_fhv0	HV	30	64
p110226_m170445	HC1HC2HC2a	p110226_m170445_HC1HC2HC2a_0c_fvh0	VH	30	64
		p110226_m170445_HC1HC2HC2a_0c_fhh0	HH	30	64
		p110226_m170445_HC1HC2HC2a_0c_fvv0	VV	30	64
		p110226_m170445_HC1HC2HC2a_0c_fhv0	HV	30	64

Table 1: Data inventory of the Adelaide dataset including the polarisations, operated bandwidth and the multi-look factor of the number of azimuth samples incoherently averaged after focusing. Colours indicate the summing of the different channels (see file name convention).

Dataset	Track	0c	Polarization	Bandwidth (MHz)	multi-look factor
p110219_m112000	KM1aKM2a	p110219_m112000_KM1aKM2a_0c_fvv0	VV	30	64
	KM2aKM3a	p110219_m112000_KM2aKM3a_0c_fvv0	VV	30	64
	KM3aKM4	p110219_m112000_KM3aKM4_0c_fvv0	VV	30	64
	KM4KM5	p110219_m112000_KM4KM5_0c_fvv0	VV	30	64
p110219_m125706	KM5KM6	p110219_m125706_KM5KM6_0c_fvv0	VV	30	64
	KM6KM7	p110219_m125706_KM6KM7_0c_fvv0	VV	30	64
	KM7KM8	p110219_m125706_KM7KM8_0c_fvv0	VV	30	64
p110219_m132840	KM8KM9a	p110219_m132840_KM8KM9a_0c_fvva	VV	30	64
		p110219_m132840_KM8KM9a_0c_fvvb	VV	30	64
		p110219_m132840_KM8KM9a_0c_fvv0	VV	30	64
	KM9aKM10	p110219_m132840_KM9aKM10_0c_fvvb	VV	30	64
		p110219_m132840_KM9aKM10_0c_fvva	VV	30	64
		p110219_m132840_KM9aKM10_0c_fvv0	VV	30	64

Table 2: Data inventory of the Coastal flight dataset including the polarisations, operated bandwidth and the multi-look factor of the number of azimuth samples incoherently averaged after focusing. Colours indicate the summing of the different channels (see file name convention).

Dataset	Track	0c	Polarization	Bandwidth (MHz)	multi-look factor
p110219_m155222 (complete)	jsew1	p110219_m155222_jsew1_0c_dvv0	VV	30	128
		p110219_m155222_jsew1_0c_dvv1	VV	30	128
		p110219_m155222_jsew1_0c_dvv2	VV	30	128
		p110219_m155222_jsew1_0c_dvv3	VV	30	128
		p110219_m155222_jsew1_0c_dvv4	VV	30	128
		p110219_m155222_jsew1_0c_svv0	VV	85	128
		p110219_m155222_jsew1_0c_svv1	VV	85	128
		p110219_m155222_jsew1_0c_svv2	VV	85	128
		p110219_m155222_jsew1_0c_svv3	VV	85	128
		p110219_m155222_jsew1_0c_svv4	VV	85	128
	jsns1	p110219_m155222_jsns1_0c_dvv1	VV	30	128
		p110219_m155222_jsns1_0c_dvv2	VV	30	128
		p110219_m155222_jsns1_0c_dvv3	VV	30	128
		p110219_m155222_jsns1_0c_dvv4	VV	30	128
		p110219_m155222_jsns1_0c_svv1	VV	85	128
		p110219_m155222_jsns1_0c_svv2	VV	85	128
		p110219_m155222_jsns1_0c_svv3	VV	85	128
		p110219_m155222_jsns1_0c_svv4	VV	85	128
	jswe1	p110219_m155222_jswe1_0c_dvv1	VV	30	128
		p110219_m155222_jswe1_0c_dvv2	VV	30	128
		p110219_m155222_jswe1_0c_dvv3	VV	30	128
		p110219_m155222_jswe1_0c_dvv4	VV	30	128
		p110219_m155222_jswe1_0c_svv1	VV	85	128
		p110219_m155222_jswe1_0c_svv2	VV	85	128
		p110219_m155222_jswe1_0c_svv3	VV	85	128
		p110219_m155222_jswe1_0c_svv4	VV	85	128

Table 3: Data inventory of the Multi-aperture dataset including the polarisations, operated bandwidth and the multi-look factor of the number of azimuth samples incoherently averaged after focusing. Colours indicate the summing of the different channels (see file name convention).

Dataset	Track	0c	Polarization	Bandwidth (MHz)	multi-look factor
p110219_m180339	jsns2	p110219_m180339_jsns2_0c_dvv1	VV	6	128
		p110219_m180339_jsns2_0c_dvv1	VV	6	128
		p110219_m180339_jsns2_0c_dvv1	VV	6	128
		p110219_m180339_jsns2_0c_dvv1	VV	6	128
		p110219_m180339_jsns2_0c_svv1	VV	85	128
		p110219_m180339_jsns2_0c_svv2	VV	85	128
		p110219_m180339_jsns2_0c_svv3	VV	85	128
		p110219_m180339_jsns2_0c_svv4	VV	85	128

Table 3 continued: Data inventory of the Multi-aperture dataset including the polarisations, operated bandwidth and the multi-look factor of the number of azimuth samples incoherently averaged after focusing. Colours indicate the summing of the different channels (see file name convention).

Dataset	Track	0c	Polarization	Bandwidth (MHz)	multi-look factor
p110214_m111956	EC	p110214_m111956_EC_0c_dhh0*	HH	6	128
		p110214_m111956_EC_0c_dhv0*	HV	6	128
		p110214_m111956_EC_0c_dvh0	VH	6	128
		p110214_m111956_EC_0c_dvv0	VV	6	128
		p110214_m111956_EC_0c_shh0	HH	85	128
		p110214_m111956_EC_0c_shv0	HV	85	128
		p110214_m111956_EC_0c_svh0	VH	85	128
		p110214_m111956_EC_0c_svv0	VV	85	128
p110214_m113955	EC	p110214_m113955_EC_0c_dhh0*	HH	6	128
		p110214_m113955_EC_0c_dhv0*	HV	6	128
		p110214_m113955_EC_0c_dvh0	VH	6	128
		p110214_m113955_EC_0c_dvv0	VV	6	128
		p110214_m113955_EC_0c_shh0	HH	85	128
		p110214_m113955_EC_0c_shv0	HV	85	128
		p110214_m113955_EC_0c_svh0	VH	85	128
		p110214_m113955_EC_0c_svv0	VV	85	128

Table 4: Data inventory of the IceGrav dataset including the polarisations, operated bandwidth and the multi-look factor of the number of azimuth samples incoherently averaged after focusing. Colours indicate the summing of the different channels (see file name convention). The asterisk symbol (*) indicates the data has been corrected for the Radio Frequency Interference of the ICARS instrument. Data of the p110217_m113112 track is not available as the altitude over the ice could not be retrieved.

Dataset	Track	0c	Polarization	Bandwidth (MHz)	multi-look factor
p110214_m133359	ED	p110214_m133359_ED_0c_dhh0*	HH	6	128
		p110214_m133359_ED_0c_dhv0*	HV	6	128
		p110214_m133359_ED_0c_dvh0	VH	6	128
		p110214_m133359_ED_0c_dvv0	VV	6	128
		p110214_m133359_ED_0c_shh0	HH	85	128
		p110214_m133359_ED_0c_shv0	HV	85	128
		p110214_m133359_ED_0c_svh0	VH	85	128
		p110214_m133359_ED_0c_svv0	VV	85	128
p110214_m145525	ED	p110214_m145525_ED_0c_dhh0*	HH	6	128
		p110214_m145525_ED_0c_dhv0*	HV	6	128
		p110214_m145525_ED_0c_dvh0	VH	6	128
		p110214_m145525_ED_0c_dvv0	VV	6	128
		p110214_m145525_ED_0c_shh0	HH	85	128
		p110214_m145525_ED_0c_shv0	HV	85	128
		p110214_m145525_ED_0c_svh0	VH	85	128
		p110214_m145525_ED_0c_svv0	VV	85	128
p110214_m151654	ED	p110214_m151654_ED_0c_dhh0*	HH	6	32
		p110214_m151654_ED_0c_dhv0*	HV	6	32
		p110214_m151654_ED_0c_dvh0	VH	6	32
		p110214_m151654_ED_0c_dvv0	VV	6	32
		p110214_m151654_ED_0c_shh0	HH	85	32
		p110214_m151654_ED_0c_shv0	HV	85	32
		p110214_m151654_ED_0c_svh0	VH	85	32
		p110214_m151654_ED_0c_svv0	VV	85	32

Table 4 continued: Data inventory of the IceGrav dataset including the polarisations, operated bandwidth and the multi-look factor of the number of azimuth samples incoherently averaged after focusing. Colours indicate the summing of the different channels (see file name convention). The asterisk symbol (*) indicates the data has been corrected for the Radio Frequency Interference of the ICARS instrument. Data of the p110217_m113112 track is not available as the altitude over the ice could not be retrieved.

Dataset	Track	0c	Polarization	Bandwidth (MHz)	multi-look factor
p110214_m151811	ED	p110214_m151811_ED_0c_dhh0*	HH	6	128
		p110214_m151811_ED_0c_dhv0*	HV	6	128
		p110214_m151811_ED_0c_dvh0	VH	6	128
		p110214_m151811_ED_0c_dvv0	VV	6	128
		p110214_m151811_ED_0c_shh0	HH	85	128
		p110214_m151811_ED_0c_shv0	HV	85	128
		p110214_m151811_ED_0c_svh0	VH	85	128
		p110214_m151811_ED_0c_svv0	VV	85	128
p110215_m101537	EB	p110215_m101537_EB_0c_dhh0*	HH	6	128
		p110215_m101537_EB_0c_dhv0*	HV	6	128
		p110215_m101537_EB_0c_dvh0	VH	6	128
		p110215_m101537_EB_0c_dvv0	VV	6	128
		p110215_m101537_EB_0c_shh0	HH	85	128
		p110215_m101537_EB_0c_shv0	HV	85	128
		p110215_m101537_EB_0c_svh0	VH	85	128
		p110215_m101537_EB_0c_svv0	VV	85	128
p110215_m133612	EA	p110215_m133612_EA_0c_dhh0*	HH	6	128
		p110215_m133612_EA_0c_dhv0*	HV	6	128
		p110215_m133612_EA_0c_dvh0	VH	6	128
		p110215_m133612_EA_0c_dvv0	VV	6	128
		p110215_m133612_EA_0c_shh0	HH	85	128
		p110215_m133612_EA_0c_shv0	HV	85	128
		p110215_m133612_EA_0c_svh0	VH	85	128
		p110215_m133612_EA_0c_svv0	VV	85	128

Table 4 continued: Data inventory of the IceGrav dataset including the polarisations, operated bandwidth and the multi-look factor of the number of azimuth samples incoherently averaged after focusing. Colours indicate the summing of the different channels (see file name convention). The asterisk symbol (*) indicates the data has been corrected for the Radio Frequency Interference of the ICARS instrument. Data of the p110217_m113112 track is not available as the altitude over the ice could not be retrieved.

Dataset	Track	0c	Polarization	Bandwidth (MHz)	multi-look factor
p110217_m105125	EI	p110217_m105125_EI_0c_dhh0*	HH	6	128
		p110217_m105125_EI_0c_dhv0*	HV	6	128
		p110217_m105125_EI_0c_dvh0	VH	6	128
		p110217_m105125_EI_0c_dvv0	VV	6	128
		p110217_m105125_EI_0c_shh0	HH	85	128
		p110217_m105125_EI_0c_shv0	HV	85	128
		p110217_m105125_EI_0c_svh0	VH	85	128
		p110217_m105125_EI_0c_svv0	VV	85	128
p110217_m113112	EI	p110217_m113112_EI_0c_fvv0	VV	6	
p110217_m132956	EJ	p110217_m132956_EJ_0c_dhh0*	HH	6	128
		p110217_m132956_EJ_0c_dhv0*	HV	6	128
		p110217_m132956_EJ_0c_dvh0	VH	6	128
		p110217_m132956_EJ_0c_dvv0	VV	6	128
		p110217_m132956_EJ_0c_shh0	HH	85	128
		p110217_m132956_EJ_0c_shv0	HV	85	128
		p110217_m132956_EJ_0c_svh0	VH	85	128
		p110217_m132956_EJ_0c_svv0	VV	85	128
p110218_m100213	EK	p110218_m100213_EK_0c_dhh0*	HH	6	128
		p110218_m100213_EK_0c_dhv0*	HV	6	128
		p110218_m100213_EK_0c_dvh0	VH	6	128
		p110218_m100213_EK_0c_dvv0	VV	6	128
		p110218_m100213_EK_0c_shh0	HH	85	128
		p110218_m100213_EK_0c_shv0	HV	85	128
		p110218_m100213_EK_0c_svh0	VH	85	128
		p110218_m100213_EK_0c_svv0	VV	85	128

Table 4 continued: Data inventory of the IceGrav dataset including the polarisations, operated bandwidth and the multi-look factor of the number of azimuth samples incoherently averaged after focusing. Colours indicate the summing of the different channels (see file name convention). The asterisk symbol (*) indicates the data has been corrected for the Radio Frequency Interference of the ICARS instrument. Data of the p110217_m113112 track is not available as the altitude over the ice could not be retrieved.

Dataset	Track	0c	Polarization	Bandwidth (MHz)	multi-look factor
	epica	p110218_m100213_epica_0c_dhh0	HH	6	64
		p110218_m100213_epica_0c_dhv0	HV	6	64
		p110218_m100213_epica_0c_dvh0	VH	6	64
		p110218_m100213_epica_0c_dvv0	VV	6	64
		p110218_m100213_epica_0c_shh0	HH	85	64
		p110218_m100213_epica_0c_shv0	HV	85	64
		p110218_m100213_epica_0c_svh0	VH	85	64
		p110218_m100213_epica_0c_svv0	VV	85	64
p110218_m131313	EL	p110218_m131313_EL_0c_dhh0*	HH	6	128
		p110218_m131313_EL_0c_dhv0*	HV	6	128
		p110218_m131313_EL_0c_dvh0	VH	6	128
		p110218_m131313_EL_0c_dvv0	VV	6	128
		p110218_m131313_EL_0c_shh0	HH	85	128
		p110218_m131313_EL_0c_shv0	HV	85	128
		p110218_m131313_EL_0c_svh0	VH	85	128
		p110218_m131313_EL_0c_svv0	VV	85	128
p110220_m105216	EM	p110220_m105216_EM_0c_dhh0*	HH	6	64
		p110220_m105216_EM_0c_dhv0*	HV	6	64
		p110220_m105216_EM_0c_dvh0	VH	6	64
		p110220_m105216_EM_0c_dvv0	VV	6	64
		p110220_m105216_EM_0c_shh0	HH	85	64
		p110220_m105216_EM_0c_shv0	HV	85	64
		p110220_m105216_EM_0c_svh0	VH	85	64
		p110220_m105216_EM_0c_svv0	VV	85	64

Table 4 continued: Data inventory of the IceGrav dataset including the polarisations, operated bandwidth and the multi-look factor of the number of azimuth samples incoherently averaged after focusing. Colours indicate the summing of the different channels (see file name convention). The asterisk symbol (*) indicates the data has been corrected for the Radio Frequency Interference of the ICARS instrument. Data of the p110217_m113112 track is not available as the altitude over the ice could not be retrieved.

Dataset	Track	0c	Polarization	Bandwidth (MHz)	multi-look factor
	EN	p110220_m105216_EN_0c_dhh0*	HH	6	128
		p110220_m105216_EN_0c_dhv0*	HV	6	128
		p110220_m105216_EN_0c_dvh0	VH	6	128
		p110220_m105216_EN_0c_dvv0	VV	6	128
		p110220_m105216_EN_0c_shh0	HH	85	128
		p110220_m105216_EN_0c_shv0	HV	85	128
		p110220_m105216_EN_0c_svh0	VH	85	128
		p110220_m105216_EN_0c_svv0	VV	85	128
p110220_m131402	EM	p110220_m131402_EM_0c_dhh0*	HH	6	64
		p110220_m131402_EM_0c_dhv0*	HV	6	64
		p110220_m131402_EM_0c_dvh0	VH	6	64
		p110220_m131402_EM_0c_dvv0	VV	6	64
		p110220_m131402_EM_0c_shh0	HH	85	64
		p110220_m131402_EM_0c_shv0	HV	85	64
		p110220_m131402_EM_0c_svh0	VH	85	64
		p110220_m131402_EM_0c_svv0	VV	85	64
p110220_m140124	EM	p110220_m140124_EM_0c_dhh0*	HH	6	128
		p110220_m140124_EM_0c_dhv0*	HV	6	128
		p110220_m140124_EM_0c_dvh0	VH	6	128
		p110220_m140124_EM_0c_dvv0	VV	6	128
		p110220_m140124_EM_0c_shh0	HH	85	128
		p110220_m140124_EM_0c_shv0	HV	85	128
		p110220_m140124_EM_0c_svh0	VH	85	128
		p110220_m140124_EM_0c_svv0	VV	85	128

Table 4 continued: Data inventory of the IceGrav dataset including the polarisations, operated bandwidth and the multi-look factor of the number of azimuth samples incoherently averaged after focusing. Colours indicate the summing of the different channels (see file name convention). The asterisk symbol (*) indicates the data has been corrected for the Radio Frequency Interference of the ICARS instrument. Data of the p110217_m113112 track is not available as the altitude over the ice could not be retrieved.

Dataset	Track	0c	Polarization	Bandwidth (MHz)	multi-look factor
p110222_m104136	EP	p110222_m104136_EP_0c_dhh0*	HH	6	128
		p110222_m104136_EP_0c_dhv0*	HV	6	128
		p110222_m104136_EP_0c_dvh0	VH	6	128
		p110222_m104136_EP_0c_dvv0	VV	6	128
		p110222_m104136_EP_0c_shh0	HH	85	128
		p110222_m104136_EP_0c_shv0	HV	85	128
		p110222_m104136_EP_0c_svh0	VH	85	128
		p110222_m104136_EP_0c_svv0	VV	85	128
p110222_m131359	EQ	p110222_m131359_EQ_0c_dhh0*	HH	6	128
		p110222_m131359_EQ_0c_dhv0*	HV	6	128
		p110222_m131359_EQ_0c_dvh0	VH	6	128
		p110222_m131359_EQ_0c_dvv0	VV	6	128
		p110222_m131359_EQ_0c_shh0	HH	85	128
		p110222_m131359_EQ_0c_shv0	HV	85	128
		p110222_m131359_EQ_0c_svh0	VH	85	128
		p110222_m131359_EQ_0c_svv0	VV	85	128
p110223_m100847	ER	p110223_m100847_ER_0c_dvv0	VV	6	128
		p110223_m100847_ER_0c_svv0	VV	85	128
p110223_m132504	ES	p110223_m132504_ES_0c_dvv0	VV	6	128
		p110223_m132504_ES_0c_svv0	VV	85	128
p110224_m114727	trollEA30	p110224_m114727_trollEA30_0c_dvv0	VV	6	128
		p110224_m114727_trollEA30_0c_svv0	VV	85	128
p110224_m130052	crossing	p110224_m130052_crossing_0c_dvv0	VV	6	128
		p110224_m130052_crossing_0c_svv0	VV	85	128

Table 4 continued: Data inventory of the IceGrav dataset including the polarisations, operated bandwidth and the multi-look factor of the number of azimuth samples incoherently averaged after focusing. Colours indicate the summing of the different channels (see file name convention). The asterisk symbol (*) indicates the data has been corrected for the Radio Frequency Interference of the ICARS instrument. Data of the p110217_m113112 track is not available as the altitude over the ice could not be retrieved.

Dataset	Track	0c	Polarization	Bandwidth (MHz)	multi-look factor
p110224_m141654	crossing	p110224_m141654_crossing_0c_dvv0	VV	6	128
		p110224_m141654_crossing_0c_svv0	VV	85	128
p110224_m155704	crossing	p110224_m155704_crossing_0c_dvv0	VV	6	128
		p110224_m155704_crossing_0c_svv0	VV	85	128

Table 4 continued: Data inventory of the IceGrav dataset including the polarisations, operated bandwidth and the multi-look factor of the number of azimuth samples incoherently averaged after focusing. Colours indicate the summing of the different channels (see file name convention). The asterisk symbol (*) indicates the data has been corrected for the Radio Frequency Interference of the ICARS instrument. Data of the p110217_m113112 track is not available as the altitude over the ice could not be retrieved.

2 READING OF PROCESSED DATA

The fully focussed (range and azimuth compressed) POLARIS data is available as an intensity data product. The level-0c data, already range compressed, were first focussed in azimuth to obtain a fully focussed SAR image. Next these data were multi-looked to obtain an intensity product. More information about the applied processing tools can found in the first POLARIS Proof of Concept report [3].

Each processed data file (filename with <AL_out> as suffix) is provided together with an information file (filename with <AL_out_info.mat> as suffix). The latter is a MATLAB file, containing information of the processed data file as outlined in Table 5. The processed data file can be read into matrix format, with the rows and columns being the number of range samples and azimuth samples of the processed data (denoted Nrg and NazProc, respectively). Each intensity value for the processed data represents 4 Bytes (float32). Each 4*Nrg Bytes corresponds to a column of the data matrix. For MATLAB, this reads:

```
processedData=zeros(Nrg,NazProc);
for k=1:NazProc
    processedData(:,k)=fread(fid,Nrg,'float32');
end;
figure
imagesc(10*log(processedData));
```

Parameter	Variable name
# range samples	Nrg
# azimuth samples	NazProc
Altitude wrt the geoid (m)	altProc
Altitude over the ice surface (m)	flightAltitudeOverIceProc
Along track distance (m)	Azimuth_distance_Proc
Longitude (°)	LonProc
Latitude (°)	latProc
Aircraft roll angle (°)	rollProc
Mean velocity over the track (m/s)	v_mean
Receive window start time delay w.r.t. first pulse (s)	tau_min
Pulse length (s)	tau_pulse
Pulse Repetition Frequency (Hz)	PRF
Sampling frequency (Hz)	fS
Carrier frequency (Hz)	fC

Table 5: Parameters of the processed data contained in the info file.

3 ADELAIDE DATASET

Figure 3 gives an overview of the flown Adelaide data tracks. The data has been acquired partly using a transmit bandwidth of 6 and 30 MHz, as is indicated in Table 1. Sample plots of the power and the differential power are shown with respect to a reference altitude for each track. Beside this an along track visualisation is given for the airplane longitude, latitude, attitude over ice and the roll angle.

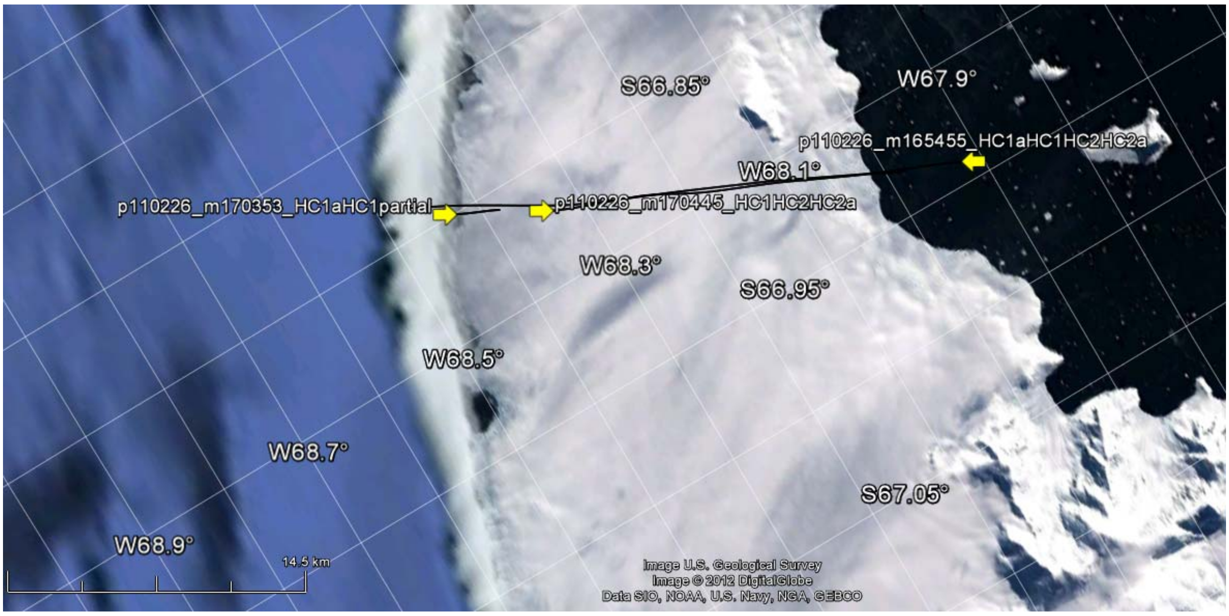

Figure 3: Google Earth plot of the flown tracks

3.1 Processed Data: p110226_m165455_HC1aHC1HC2HC2a

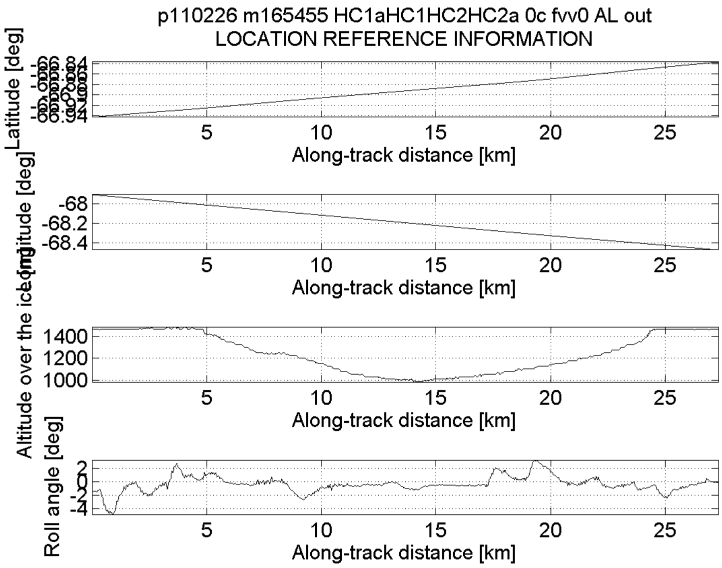

Figure 4: Location information

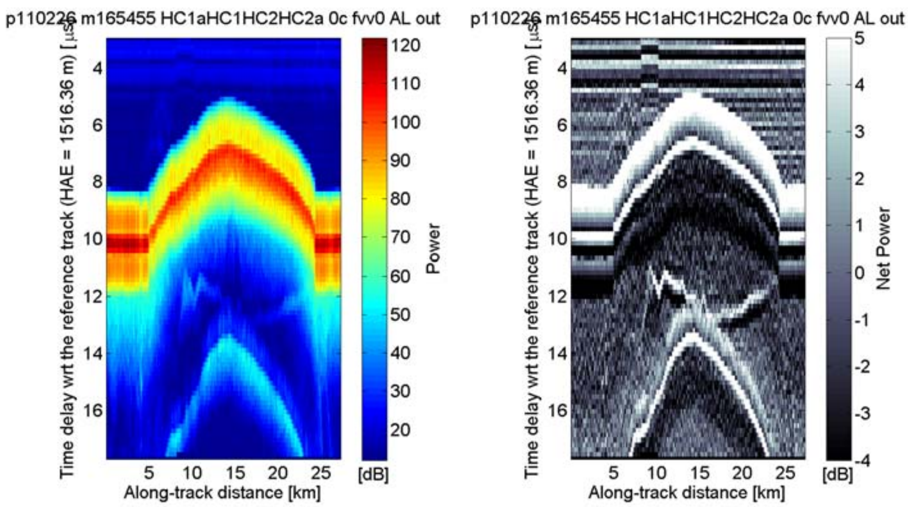

Figure 5: VV Polarisation of the p110226_m165455_HC1aHC1HC2HC2a track, 6 MHz bandwidth. (Left) power plot, (Right) differential plot of the power, both displayed with respect to a reference WGS84 altitude track.

3.2 Processed Data: p110226_m170353_HC1aHC1partial

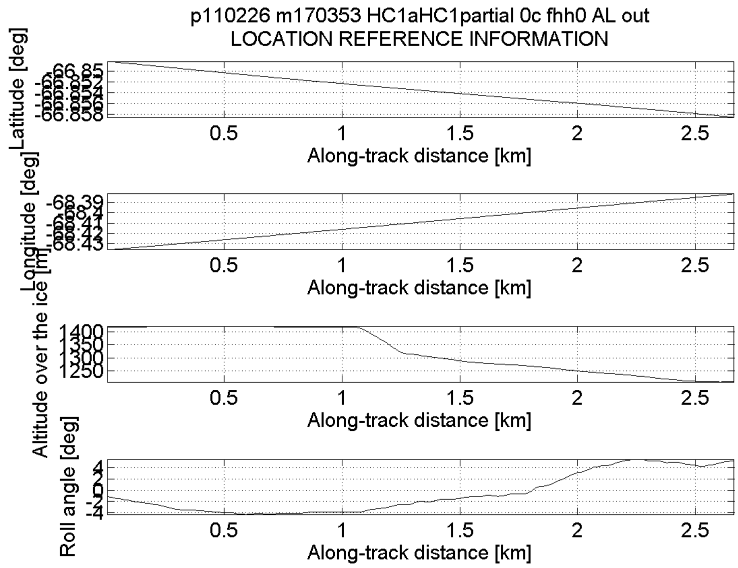

Figure 6: Location information

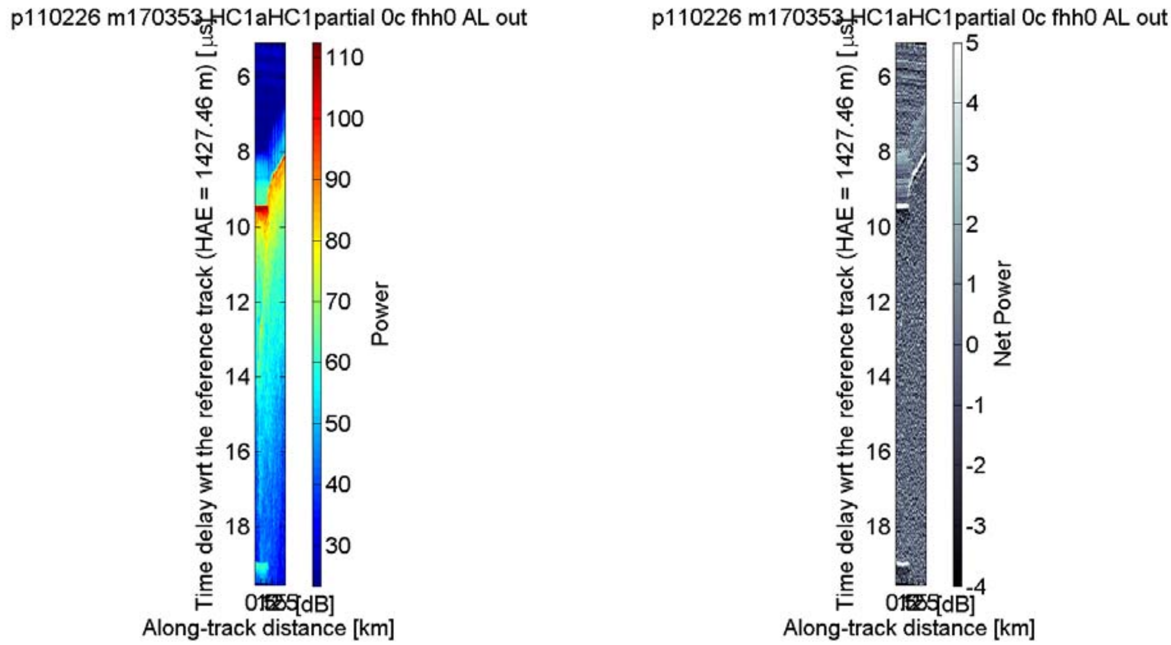

Figure 7: HH Polarisation of the p110226_m170353_HC1aHC1partial track, 30 MHz bandwidth. (Left) power plot, (Right) differential plot of the power, both displayed with respect to a reference WGS84 altitude track. Other polarisations have similar results and are for this reason not shown.

European Space Agency
Agence spatiale européenne

3.3 Processed Data: p110226_m170445_HC1HC2HC2a

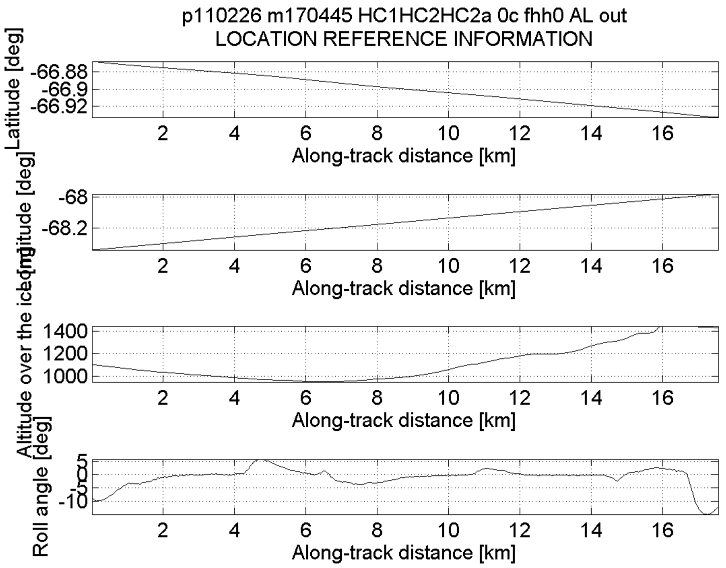

Figure 8: Location information

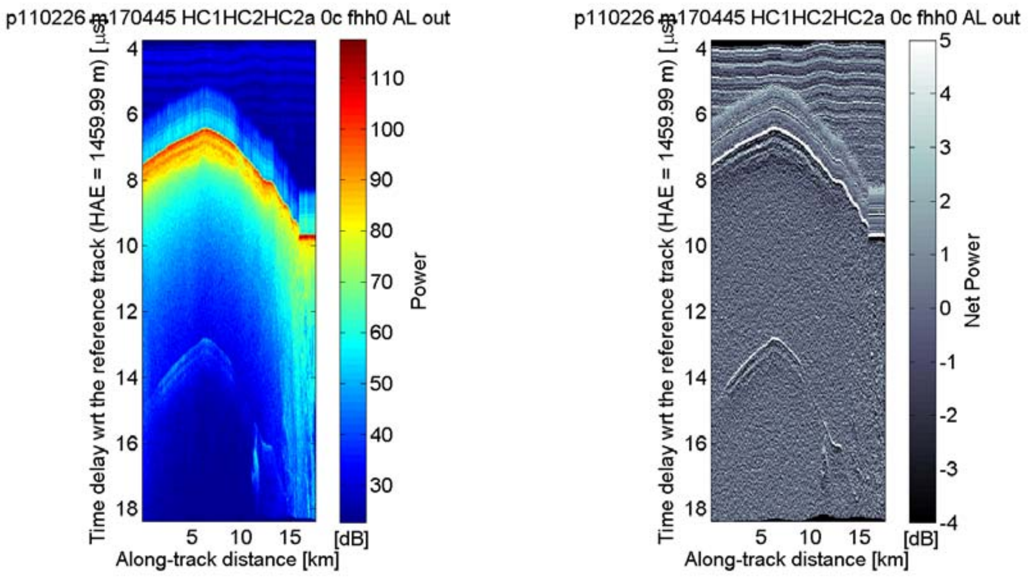

Figure 9: HH Polarisation of the p110226_m170445_HC1HC2HC2a track, 30 MHz bandwidth. (Left) power plot, (Right) differential plot of the power, both displayed with respect to a reference WGS84 altitude track. Other polarisations have similar results and are for this reason not shown.

European Space Agency
Agence spatiale européenne

4 COASTAL FLIGHT DATASET

Figure 10 gives an overview of the flown Coastal flight tracks. All the data has been acquired using a bandwidth of 30 MHz. For some tracks, the antenna was operated in multiple modes (e.g. channel combinations 1+2+3+4, 1+4 and 2+3), as is indicated in by the colours in Table 2 and explained in the file name convention. Sample plots of the power and the differential power are shown with respect to a reference altitude for each track. Beside this an along track visualisation is given for the airplane longitude, latitude, attitude over ice and the roll angle.

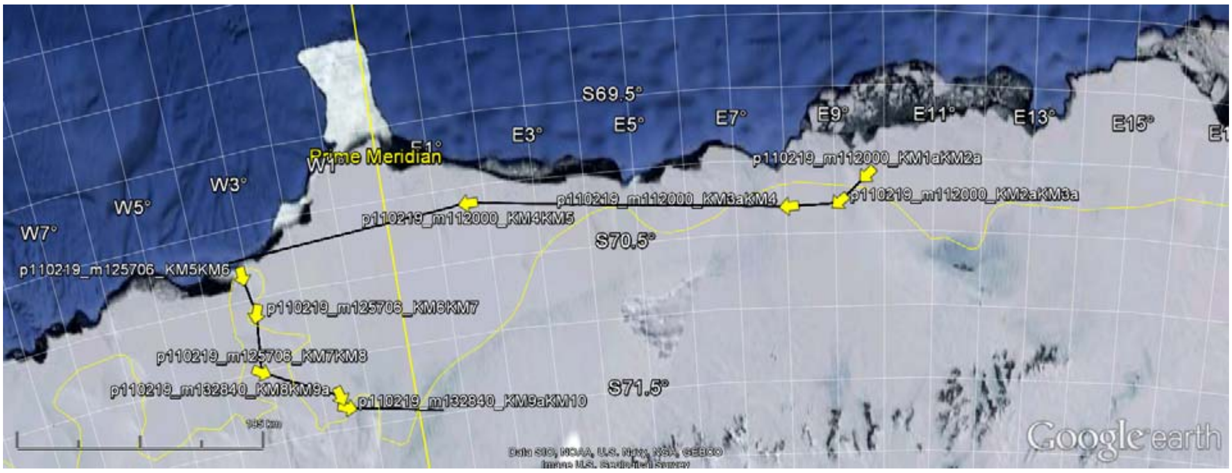

Figure 10: Google Earth plot of the flown tracks

4.1 Processed Data: p110219_m112000_KM1aKM2a

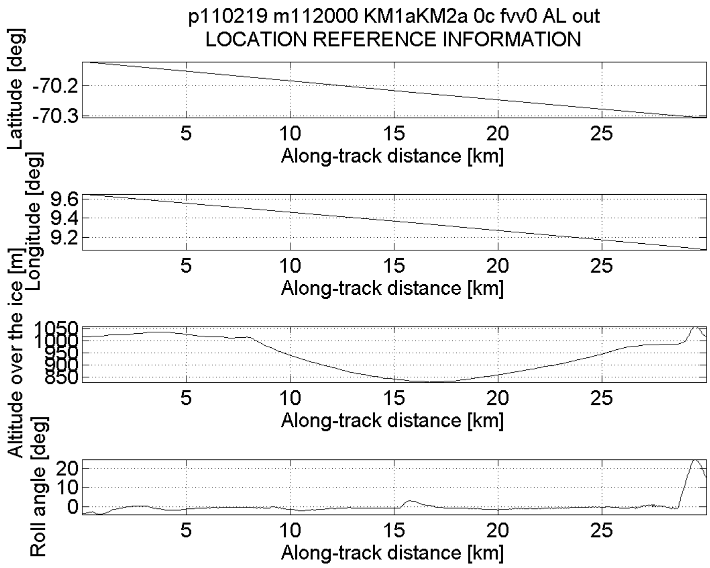

Figure 11: Location information

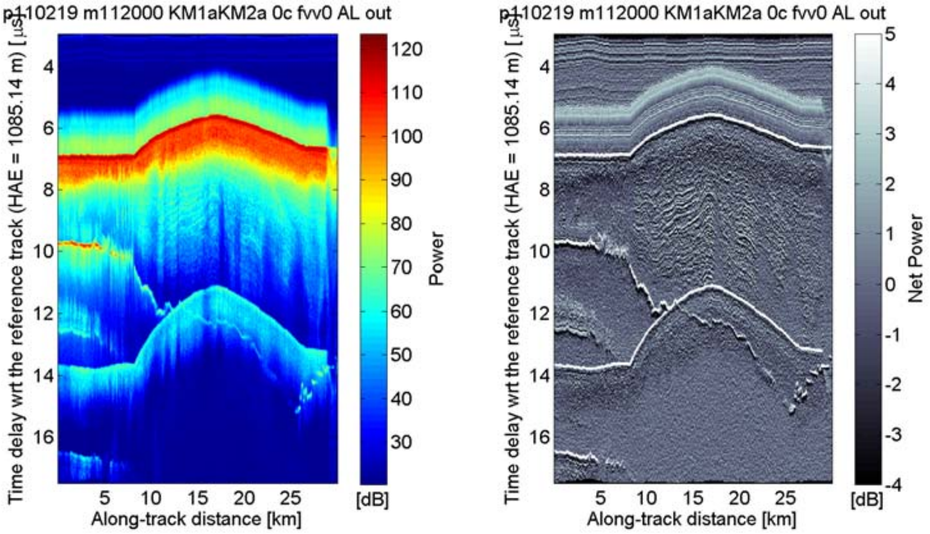

Figure 12: VV Polarisation of the p110219_m112000_KM1aKM2a track, 30 MHz bandwidth. (Left) power plot, (Right) differential plot of the power, both displayed with respect to a reference WGS84 altitude track

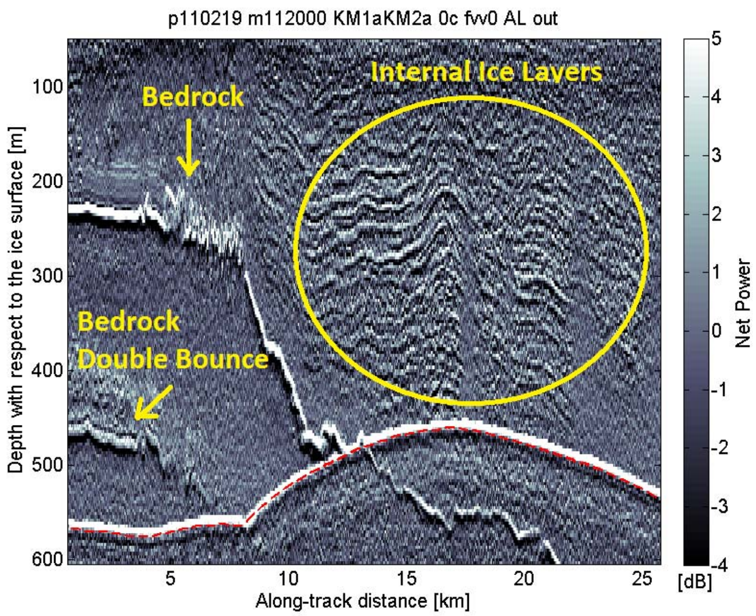

Figure 13: Differential power plot showing the internal ice layers of track p110219_m112000_KM1aKM2a, with a bandwidth of 30MHz. The red dashed line indicates the double bounce of the surface.

4.2 Processed Data: p110219_m112000_KM2aKM3a

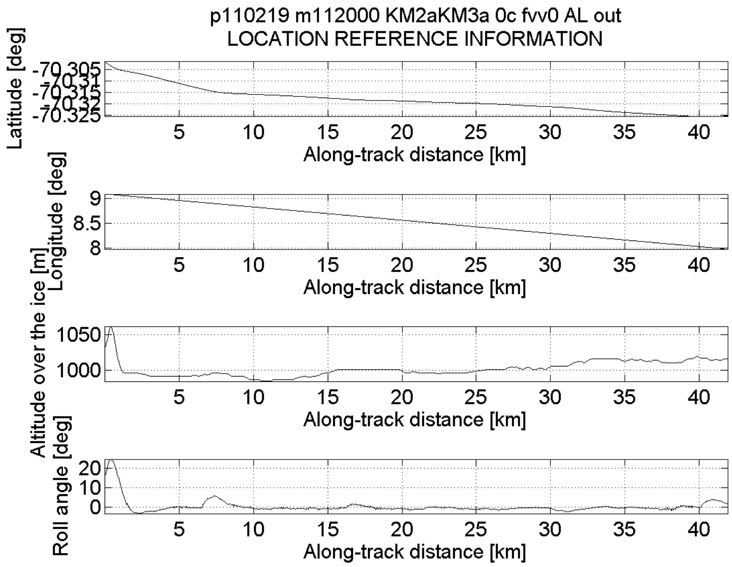

Figure 14: Location information

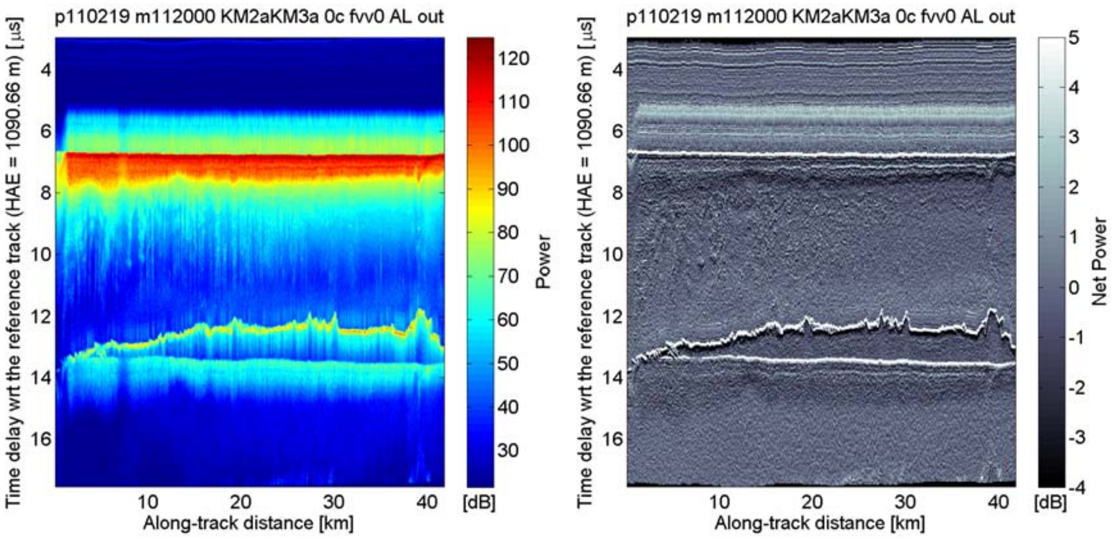

Figure 15: VV Polarisation of the p110219_m112000_KM2aKM3a track, 30 MHz bandwidth. (Left) power plot, (Right) differential plot of the power, both displayed with respect to a reference WGS84 altitude track

4.3 Processed Data: p110219_m112000_KM3aKM4

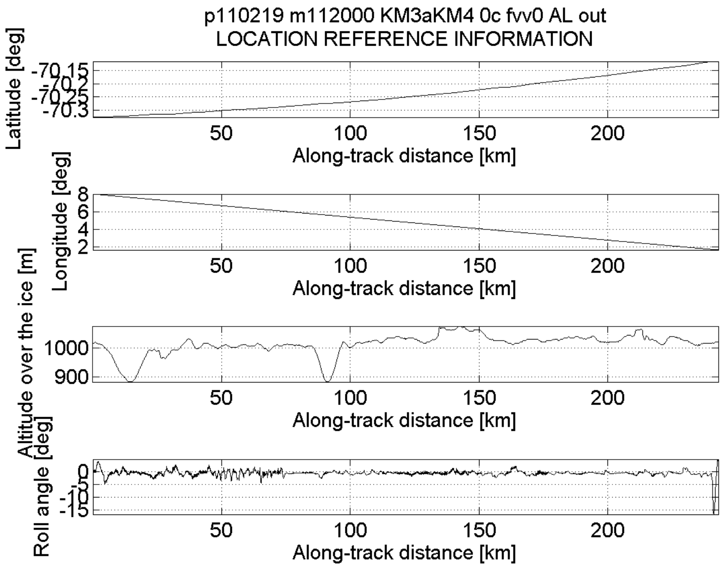

Figure 16: Location information

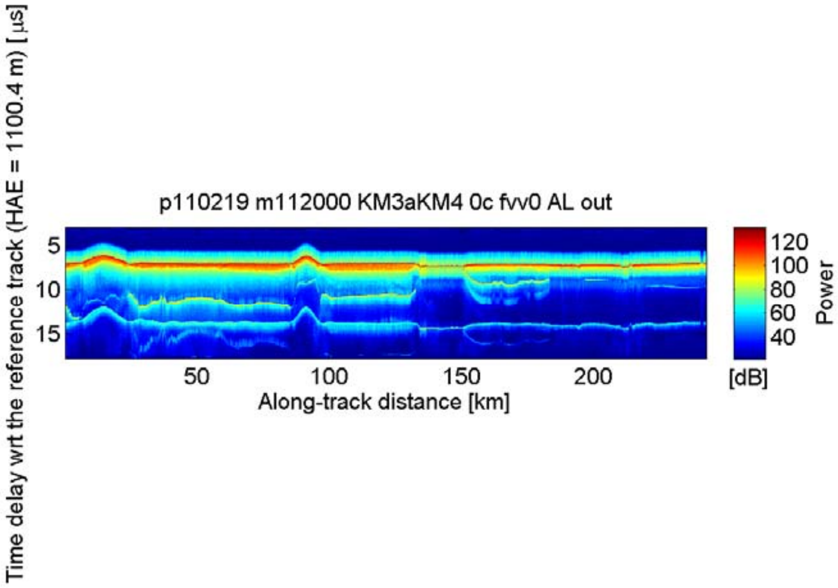

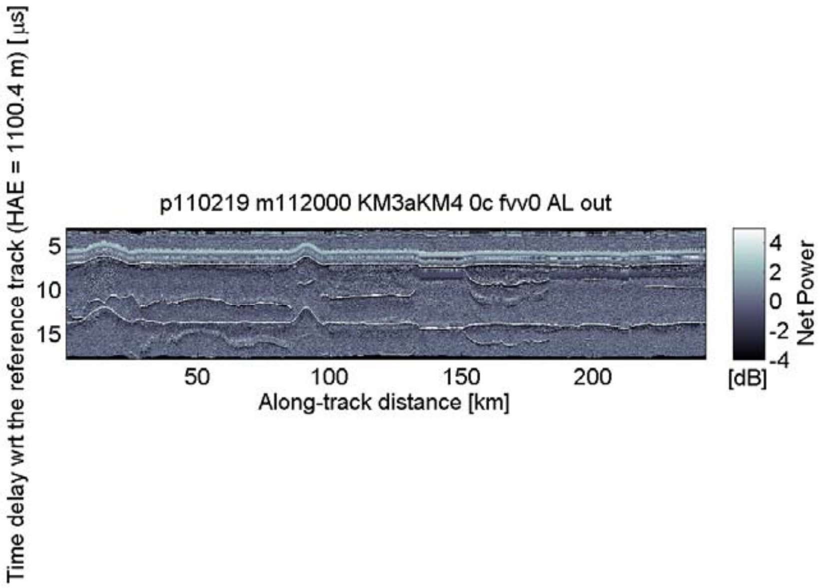

Figure 17: VV Polarisation of the p110219_m112000_KM3aKM4 track, 30 MHz bandwidth. (Top) power plot, (Bottom) differential plot of the power, both displayed with respect to a reference WGS84 altitude track

4.4 Processed Data: p110219_m112000_KM4KM5

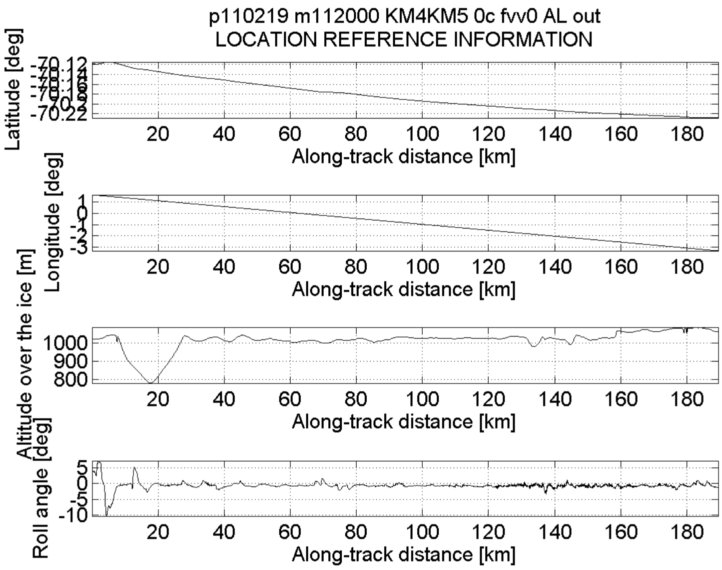

Figure 18: Location information

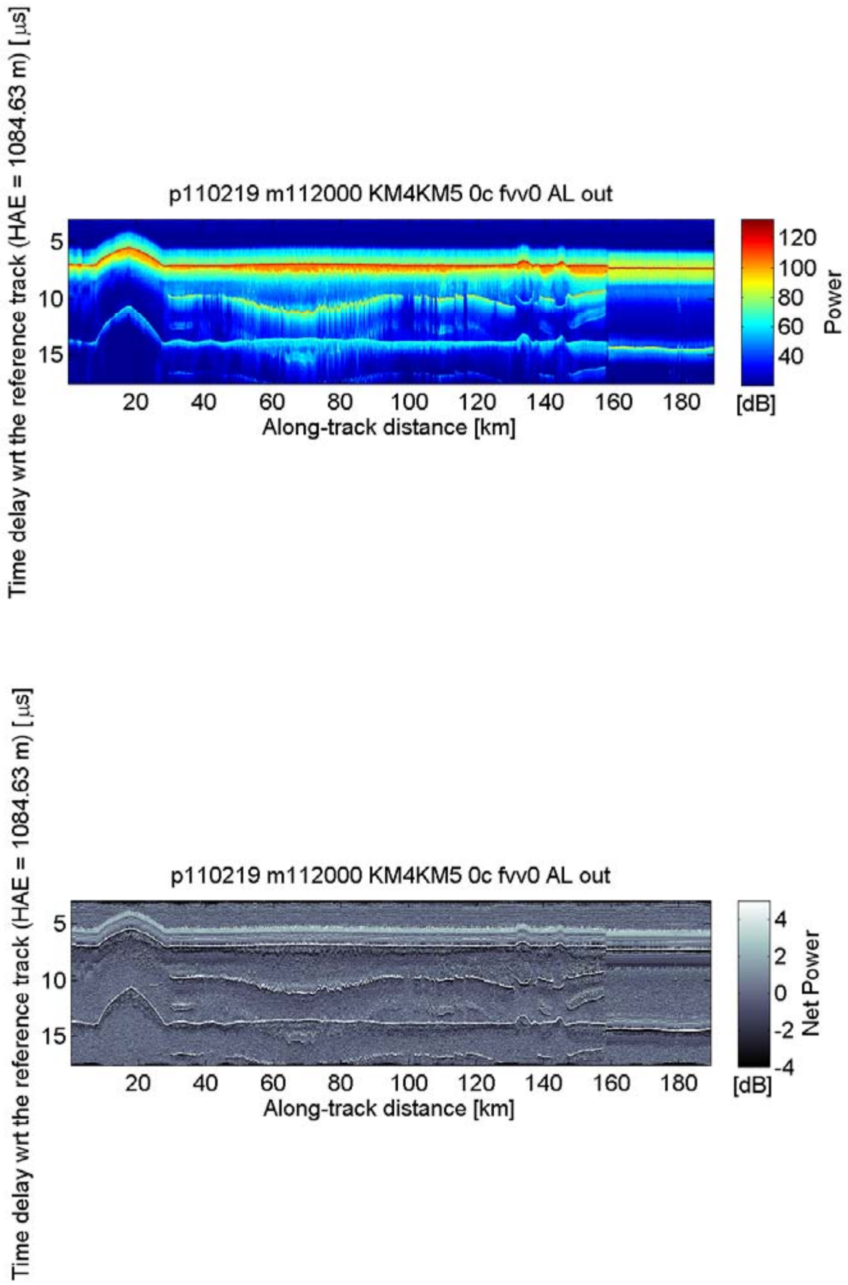

Figure 19: VV Polarisation of the p110219_m112000_KM4KM5 track, 30 MHz bandwidth. (Top) power plot, (Bottom) differential plot of the power, both displayed with respect to a reference WGS84 altitude track

4.5 Processed Data: p110219_m125706_KM5KM6

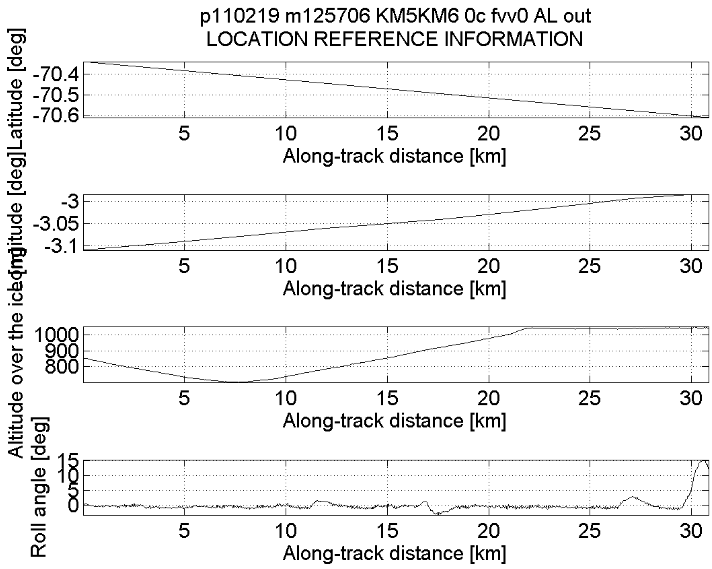

Figure 20: Location information

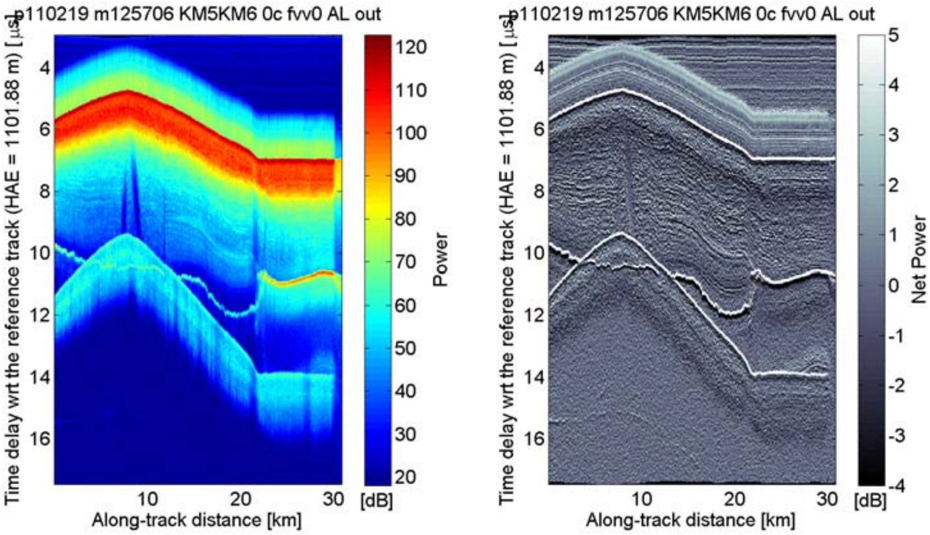

Figure 21: VV Polarisation of the p110219_m125706_KM5KM6 track, 30 MHz bandwidth. (Left) power plot, (Right) differential plot of the power, both displayed with respect to a reference WGS84 altitude track

4.6 Processed Data: p110219_m125706_KM6KM7

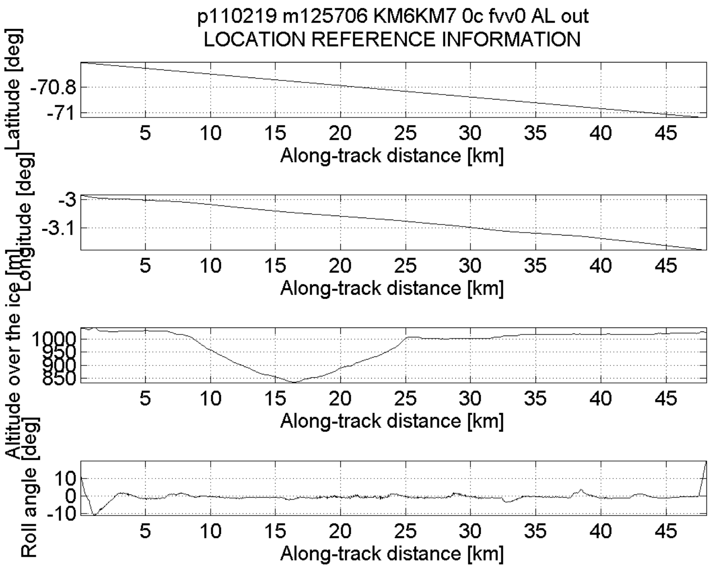

Figure 22: Location information

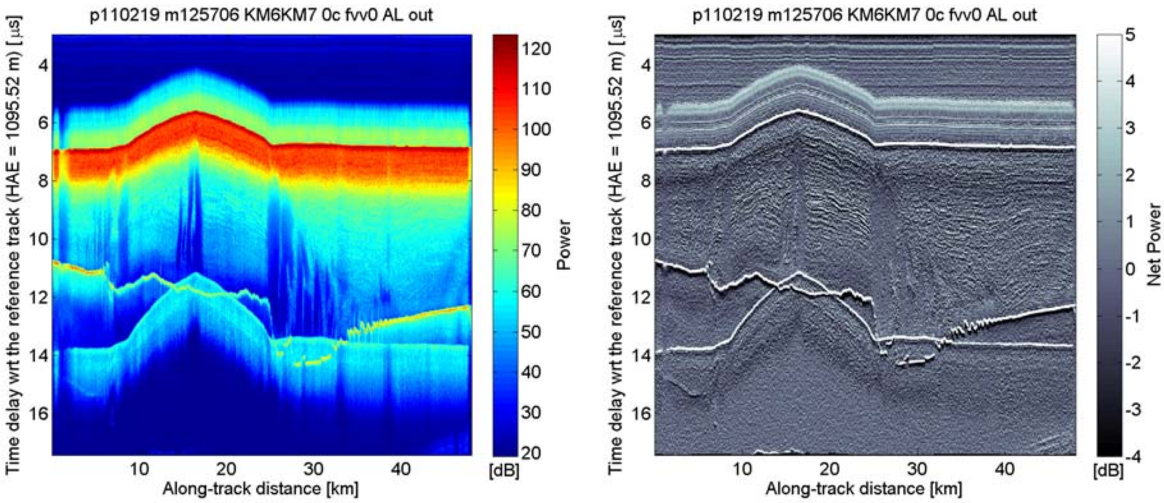

Figure 23: VV Polarisation of the p110219_m125706_KM6KM7 track, 30 MHz bandwidth. (Left) power plot, (Right) differential plot of the power, both displayed with respect to a reference WGS84 altitude track

4.7 Processed Data: p110219_m125706_KM7KM8

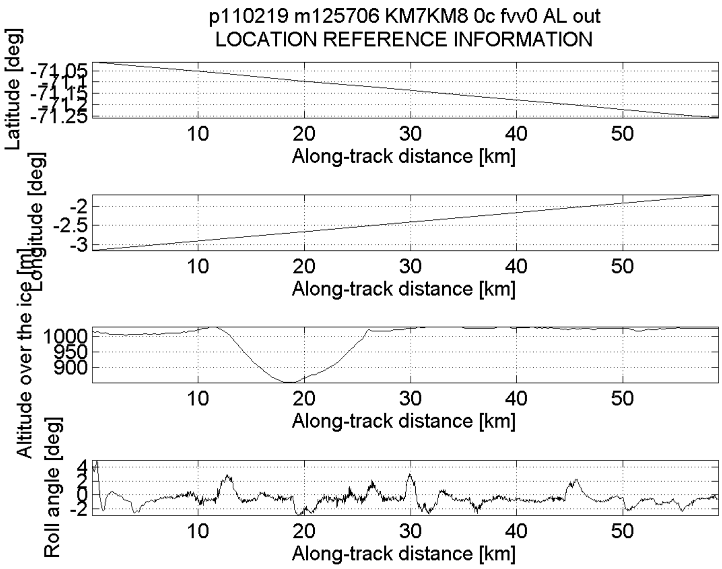

Figure 24: Location information

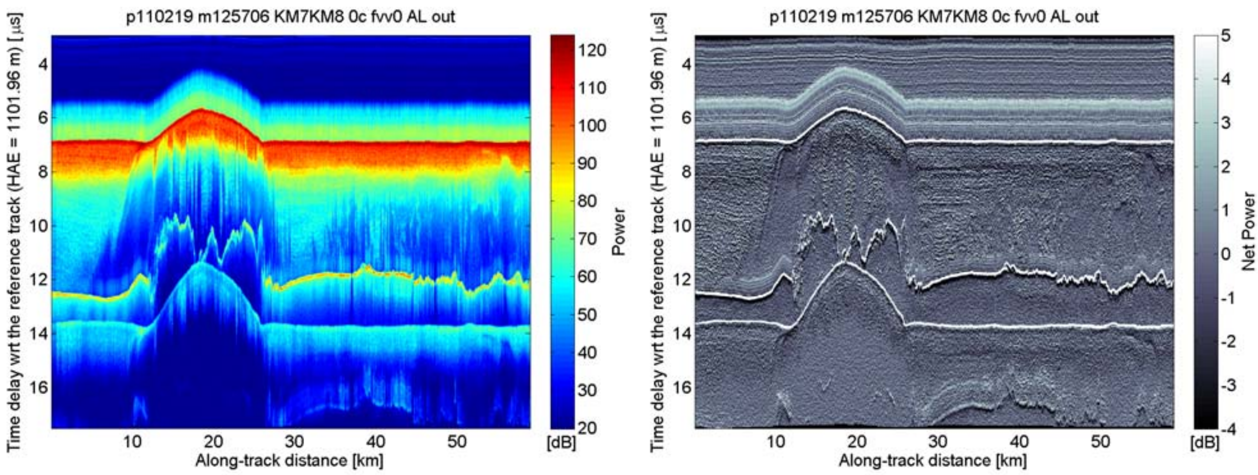

Figure 25: VV Polarisation of the p110219_m125706_KM7KM8 track, 30 MHz bandwidth. (Left) power plot, (Right) differential plot of the power, both displayed with respect to a reference WGS84 altitude track

4.8 Processed Data: p110219_m125706_KM8KM9a

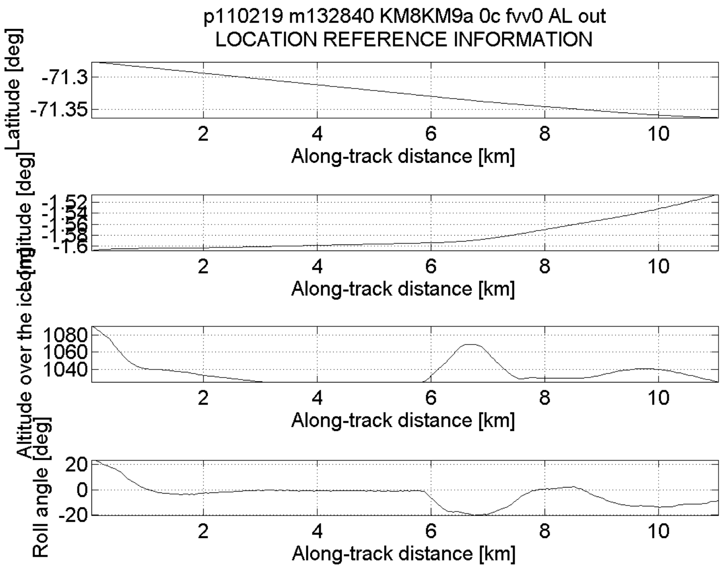

Figure 26: Location information

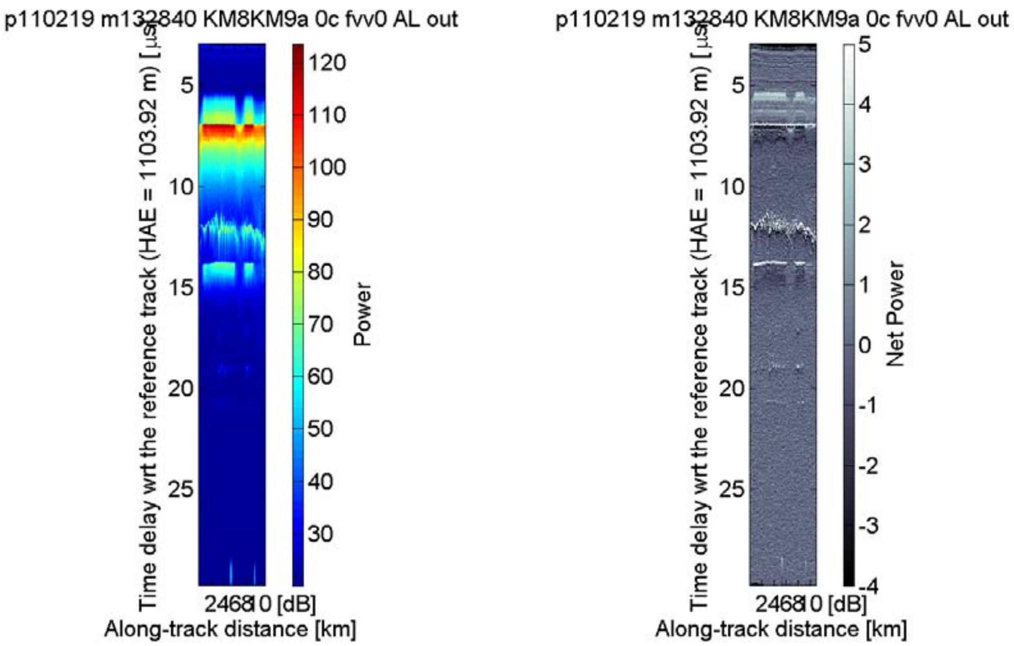

Figure 27: VV Polarisation of the p110219_m125706_KM8KM9a track, 30 MHz bandwidth. (Left) power plot, (Right) differential plot of the power, both displayed with respect to a reference WGS84 altitude track. Other antenna modes have similar results and are for this reason not shown.

4.9 Processed Data: p110219_m125706_KM9aKM10

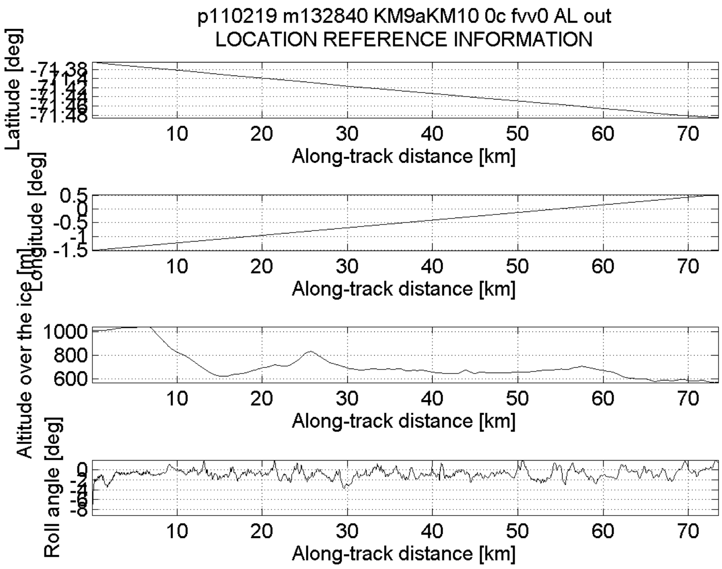

Figure 28: Location information

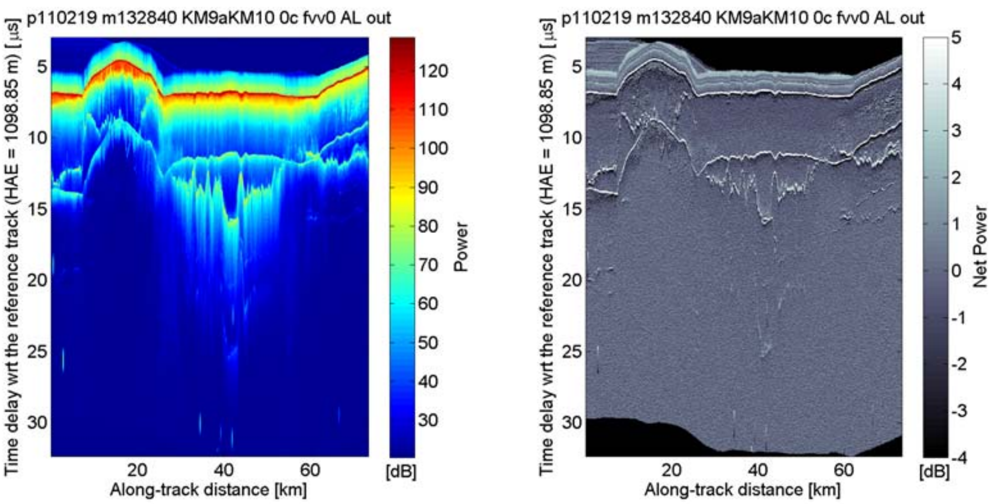

Figure 29: VV Polarisation of the p110219_m125706_KM9aKM10 track, 30 MHz bandwidth. (Left) power plot, (Right) differential plot of the power, both displayed with respect to a reference WGS84 altitude track. Other antenna modes have similar results and are for this reason not shown.

5 MULTI-APERTURE DATASET

The Multi-aperture dataset has been acquired over the Jutulstraumen glacier, for which the flown tracks are visualized in Figure 30. The operated bandwidths, antenna operation modes and acquired polarizations are summarized in Table 3. Below sample plots of the power and the differential power are shown with respect to a reference altitude for each track. Beside this an along track visualisation is given for the airplane longitude, latitude, attitude over ice and the roll angle.

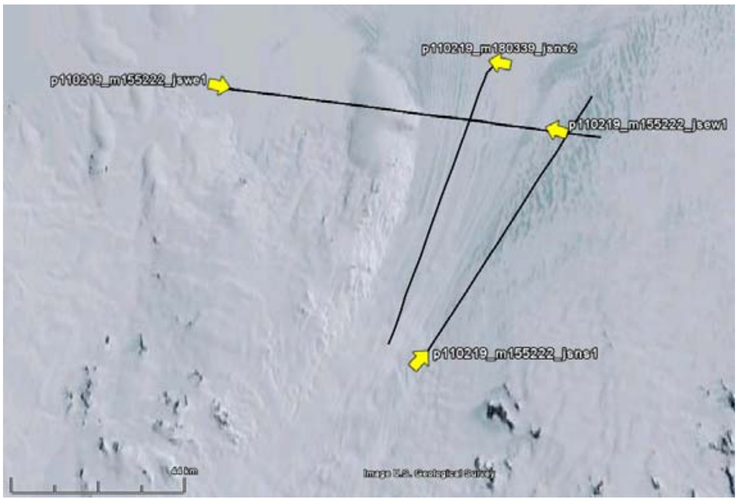

Figure 30: Google Earth plot of the flown tracks

5.1 Processed Data: p110219_m155222_jsew1

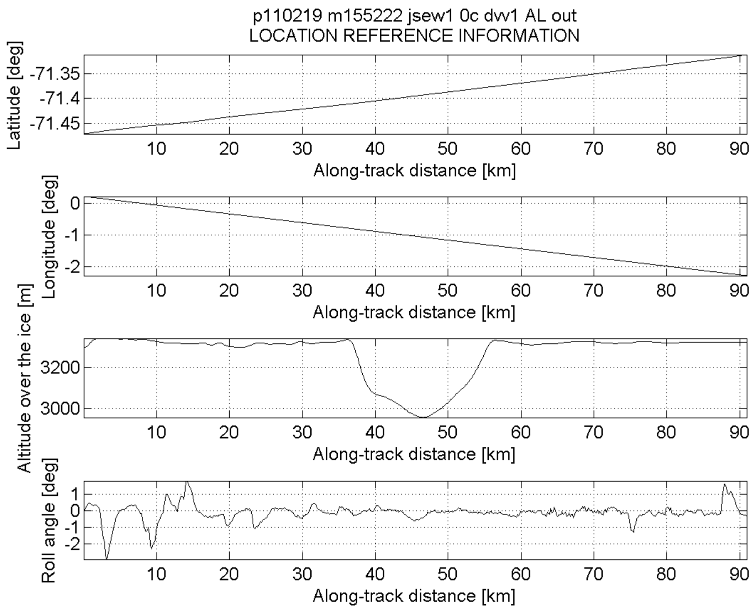

Figure 31: Location information

European Space Agency
Agence spatiale européenne

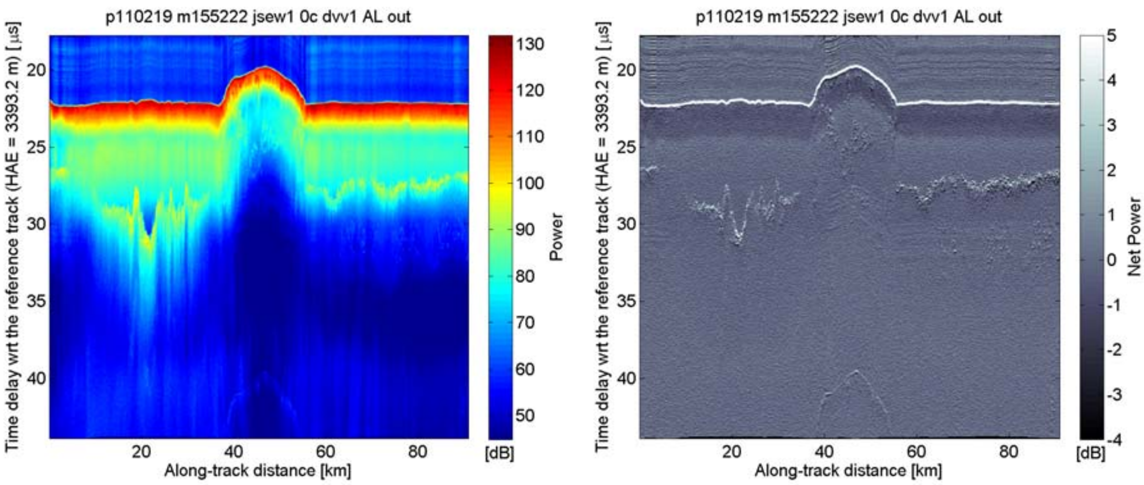

Figure 32: VV Polarisation of channel 1 of the p110219_m155222_jsew1 track, 30 MHz bandwidth. (Left) power plot, (Right) differential plot of the power, both displayed with respect to a reference WGS84 altitude track. Other channels have similar results and are for this reason not shown.

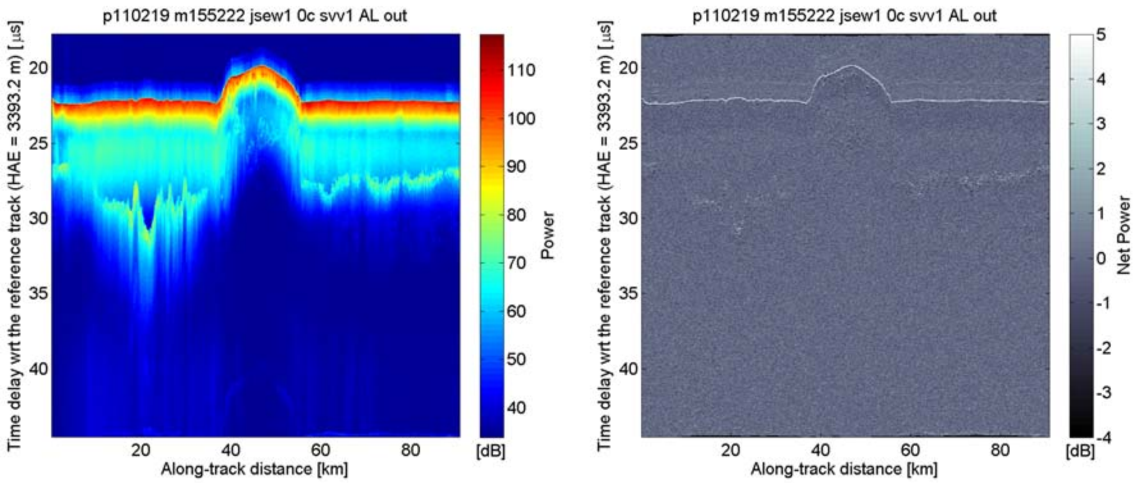

Figure 33: VV Polarisation of channel 1 of the p110219_m155222_jsew1 track, 85 MHz bandwidth. (Left) power plot, (Right) differential plot of the power, both displayed with respect to a reference WGS84 altitude track. Other channels have similar results and are for this reason not shown.

5.2 Processed Data: p110219_m155222_jsns1

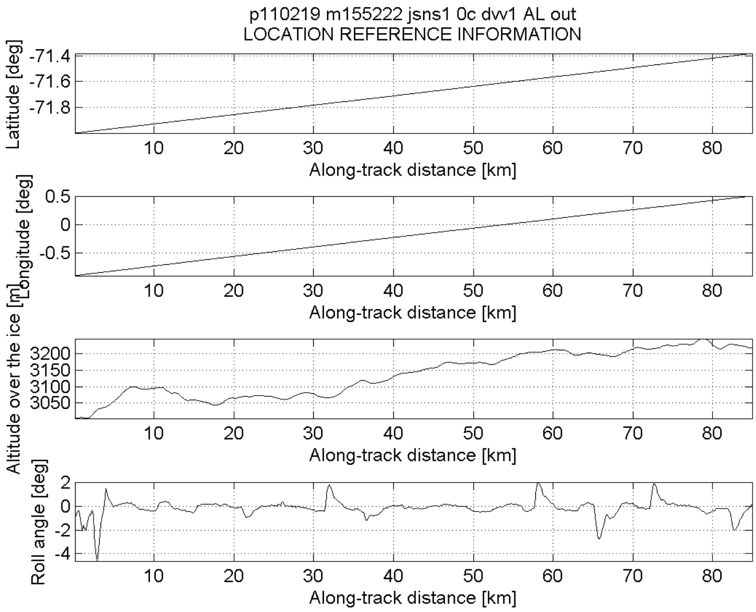

Figure 34: Location information

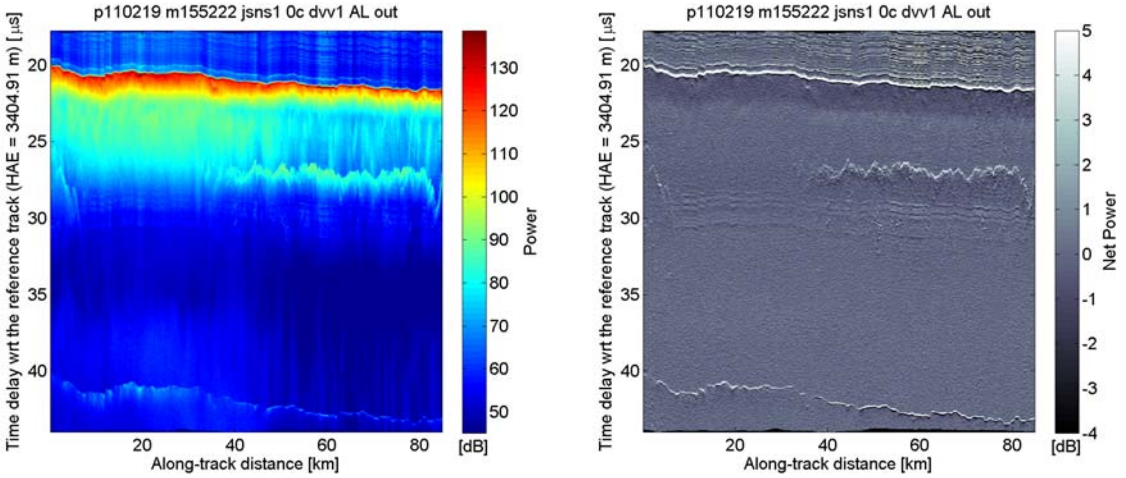

Figure 35: VV Polarisation of channel 1 of the p110219_m155222_jsns1 track, 30 MHz bandwidth. (Left) power plot, (Right) differential plot of the power, both displayed with respect to a reference WGS84 altitude track. Other channels have similar results and are for this reason not shown.

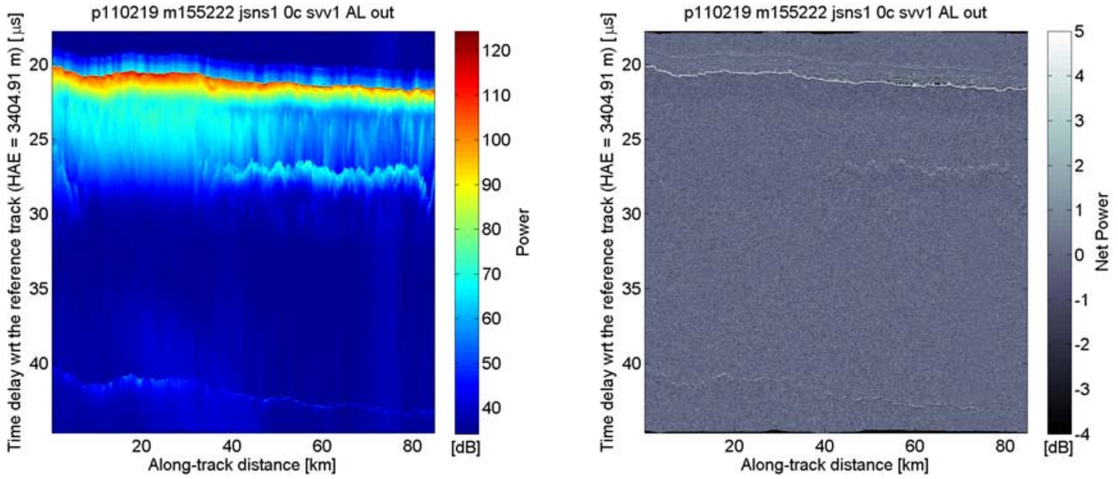

Figure 36: VV Polarisation of channel 1 of the p110219_m155222_jsns1 track, 85 MHz bandwidth. (Left) power plot, (Right) differential plot of the power, both displayed with respect to a reference WGS84 altitude track. Other channels have similar results and are for this reason not shown.

5.3 Processed Data: p110219_m155222_jswe1

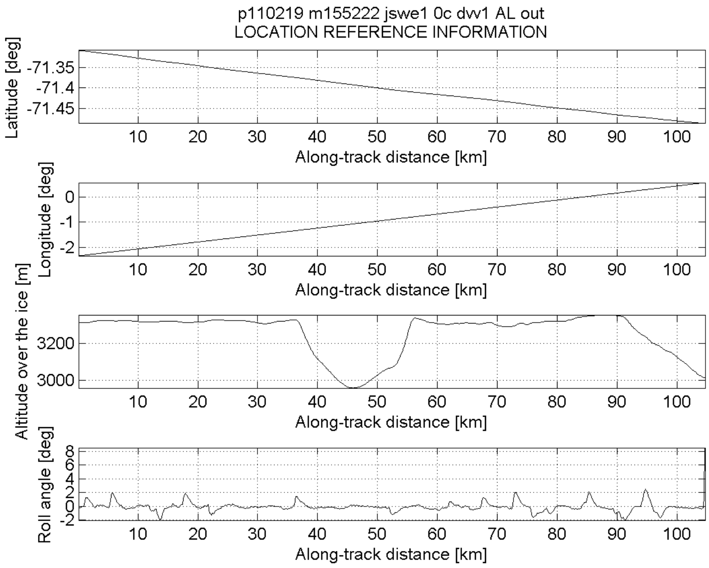

Figure 37: Location information

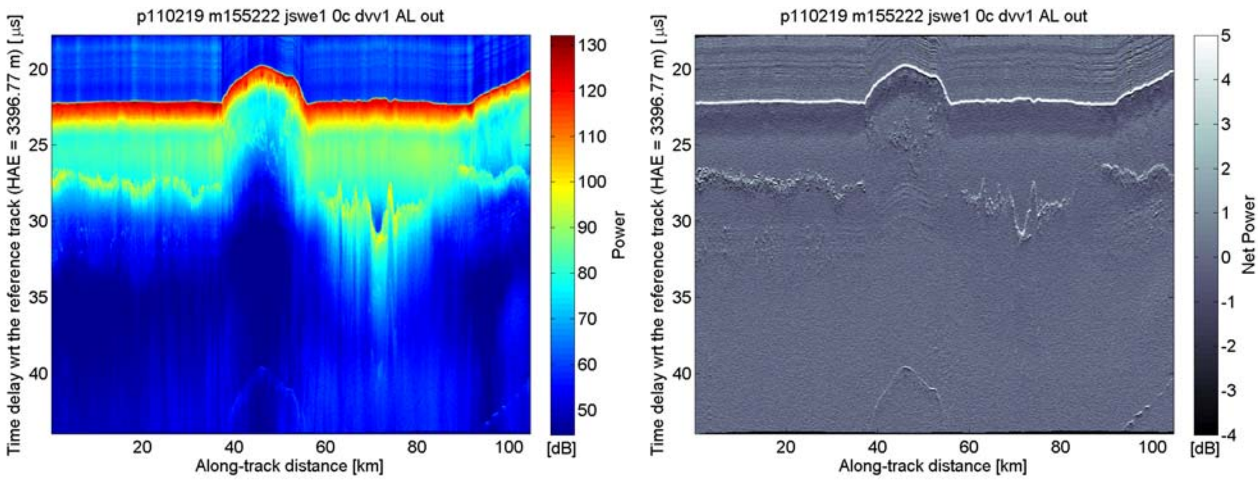

Figure 38: VV Polarisation of channel 1 of the p110219_m155222_jswe1 track, 30 MHz bandwidth. (Left) power plot, (Right) differential plot of the power, both displayed with respect to a reference WGS84 altitude track. Other channels have similar results and are for this reason not shown.

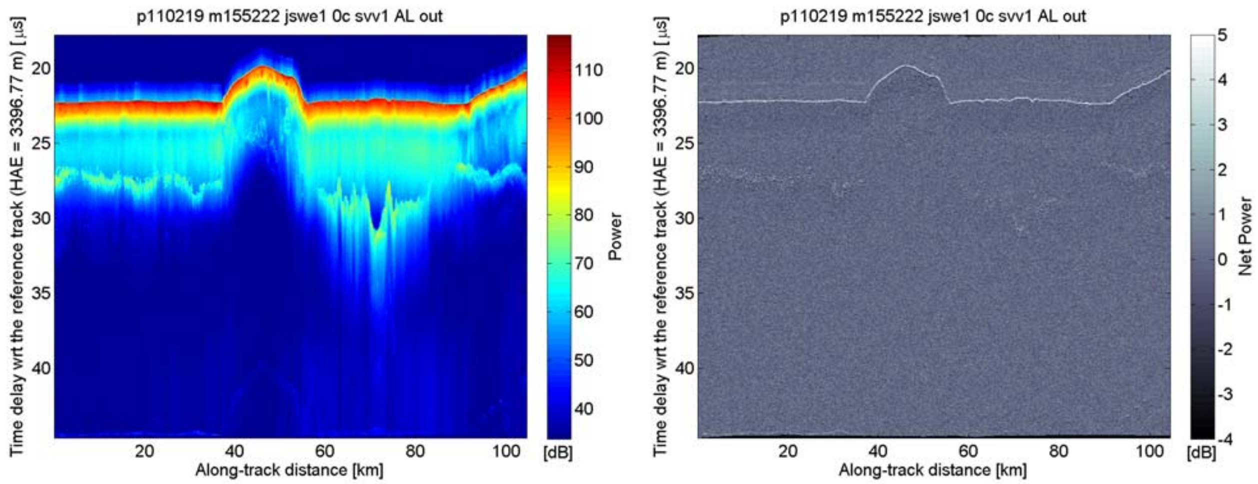

Figure 39: VV Polarisation of channel 1 of the p110219_m155222_jswe1 track, 85 MHz bandwidth. (Left) power plot, (Right) differential plot of the power, both displayed with respect to a reference WGS84 altitude track. Other channels have similar results and are for this reason not shown.

5.4 Processed Data: p110219_m180339_jsns2

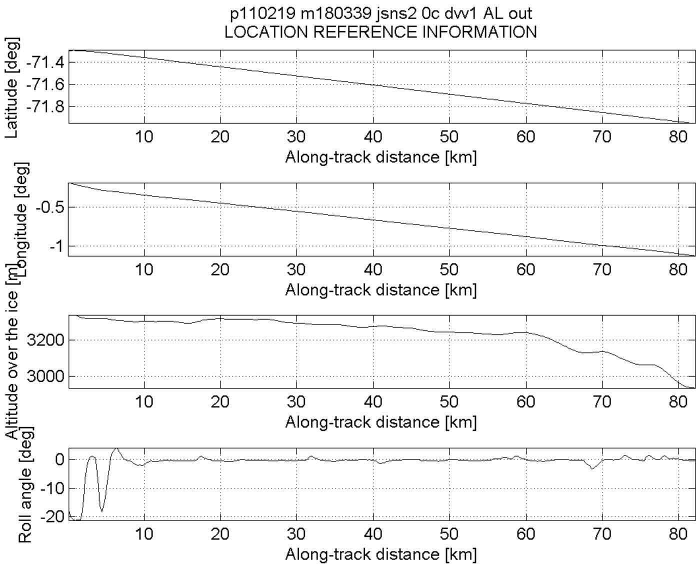

Figure 40: Location information

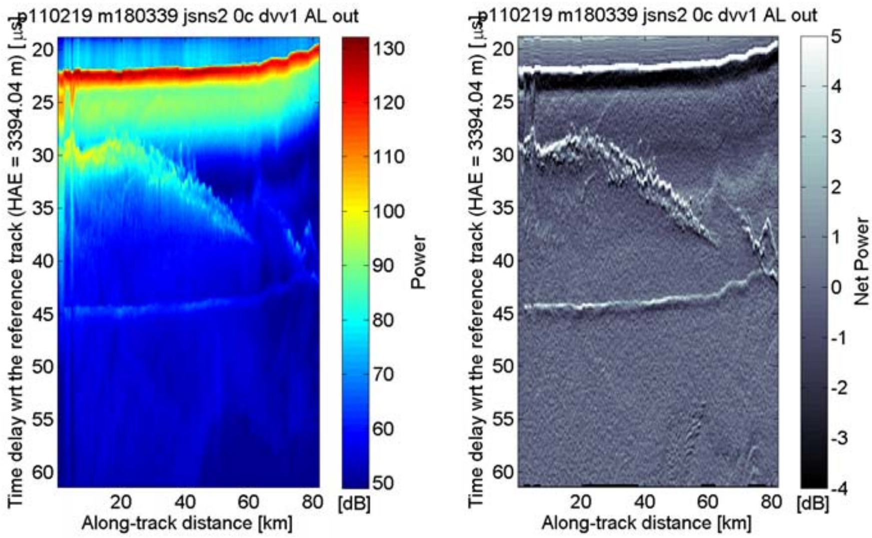

Figure 41: VV Polarisation of channel 1 of the p110219_m180339_jsns2 track, 30 MHz bandwidth. (Left) power plot, (Right) differential plot of the power, both displayed with respect to a reference WGS84 altitude track. Other channels have similar results and are for this reason not shown.

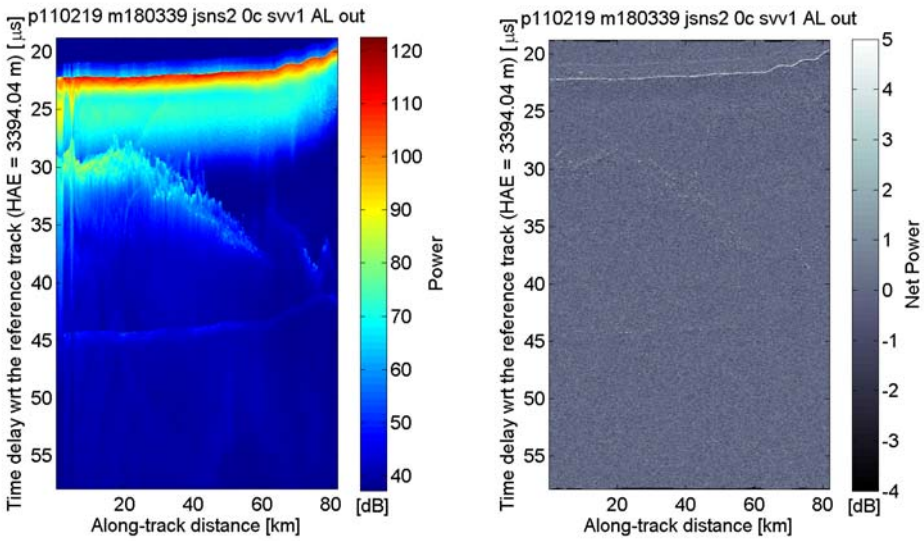

Figure 42: VV Polarisation of channel 1 of the p110219_m180339_jsns2 track, 85 MHz bandwidth. (Left) power plot, (Right) differential plot of the power, both displayed with respect to a reference WGS84 altitude track. Other channels have similar results and are for this reason not shown.

6 ICEGRAV

Figure 43 gives an overview of the flown IceGrav data tracks. The data have been acquired for multiple polarisations using a bandwidth of 6/85 MHz, as is summarized in Table 4. Sample plots of the power and the differential power are shown with respect to a reference altitude for only a small subset of the processed tracks. Beside this an along track visualisation is given for the airplane longitude, latitude, attitude over ice and the roll angle. Example plots for all IceGrav tracks are provided together with the processed data.

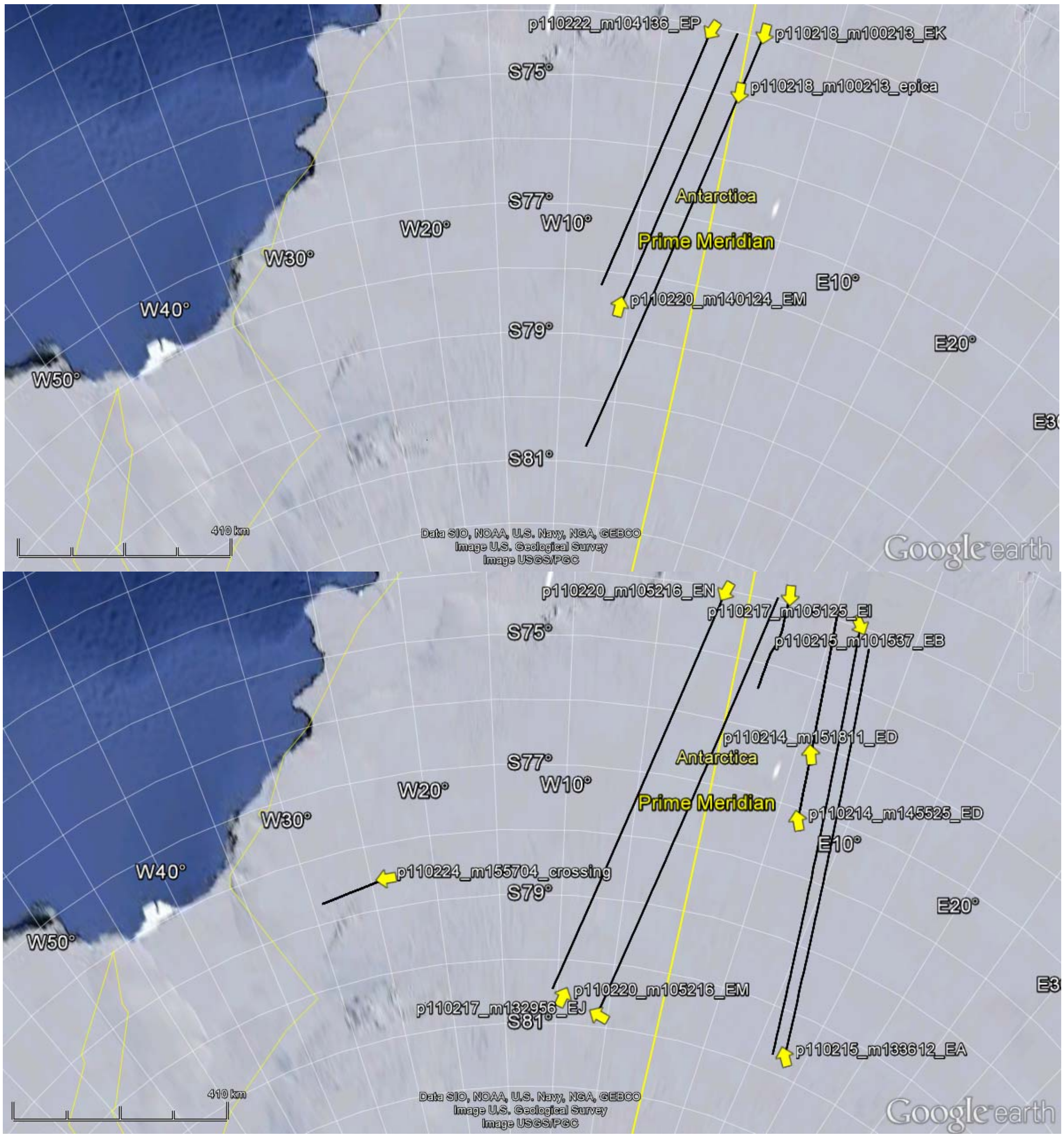

Figure 43: Google Earth plot of the flown tracks

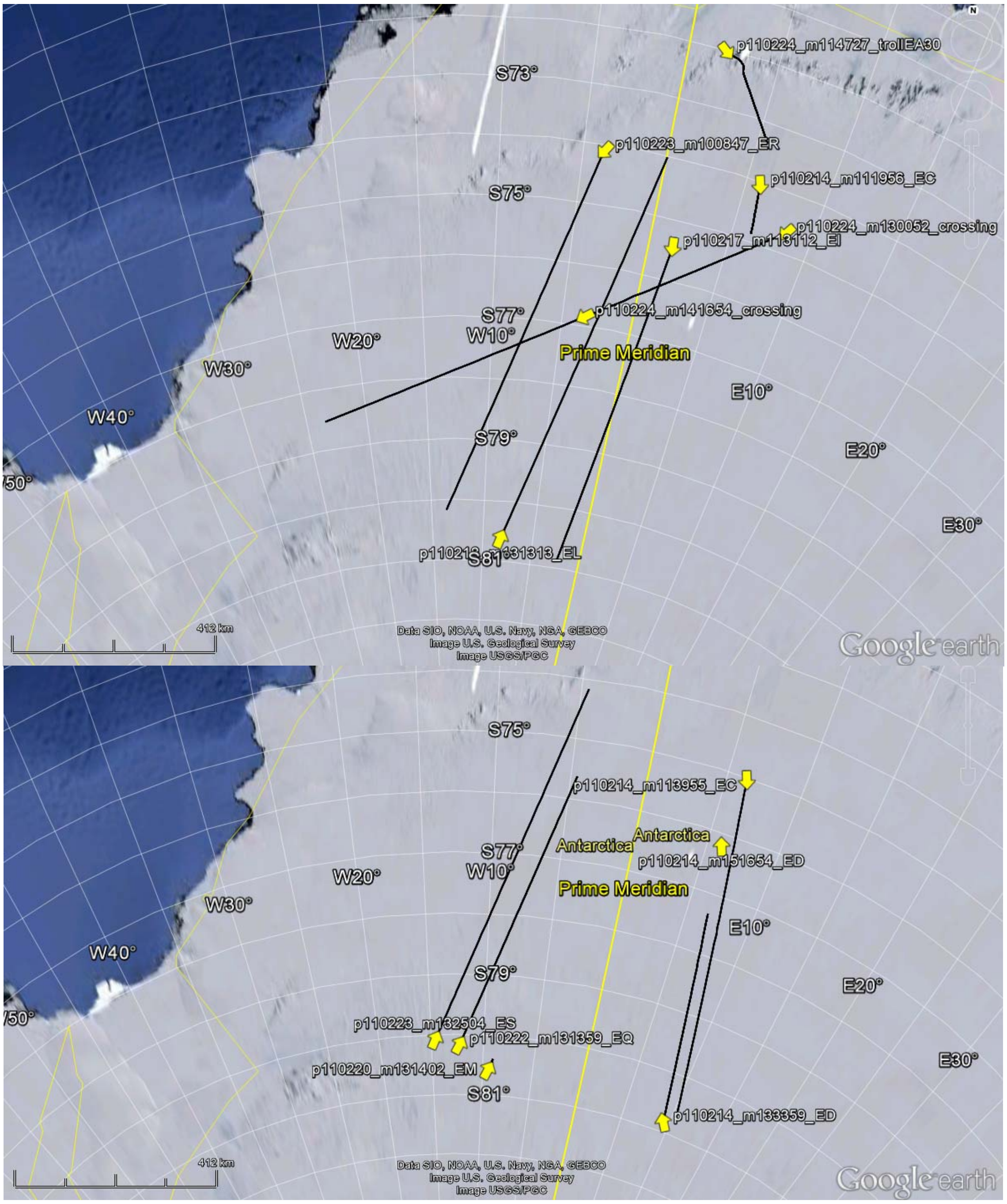

Figure 43 continued: Google Earth plot of the flown tracks

European Space Agency
Agence spatiale européenne

6.1 Processed Data: p110220_m140124_EM

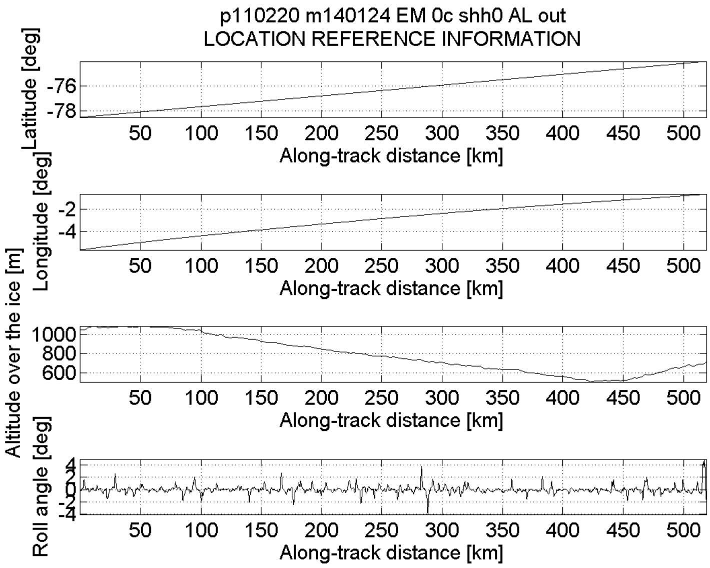

Figure 44: Location information

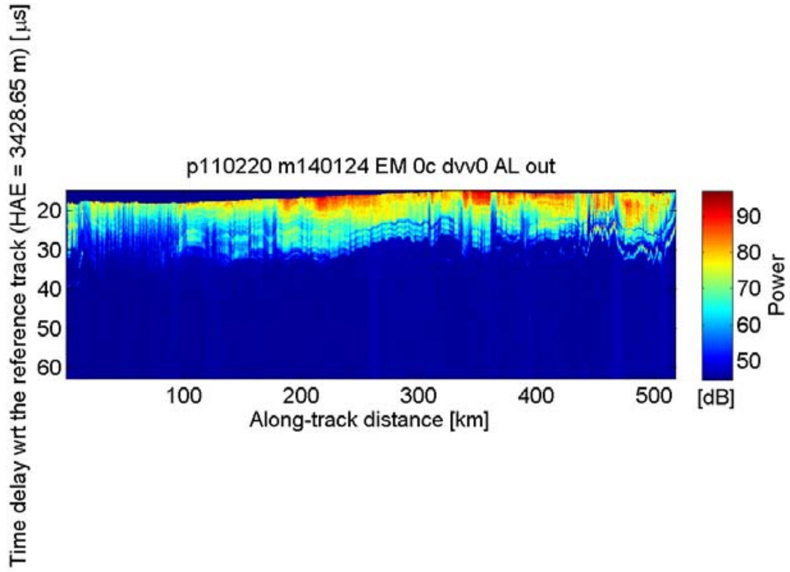

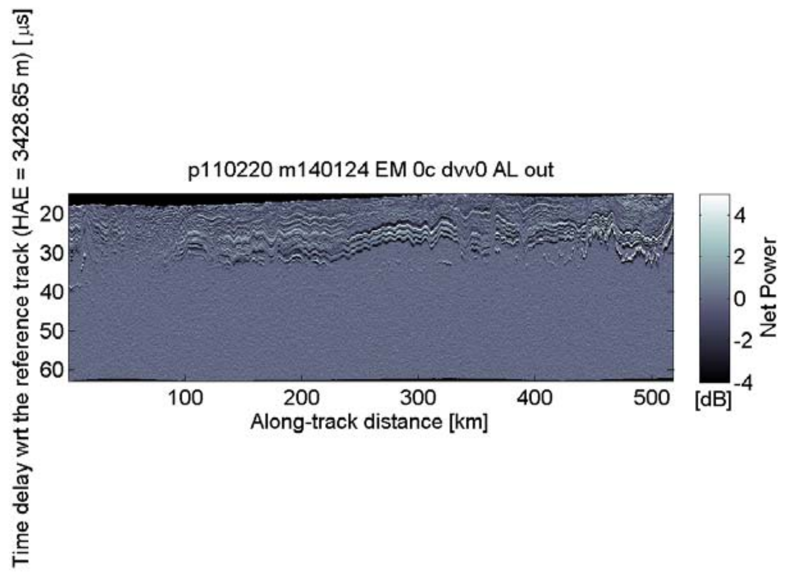

Figure 45: VV Polarisation of the p110220_m140124_EM track, 6 MHz bandwidth. (Top) power plot, (Bottom) differential plot of the power, both displayed with respect to a reference WGS84 altitude track

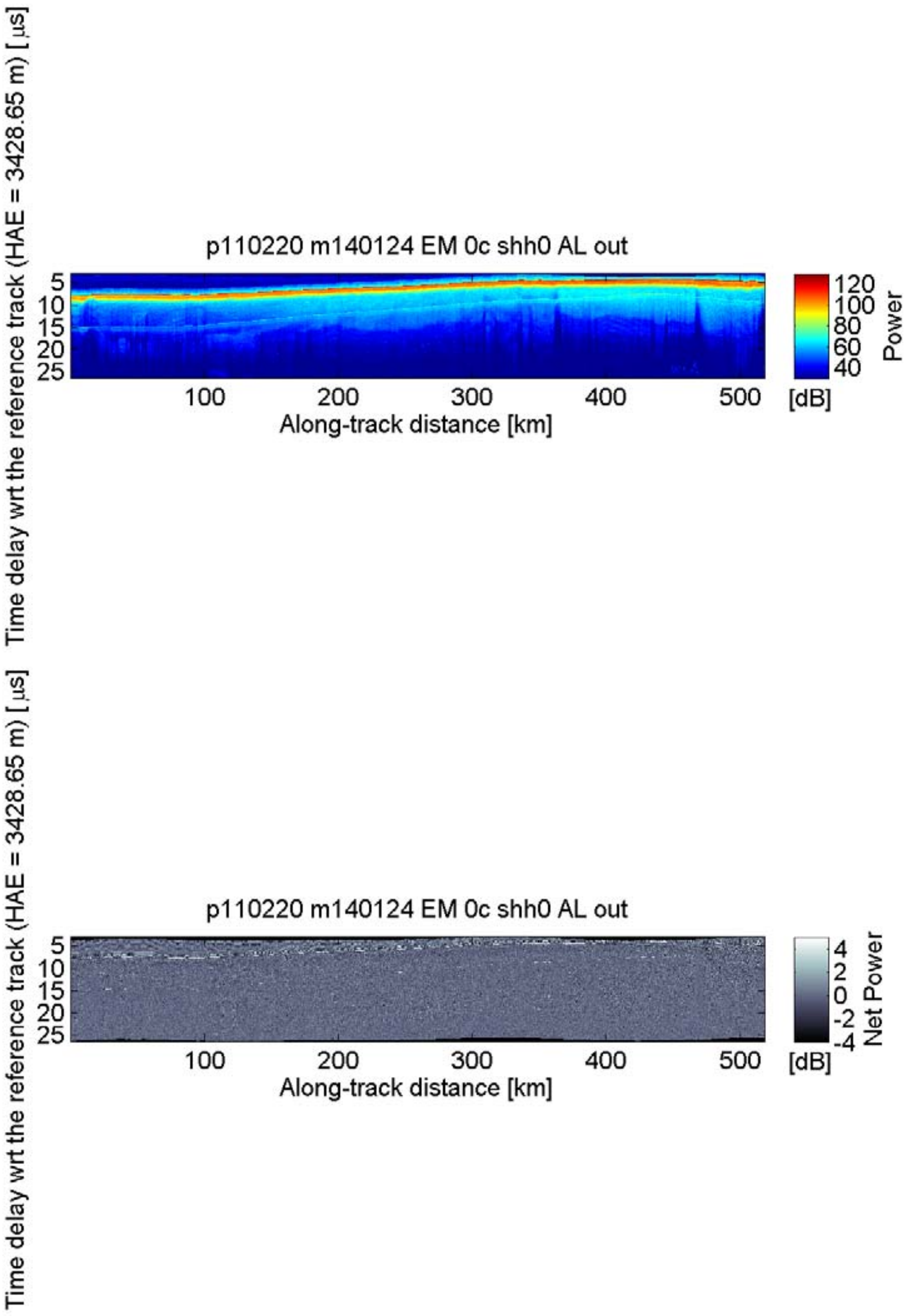

Figure 46: VV Polarisation of the p110220_m140124_EM track, 85 MHz bandwidth. (Top) power plot, (Bottom) differential plot of the power, both displayed with respect to a reference WGS84 altitude track

6.2 Processed Data: p110214_m133359_ED + RFI correction comparison

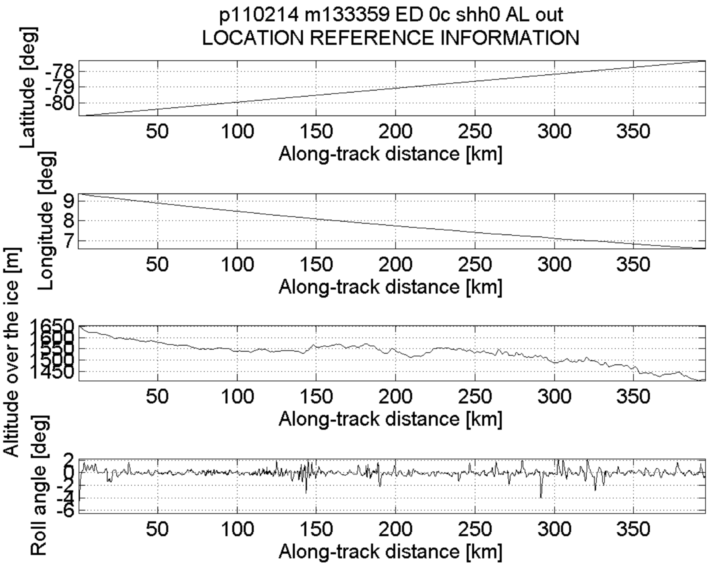

Figure 47: Location information

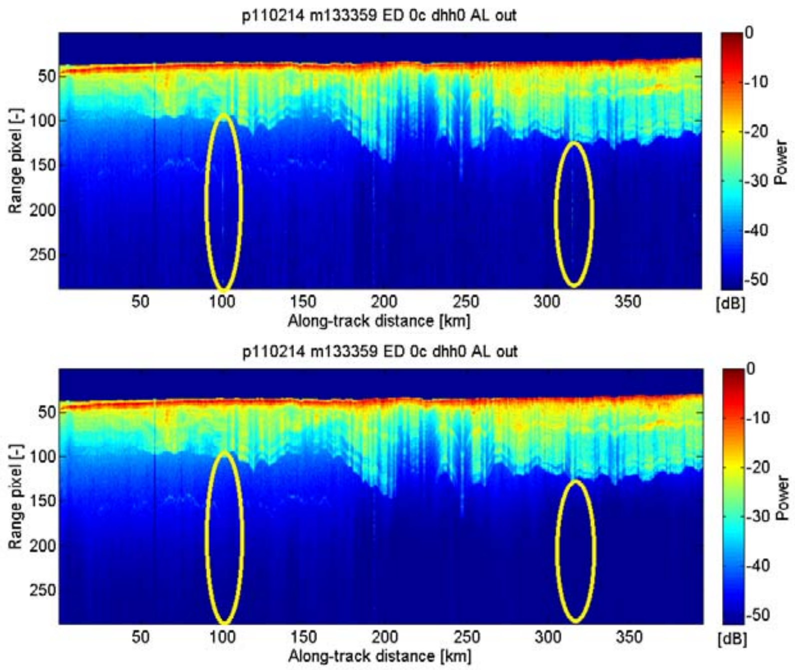

Figure 48: (Top) before Radio Frequency Interference correction, (Bottom) after. Highlighted regions indicate the most clear changes, as the smaller changes are difficult to observe when printed

6.3 Processed Data: p110224_m114727_trollEA30

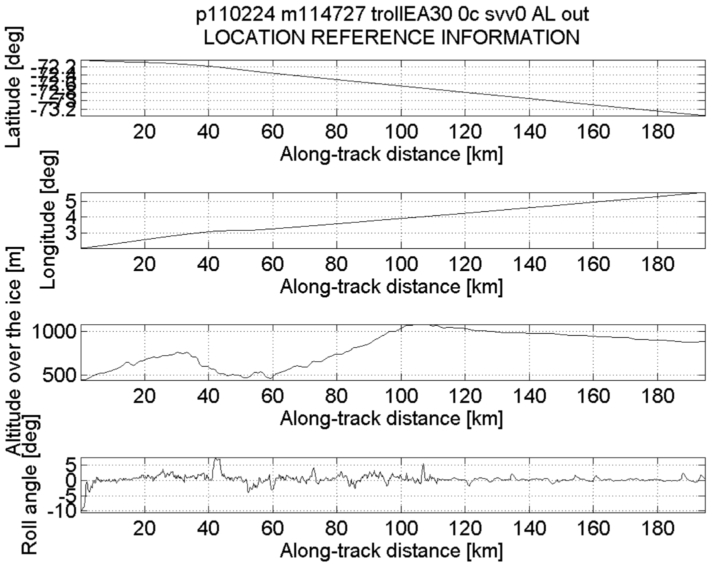

Figure 49: Location information

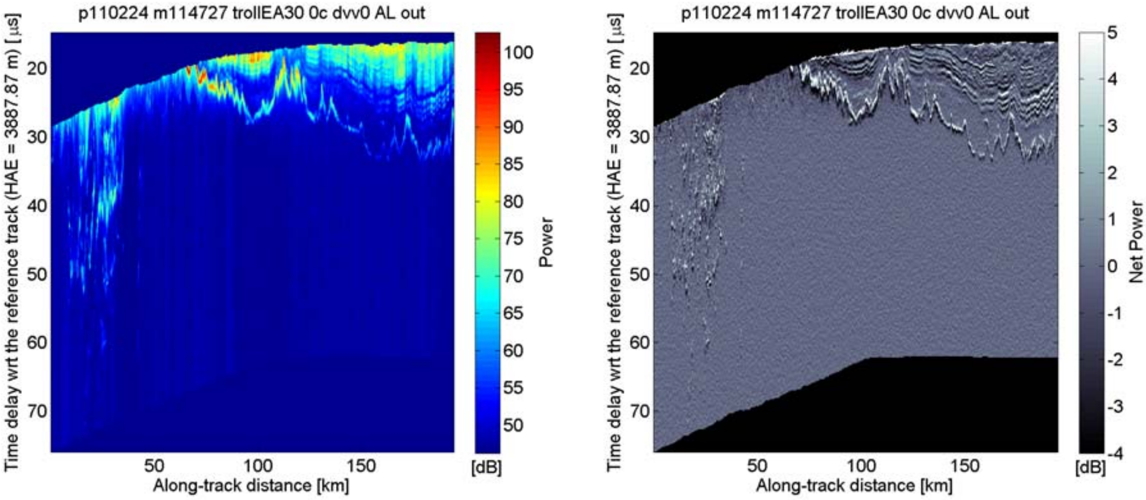

Figure 50: VV Polarisation of the p110224_m114727_trollEA30 track, 6 MHz bandwidth. (Left) power plot, (Right) differential plot of the power, both displayed with respect to a reference WGS84 altitude track.

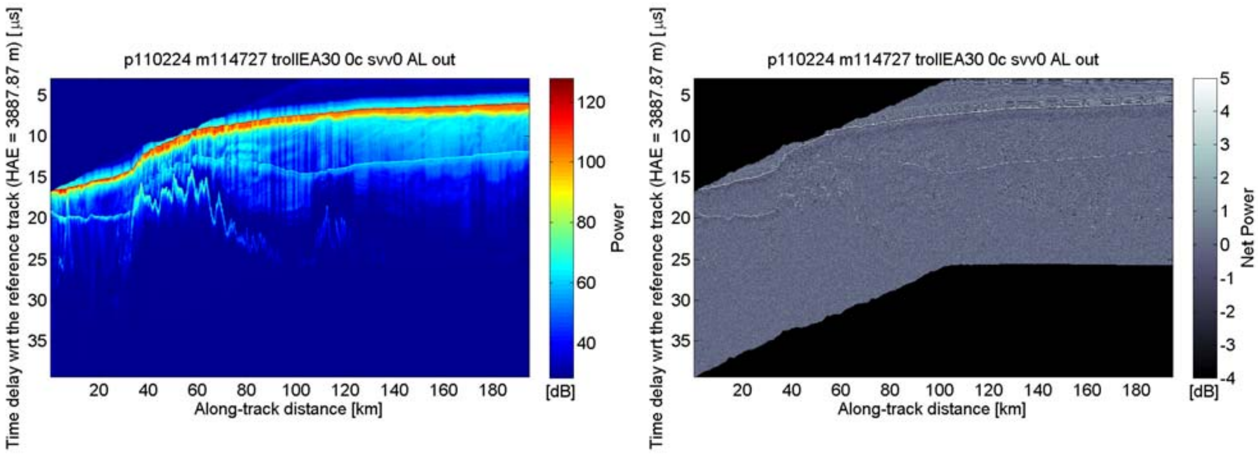

Figure 51: VV Polarisation of the p110224_m114727_trollEA30 track, 85 MHz bandwidth. (Left) power plot, (Right) differential plot of the power, both displayed with respect to a reference WGS84 altitude track

References

[1] J. Dall, A. Kusk, S.S. Kristensen, R. Forsberg and U. Nielsen, POLARIS Validation experiment during the 2010/2011 IceGrav campaign; Final Report. ESA Contract No 4000103505/11/NL/JA/fk, February 2012.

[2] J. Dall and A. Kusk, P-Band Ice Sounding Radar Demonstrator Development; Campaign Report, ESA Contract No 19307/05/NL/JA, April 2009.

[3] M. Villano and F. Hélière, P-Band Ice Sounding Radar Demonstrator Development; Delivered Data and Processing Tools, June 2009.

EUROPEAN SPACE AGENCY CONTRACT REPORT

ESA Contract No. 4000103505/11/NL/JA/fk

POLARIS validation experiment during the 2010/11 IceGrav campaign; Final Report

Jørgen Dall, Anders Kusk, Steen Savstrup Kristensen,

Rene Forsberg, and Ulrik Nielsen

February 2012

National Space Institute
Technical University of Denmark
Ørsteds Plads, building 348
DK-2800 Kongens Lyngby, Denmark
Phone : +45 4525 3800
Fax: +45 4593 1634
http://www.space.dtu.dk

ESA STUDY CONTRACT REPORT

ESA CONTRACT No	SUBJECT		CONTRACTOR
40000101xxx/10NL/JA/fk	Technical Assistance for POLARIS during the 2010/2011 IceGrav validation experiment		DTU Space
*** ESA CR( )No**	*** STAR CODE**	**No of volumes:** 1 **This is Volume No:** 1	**Contractor's Ref.** FR_v1

ABSTRACT:

In February 2011, the ESA POLARIS system was flown for the first time in the Antarctic, as part of the ICEGRAV project. This report describes the campaign planning and implementation, data processing, quality assessment, and analysis of the processed data wrt. to the five objectives: 1) The detection and mapping of deep ice layers and bedrock at up to 4 km depth in cold ice; 2) Sensitivity limit (depth) in warm ice; 3) Observability of radar reflection horizons under various conditions: 4) Potential of polarimetry for observing ice anisotropy in flowing ice and dynamical regions; 5) Acquisition of multiple phase-centre data in order to develop processing techniques for suppression of across-track surface clutter and enhancing shallow ice layers.An extensive data set to address these objectives has been acquired. 1) and 4) have been addressed on gravimetry flights south of Troll, including an overflight of the EPICA/Kohnen drilling site. 2) has been investigated on dedicated flights over Adelaide Island and over Fimbulisen ice shelf on the Queen Maud Land coast. 3) has been addressed by the aforementioned acquisitions, as well as acquisitions over the Jutulstraumen glacier. Finally, multi-aperture data for 5) have been acquired on a dedicated flight with acquisitions parallel to and crossing the Jutulstraumen glacier. The main results are summarised below:

1) POLARIS could detect bedrock at 3 km depth in the cold ice regions covered by the IceGrav tracks, although not consistently. Internal layers were consistently observed below 2 km depth.

2+3) POLARIS was able to penetrate the major part of the warm ice test sites. At Adelaide Island the penetration limit seems to be around 500 m, whereas along Fimbulisen, the maximum observed penetration depth was 700 m. Internal layers in the warm ice regions were observed down to 400 m depth. The basal return from the 700 m thick ice Jutulstraumen glacier was easily detectable, even with a short pulse at high altitude, but no internal layers could be observed

4) At the EPICA/Kohnen drilling site, differences between HH and VV reflection horizons were clearly observed down to below 2 km depth.

5) A preliminary analysis of the acquired clutter suppression data indicates they can indeed be used for investigating clutter suppression, despite a problem with the large antenna transmit pattern.

Names of authors: Jørgen Dall, Anders Kusk, Steen Savstrup Kristensen, Rene Forsberg, and Ulrik Nielsen

** NAME OF ESA STUDY MANAGER	** ESA BUDGET HEADING
DIV: **DIRECTORATE:**	

Table of contents

1 Introduction

In order to better understand and model the response of the continental ice sheets to climate change, it is desirable to map the thickness and the basal conditions of the entire Antarctica and Greenland ice sheets with a homogeneous quality and a dense sampling. This cannot be done by ground-based survey or by aircraft, whereas a space-based ice sounding radar has the potential.

Until recently, the ITU frequency allocation did not offer any frequency suitable for ice sounding from space, but in June 2003 a 6 MHz radar band was made available in the P-band (435 MHz). In order to clarify if the attenuation at P-band is sufficiently low for an ice sounding radar to penetrate through the continental ice sheets and detect the bedrock, ESA assigned the Technical University of Denmark (DTU) to develop an airborne demonstrator, POLARIS (POLarimetric Airborne Radar Ice Sounder [1]). POLARIS has successfully profiled the bedrock topography under 3 km ice in Greenland, but in Antarctica the ice thickness locally exceeds 4 km, and according to the POLARIS ITT [2], “the Agency considers it necessary to gather real P-band data from the Antarctic ice sheet”.

Another reason to develop POLARIS was to enable development and test of novel surface clutter suppression techniques. A space-based ice sounding radar depends on surface clutter suppression in order to prevent the surface signal from masking the weak basal signal. POLARIS is designed to support coherent, multi-aperture techniques, but suitable test data have not yet been acquired.

Other open issues include detection of internal layers within the ice and the benefit of the polarimetric capability featured by POLARIS.

So far, POLARIS has been flown in Greenland three times:

March 2008:	Functional Test Flight (FTF)
May 2008:	Proof of Concept campaign (PoC) [3]
Oct. 2009:	Additional Test Campaign (ATC) [4]

The primary objective of these campaigns have been instrument test, though the PoC and ATC test sites were selected such that the data also have glaciological interest.

The IceGrav campaigns were part of a DTU airborne geophysics project in cooperation with University of Texas (UT), the Norwegian Polar Institute (NPI), University of Bergen, Instituto Antarctico in Argentina, and the British Antarctic Survey. Funding was provided by the US National Geospatial-Intelligence Agency, DTU, ESA and NASA.

The primary purpose of the IceGrav project is to support global geodesy, by providing gridded data for global gravity field models and geoid determination, and to supplement current satellite gravity missions (GOCE and GRACE). The secondary purpose is to collect magnetic, laser altimetry and ice-penetrating radar data for general geophysics, glaciology and oceanography. The first and second IceGrav campaigns took place in Jan-Feb 2010 and in Oct-Nov 2010, respectively. The third one took place in February 2011, and unlike the first two campaigns, it involved POLARIS.

Due to the constraints imposed by the gravity measurements, not all POLARIS objectives could be met by the gravity flights. ESA contributed to the February 2011 campaign by funding a day dedicated to acquisition of POLARIS data and subsequent processing and analysis of these data. This report addresses both the ESA funded and the gravimetry related acquisitions.

For the IceGrav campaigns, a DC-3T Basler long-range aircraft chartered from Kenn Borek, Air Ltd. (KBA), Canada was used. In between the second and third IceGrav campaigns, UT was using the same aircraft in Antarctica to make geophysical measurements including ice sounding with a 60 MHz ice radar originally developed by DTU. This radar remained onboard and was operated simultaneously with POLARIS in February.

2 Objectives

According to the ESA Statement of Work [5] the main objectives of the campaign are to provide quantitative feedback on:

1) The detection and mapping of deep ice layers as well as the feasibility of observing the bedrock at 4 km depth in cold ice
2) Explore the sensitivity limit (depth) in warm ice
3) Investigate the observability of radar reflection horizons under various conditions (cold/warm ice, regions of dynamical ice)
4) Explore the potential of polarimetry for observing ice anisotropy (i.e. crystal fabric orientation, COF) in flowing ice over ice divides and in dynamical regions
5) Acquisition of multiple phase-centre data in order to develop processing techniques for suppression of across-track surface clutter and enhancing shallow ice layers

Validation of the first two objectives must be ensured by means of independent bedrock topography data, e.g. from the radar operated simultaneously by University of Texas or from previous sounding campaigns. For the validation of the third and fourth objectives, the availability of ice-core data is highly desirable. Finally, the fifth objective would require data acquisition over flat and sloped terrain in combination with accurate information on the ice surface topography.

3 Equipment

3.1 Aircraft

Until this campagin, POLARIS has been flown on a Twin Otter aircraft, but since a long-range aircraft is required in order to maximize the coverage, POLARIS was flown on the KBA DC-3 shown in Figure 1 and Figure 2. In October 2010, POLARIS was installed on the DC3 and certified, and Figure 3 shows the POLARIS rack in the cabin. Two STCs have been approved, one for the two antennas and another one for the electronics in the cabin, see Appendix A.

Figure 1 The four-element POLARIS antenna mounted under the fuselage of the Basler aircraft. The 60 MHz radar antennas, originally developed by DTU, are mounted under the wings.

Figure 2 The eight-element POLARIS antenna mounted under the fuselage of the Basler aircraft.

3.2 POLARIS

Since the POLARIS system was presented in [1], an additional, eight-element antenna has been developed. Both antennas are dual-linear polarized microstrip patch antenna arrays configured as four sub-apertures. The smaller one is a four-element array and each sub-aperture is constituted by one element. The larger array is an eight-element array, and each sub-aperture is constituted by a pair of neighboring elements. On the transmit side, the four sub-apertures are electronically combined to one large aperture, and usually this is also the case on the receive side. However, when acquiring data for

Figure 3 POLARIS rack installed in the cabin of the DC-3T Basler aircraft Air. The blue box to the right (left side of the aircraft) is an inverter, and next to that the EGI.

the development of clutter suppression techniques (the fifth objective) no such aperture combination will be applied.

The larger antenna was used for the dedicated POLARIS flights, adapting its configuration to the objectives in the best possible way. KBA has made a coarse estimate of the range reduction resulting from the parasitic drag on the antenna element, neglecting the induced drag on the antenna and the interference drag from interaction of the antenna with the fuselage. The smaller antenna is estimated to decrease range by about 3 % and the larger by about 8 %. On this background, the long gravimetry flights were flown with the smaller antenna.

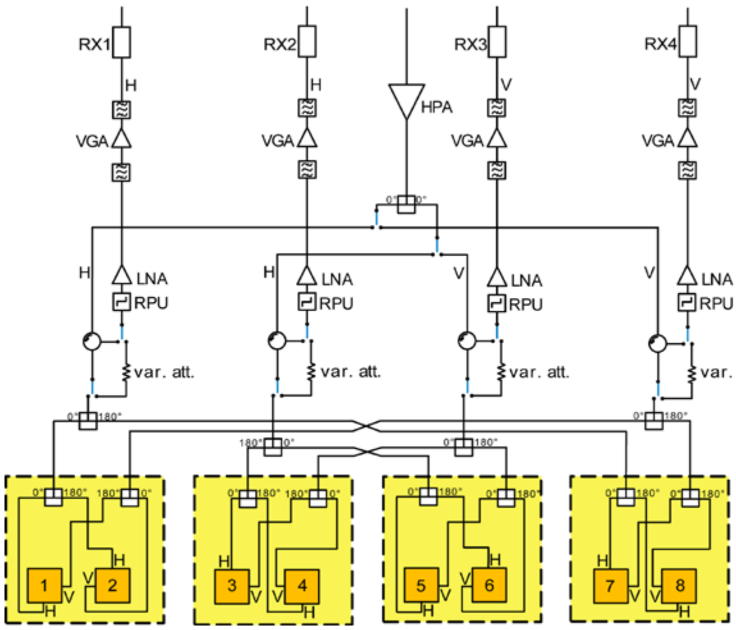

Figure 4 POLARIS with the eight-element antenna configured with one or two sub-apertures.

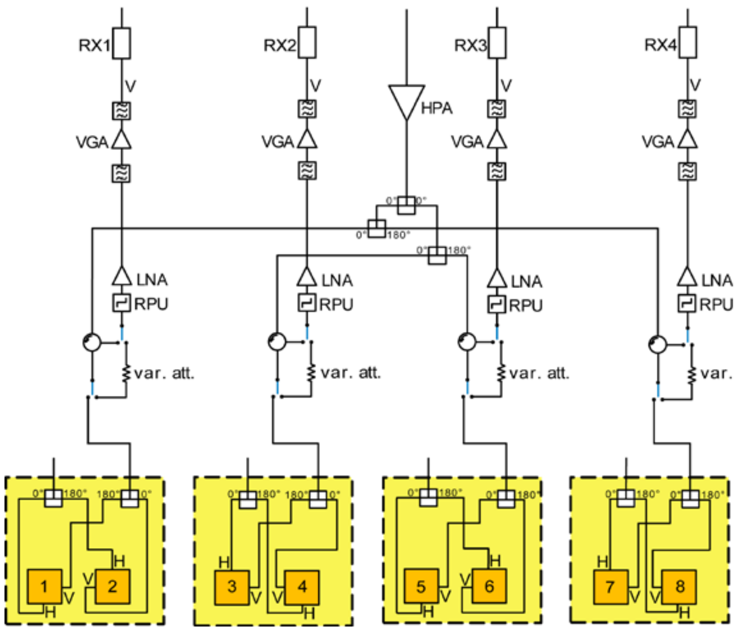

Figure 5 POLARIS with the eight-element antenna configured with four sub-apertures.

POLARIS is a highly reconfigurable system, but switching between the four-aperture configuration and configuration allowing polarimetry cannot be commanded by the operator from the graphical user interface, as the as the electronics in the AFE2 (analog front end 2) must be reconfigured. Figure 4 and Figure 5 show that the polarization switches must be replaced by power splitters, and the four power splitters at the AFE2 output must be bypassed. Unfortunately, this reconfiguration cannot be carried out when airborne, and consequently acquisition of clutter suppression data and polarimetric data calls for two separate flights.

POLARIS was flown together with a laser scanner, which can provide an accurate range to the surface of the ice sheet and a DEM, which might prove valuable when developing and testing the across track surface clutter suppression techniques.

The UT radar was operated simultaneously with POLARIS, but was switched off during the dedicated ESA flights to limit radio frequency interference (RFI).

Finally, the suite of instruments include a magnetometer and, of course, the gravimeter to be used for the primary purpose of the IceGrav campaign.

4 Test sites

Figure 6 shows the planned coverage of the IceGrav 2010/11 campaigns as of December 2010. The red lines were flown in Jan-Feb 2010, while the blue lines on the Antarctic Peninsula were planned for Oct-Nov 2010. Due to bad weather, however, about three flights were left for February 2011. Consequently, the gravity survey area at the Norwegian Troll Station (TRO) was covered with more widely separated tracks, coordinated with the latest acquisitions/plans of the Alfred Wegener Institute.

In order to suppress surface clutter, ice sounding is best carried out flying at a constant, quite low altitude over the ice surface, whereas for gravity measurements the flight altitude over the geoid should ideally be constant for each sortie. The altitude variation, though somewhat reduced by the orientation of the contour lines with respect to the flight track, is one reason why dedicated POLARIS tracks are highly desirable. Another reason is that test sites, suitable for the POLARIS objectives, are not covered by the gravimetry flights shown in Figure 6. The dedicated POLARIS tracks north of TRO were planned in close cooperation with the Norwegian Polar Institute [6].

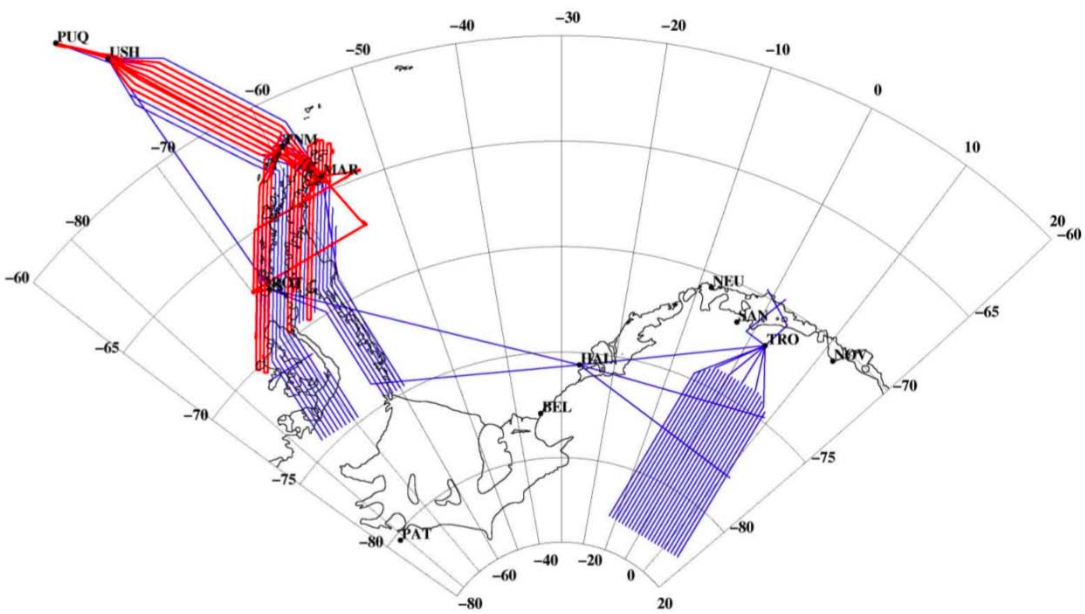

Figure 6 The coverage of the three IceGrav campaigns 2010/11.
The dedicated POLARIS flight lines are not shown.

Table 1 Objectives (rows), test sites (columns), and radar configuration/modes (entries).

		Adelaide Island	South Site	EPICA ice core site	Ice rises	Jutulstraumen ⊥	Jutulstraumen ⊥	Jutulstraumen ‖	Ice shelf
Objective 1 Limit, cold ice			Var. altitude Small ant. Long pulse	Var. altitude Small ant. Long pulse					
Objective 2 Limit, warm ice		Long pulse							Long pulse
Objective 3 Reflecting horizons	cold ice		Bandwidth compromise	Bandwidth compromise					
	warm ice	Bandwidth compromise							
	dynamic ice					Bandwidth compromise			
Objective 4 COF	ice core			One aperture Quad pol.					
	ice divide	One aperture Quad pol.			One aperture Quad pol.				
	dynamic ice					One aperture Quad pol.			
Objective 5 Surface clutter	flat terrain								High altitude Large antenna Four apertures Single pol. High bandwidth
	sloped terrain							High altitude Large antenna Four apertures Single pol. High bandwidth	
	varying roughness						High altitude Large antenna Four apertures Single pol. High bandwidth		

In Table 1, seven test sites are listed and related to the five objectives defined in Section 2. If a test site addresses an objective, one or more radar modes/parameters are specified in the corresponding table entry, cf. Section 5. Two columns are allocated for the Jutulstraumen ⊥ site (track perpendicular to the glacier), as this site addresses two objectives with incompatible radar modes/parameters. Objective 4 and 5 call for polarimetry and four apertures, respectively, and since reconfiguration is impossible when airborne, Jutulstraumen must be flown twice in the direction perpendicular to the ice flow.

To cover all objectives, four flights are required, as indicated by the coloring of the columns. The South Site and the EPICA site are mapped in combination with gravimetry measurements.

Objective 1: According to the BEDMAP Consortium's ice thickness map, the thickest ice within the IceGrav coverage is no more than about 3.3 km, but virtually nothing is known about the southern part, for which no ice sounding profiles exist, cf. Figure 7. Presumably, the deep sounding objective is best addressed in the southern end of the long gravimetry tracks (called South Site in Table 1). The elevation decreases by about 700 m from the northern end of the long tracks to the southern end, and consequently, POLARIS will be flown about 700 m higher over the surface than desired. This impacts the sensitivity, but surface clutter is not expected to be problem, as the objective is to detect the bedrock and the deep ice layers. If a dedicated POLARIS flight were allocated to cover this far away site, too few flight hours would be left to acquire data addressing the other POLARIS objectives.

At the EPICA ice core site (75°0.10' S, 0°4.07' E marked with a red dot within the IceGrav coverage in Figure 7), the ice is 2882 m thick.

Objective 2: According to the simplified model provided by ESA [7], the temperature profiles of cold ice and warm ice can be expressed as

$$\begin{aligned} T_{cold}(z) &= 223.15 + \frac{\exp(16z/12000)}{5} \\ T_{warm}(z) &= 243.15 + \frac{\exp(8z/4000)}{100} \end{aligned} \qquad (1)$$

where b is the depth of the bedrock in meters. For b equal to 4 km and 2.5 km, respectively, these profiles are plotted in Figure 8, and it is seen that warm ice is 20° warmer at the surface and about 10° warmer at the bottom. Such a high surface temperature is typically found at low elevation in a coastal area cf. Figure 9, and a bottom temperature around 0° can be due to geo-thermal heat or ocean water under an ice shelf [6]. Geo-thermal heat is expected in the southeastern corner of the IceGrav coverage, where the Recovery lakes are located, but there the surface temperature does not match that of the warm ice profile, cf. Figure 9. In Table 1, the ice shelf and the Adelaide Island on the west coast of the Antarctic Peninsula are appointed Objective-2 test sites. The upper part of the ice cap on Adelaide Island is expected to consist with the warm temperature profile, whereas basal conditions are unknown.

Objective 3: POLARIS' ability to observe radar reflection horizons under cold and warm conditions is

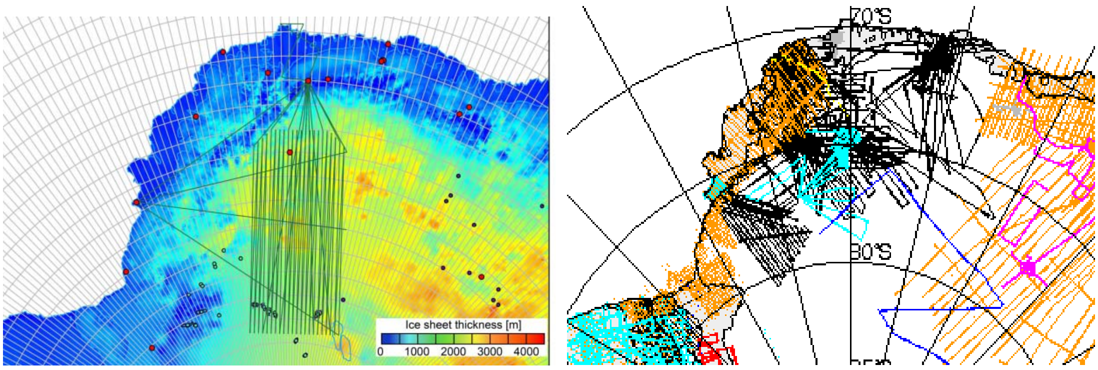

Figure 7 The BEDMAP Consortium's ice thickness map (left) and the ice sounding profiles from which it is generated (right).

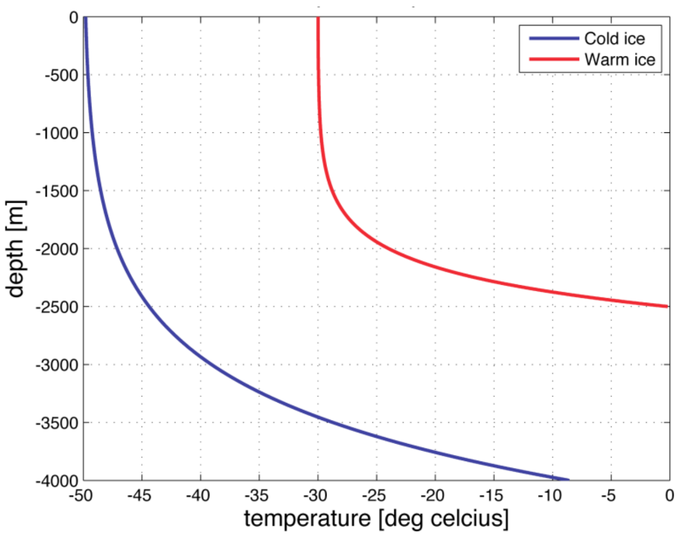

Figure 8 Temperature profiles for cold and warm ice, assuming ice thicknesses of 4 km and 2.5 km, respectively [7].

addressed by the first three test sites in Table 1. A track crossing the Jutulstraumen Glacier addresses the dynamic conditions.

Objective 4: Ice divides are found on Adelaide Island and on the ice rises [6], where polarimetric data were planned to be acquired in order to explore the potential of observing ice anisotropy (i.e. COF). COFs under dynamical conditions were planned to be studied at the Jutulstraumen Glacier. Polarimetric data were acquired at the EPICA site, where it is possible to compare the POLARIS data with the crystal orientations determined from the ice core.

Objective 5: Data for development and test of surface clutter suppression techniques were acquired over the flat ice shelf and when flying along the Jutulstraumen Glacier, taking advantage of the cross-track slope. When crossing the glacier, a varying surface roughness will be observed, such that the efficiency of the techniques can be better tested.

The test sites are illustrated in Appendix B, and the coordinates are listed in Appendix C.

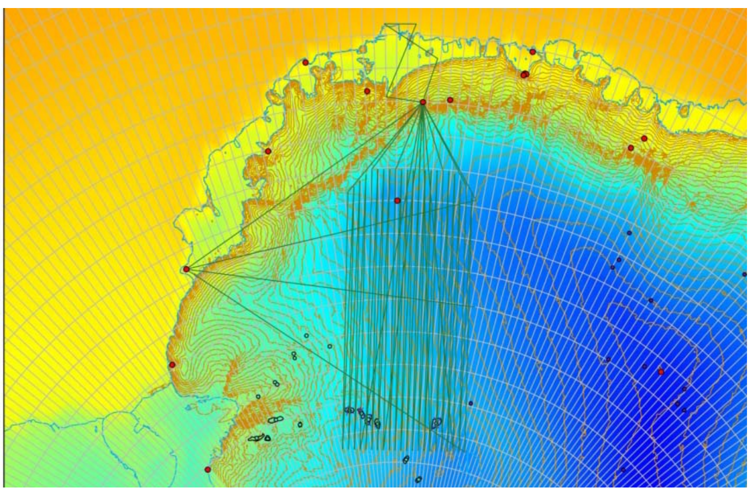

Figure 9 Average surface temperature.

5 POLARIS modes and parameters

Table 1 lists key POLARIS modes and parameters for each combination of objectives and test sites. Only the crucial modes/parameters are filled in, thereby reducing the risk of conflicts at test sites addressing multiple objectives.

As argued in Section 4, a constant absolute flight altitude is dictated by the gravimetry measurements in the southern part of the IceGrav coverage, where the POLARIS's ability to detect the bedrock under thick, cold ice and to map deep internal ice layers is to be tested. There, the smaller antenna must also be used due to the drag, cf. Section 3.2. In order to obtain the highest sensitivity, a long pulse is needed, but this may impede mapping of the entire ice profile unless a Shallow / Deep Sounding (SDS) mode, or an extraordinary high flight altitude is used.

Also when testing the penetrating through warm ice, a long pulse is required, but since the warm ice is thinner, an extremely long pulse is anyway not applicable (unless the flight altitude is extraordinary high, which in turn has an adverse effect on the sensitivity).

In case anisotropic reflection from abrupt COF changes or birefringent propagation due to a dominating crystal orientation is to be addressed, quad polarized data are required. For POLARIS, polarimetry is not supported in the 4-aperture configuration, cf. Section 3.2, so either dual-aperture or single-aperture data must be acquired. The former doubles the data rate, but it offers some surface clutter suppression potential in absence of surface slope and aircraft yaw. The ability to detect COFs is preferred to the surface clutter capability, i.e. single-aperture mode.

At a given depth, the signal-to-clutter ratio decreases with the flight altitude, because the off-nadir angle to the clutter source decreases with the altitude. Consequently, it is easier to test the benefit of applying surface clutter suppression when flying high. The larger antenna is highly preferable because the efficiency of the clutter suppression algorithms increases with the separation of the sub-apertures. The efficiency also increases with the number of sub-apertures, three being the theoretical minimum for the advanced techniques not calling for a priory knowledge of the surface topography. Unfortunately, in the four-aperture configuration, polarimetry is not supported. The need for a high bandwidth is due the fact that the angular range of the surface clutter source increases with decreasing bandwidth, and it is easier to null out a well-defined direction than a wide range of directions.

Simultaneous mapping of the ice surface and the bedrock calls for a high dynamic range and hence application of the SDS mode. Since, the ice thickness is supposed to be provided by the UT radar, POLARIS will be operated in quad pol mode during the gravimetry flights, although it reduces the effective PRF by a factor of two and hence reduces the SNR by 3 dB, corresponding to, say, two hundred meters of penetration.

In order to resolve internal layers, a high bandwidth is preferable, but the internal layers constitute a distributed target for which theory suggests that the signal-to-noise ratio decreases with increasing bandwidth. With the POLARIS geometry, the bedrock can to some extend be considered a point target, for which an increased (noise) bandwidth is compensated by a larger pulse compression gain. The compromise from the previous campaigns in Greenland will be adopted, i.e. an 85 MHz bandwidth in the shallow window and a 30 MHz bandwidth in the deep window.

The adverse effect of surface clutter is reduced with a low flight altitude. On the other hand, this shortens the pulse that can be used for shallow mapping, which in turn might imply a smaller shallow window and hence a shorter pulse for the deep window. Based on model-based SNR estimations a 2000 ft flight altitude is suggested as a compromise, where the flight altitude is not already specified in Table 1.

Table 2 specifies the modes/parameters in terms of the POLARIS operational modes that are defined in the PoC and ATC Campaign Data Inventory reports [3] [4]. Here the colouring of the row indicates the four flights. Note that for all gravimetry flights, the same mode/parameter set is used such that a unified data set is generated.

Table 2 POLARIS Setups designed for the IceGrav campaign.

Site Objective	**Altitude [ft]**	**Antenna**	**Antenna apertures**	**Mode**	**Band width [MHz]**	**Pulse length [μs]**	**Tukey**	**VGA gain [dB]**	**Delay [μs]**	**Window size [samples]**	**Deep window [m]**	**Shallow window [m]**
Adelaide Island 2. Limit, warm ice	2000 r	small[1]	1	Quad	30	2	0.10	5	min	3 K	-120/803	
South Site 1. Limit cold ice, 3. Reflecting horizons	Varying (> 7000 > 2000)	small[1]	1	Quad_SDS	6/85	10/2	0.10/0.05	30/5	15/min	14 K/6 K	85/4095 932/4942	-1620/996 -120/1844
EPICA drilling site 1. Limit cold ice, 3. Reflecting horizons 4. COF	Varying (> 2000)	small[1]	1	Quad_SDS	6/85	10/2	0.10/0.05	30/5	15/min	14 K/6 K	932/4942	-120/1844
Jutulstraumen ⊥ 3. Reflecting horizons 4. COF	3500 a (>3500)	large	2	Quad_CS2	30	2	0.10	0	min	7 K	-570/1937	
Ice rises 4. COF	3500 a (> 2188 > 3500)	large	1	Quad	30	2	0.10	0	min	4 K	-186/1110 -570/896	
Ice shelf 2. Limit, warm ice	2000 r	large	1	Quad	30	2	0.10	0	min	4 K	-120/1150	
Ice shelf 5. Surface clutter	11500 a (> 10188)	large	4	VV_SDS_CS4	30/85	15/2	0.05/0.10	16/16	19/19	10 K/7 K	-255/2054	-255/2115
Jutulstraumen ⊥ 5. Surface clutter	11500 a (> 10188)	large	4	VV_SDS_CS4	30/85	15/2	0.05/0.10	16/16	19/19	10 K/7 K	-255/2054	-255/2115
Jutulstraumen || 5. Surface clutter	11500 a (> 10188)	large	4	VV_SDS_CS4	30/85	15/2	0.05/0.10	16/16	19/19	10 K/7 K	-255/2054	-255/2115
Jutulstraumen CL 5. Surface clutter	11500 a (> 10188)	large	4	VV_SDS_CS4	6/85	15/2	0.15/0.10	16/16	19/19	14 K/10 K	-255/3442	-255/3155

r = relative to ice surface. a = absolute, i.e. relative to geoid. > = greater than relative to ice surface.

6 Measurements

The campaign in February 2011 included the following instruments:

- POLARIS, the P-band Polarimetric Airborne Radar Ice Sounder developed for ESA by DTU[1]
- HiCARS, a 60 MHz, single-pol radar ice sounder operated by UT
- a SigmaSpace scanning lidar (green) and a Riegl infrared vertical-beam laser (UT)
- numerous GPS units on several aircraft antennas, inertial navigation system (INS)
- Geometrics 823 Cesium magnetometers
- a LaCoste and Romberg gravimeter S-99 (UiB)
- a LaCoste and Romberg land gravimeter G-466 for base ties.

The GPS data and the INS data are required to processes the POLARIS data, while the 60 MHz ice sounder and the laser scanner provided auxiliary data, which can be used in combination with the POLARIS data.

The larger antenna was used for two dedicated POLARIS flights on February 19, while the smaller antenna was used for all other flights in order to maximize range, which is crucial to the gravity measurements. The smaller antenna is estimated to decrease range by about 3%, the larger by about 8%.

Table 3 list the activities involving POLARIS carried out during the IceGrav campaign. Table 4 lists the acquired POLARIS data. Due to a strike in Punta Arenas, Chile, POLARIS was shipped to Troll via Cape Town. February 3, the Basler should have arrived at Troll, but due to bad weather at Halley, it did not arrive until February 11. As a result, the gravity measurements could not await the POLARIS installation, which was instead interleaved with the first two gravity flights. Consequently, no POLARIS data were acquired from legs EH, EG, EF, and EE.

Throughout the campaign, the storage disks were a major problem, as described in Section 7.1. The “Data Gaps” column in Table 4 lists only the tracks impaired by large data gaps. Minor data gaps are typically a fraction of a range line.

As indicated in Table 4, only VV polarized data are available from the flight with the large antenna over the ice rises, as described in Section 7.4. The Jutulstraumen multi-aperture data are affected by a degraded transmit pattern, see Section 7.5

From February 23, 24 and 25 only VV polarized data are available, due to a connector failure described in Section 7.6. This also affects the February 26 data (Adelaide Island), where the H-pol antenna aperture is constituted by just a single element.

Photographic material was collected during the campaign in order to document the work performed, the instrumentation used and the locations. As an example, Figure 28 shows the Jutulstraumen Glacier seen from an altitude of about 11000 ft.

The long IceGrav gravimetry tracks (South Site) have been processed to level 0c, whereas the remaining data have been processed to level 1c. The processed flight lines are shown on Figure 10-Figure 13, along with waypoint names (see Appendix C). Aircraft turns are often, but not always, used for internal calibration purposes, and typically no data are available here. For the two flights with the large antenna (costal flight and multi-aperture flight), and for the Adelaide Island flight, there were no serious issues with the harddisk storage. For the gravimetry tracks, some parts of the flown lines are missing, and parts of the processed data have been gap-filled with zeros, as indicated on Figure 12.

Table 3 Timeline of campaign activities.

Date	Activity	Coverage
28.01.2011	POLARIS: Cape Town – Novo	
03.02.2011	POLARIS: Novo – Troll	
11.02.2011 12.02.2011	POLARIS install at Troll Gravimetry; no POLARIS data	South Site EH,EG,EF,EE
14.02.2011 15.02.2011 17.02.2011	South Site Gravimetry POLARIS	South Site EA, EB,EC,ED,EI, EJ
18.02.2011	South Site Gravimetry & POLARIS	South Site EPICA EK, EL
19.02.2011	Installation of large antenna Ice rises / Ice shelf flight Multi-aperture flight Reinstallation of small antenna	Ice Rise Ice Shelf Jutulstraumen ⊥ Jutulstraumen ⊥
20.02.2011 22.02.2011 23.02.2011	Gravimetry & POLARIS	South Site EN,EM,EP,EQ,ER,ES
24.02.2011	Gravimetry & POLARIS	South Site Troll – Halley
25.02.2011	Gravimetry & POLARIS	Halley – Rothera
26.02.2011	POLARIS	Adelaide Island
27.02.2011	POLARIS uninstall at Rothera	
28.02.2011	Rothera – Ushuaia	

Table 4 POLARIS data acquired during the IceGrav campaign.

Date	Leg	Site name in CIP	Mode	# ant elem.	Data gaps	Comment
11.02.2011	EH1-EH2	South Site				No data
11.02.2011	EG2-EG1	South Site				No data
12.02.2011	EF1-EF2	South Site				No data
12.02.2011	EE2-EE1	South Site				No data
14.02.2011	EC1-EC2	South Site	Quad_SDS	4	Large	
14.02.2011	ED2-ED1	South Site	Quad_SDS	4		
15.02.2011	EB1-EB2	South Site	Quad_SDS	4		
15.02.2011	EA2-EA1	South Site	Quad_SDS	4	Large	
17.02.2011	EI1-EI2	South Site	VV_SDS	4	Large	
17.02.2011	EJ2-EJ1	South Site	Quad_SDS	4		
18.02.2011	EK1-EK2	South Site	Quad_SDS	4		
18.02.2011	EL2-EL1	South Site	Quad_SDS	4		
19.02.2011	KM1a-KM2a	Ice Rises	VV	8		
19.02.2011	KM2a-KM3a	Ice Rises	VV	8		
19.02.2011	KM3a-KM4	Ice Rises	VV	8		
19.02.2011	KM4-KM5	Ice Rises	VV	8		
19.02.2011	KM5-KM6	Ice Rises	VV	8		
19.02.2011	KM6-KM7	Ice Rises	VV	8		
19.02.2011	KM7-KM8	Ice Rises	VV	8		
19.02.2011	KM9a-KM10	Ice Rises	VV_CS2	8		
19.02.2011	JD1-JD2	Jutulstraumen||	VV_CS4	8		Two pulses
19.02.2011	JD4-JD5	JutulstraumenCL	VV_CS4	8		Two pulses
19.02.2011	JD3-KM10	Jutulstraumen⊥	VV_CS4	8		Two pulses
20.02.2011	EN1-EN2	South Site	Quad_SDS	4		No cal. data
20.02.2011	EM2-EM1	South Site	Quad_SDS	4	Large	No cal. data
22.02.2011	EP1-EP2	South Site	Quad_SDS	4		
22.02.2011	EQ2-EQ1	South Site	Quad_SDS	4		
23.02.2011	ER1-ER2	South Site	VV_SDS	4		
23.02.2011	ES2-ES1	South Site	VV_SDS	4		
24.02.2011	Troll-Halley	South Site	VV_SDS	4		
25.02.2011	Halley-Rothera	NA	VV	4	Large	No nav. data
26.02.2011	HC1-HC2	Adelaide	Quad_SDS	V: 4, H: 1		

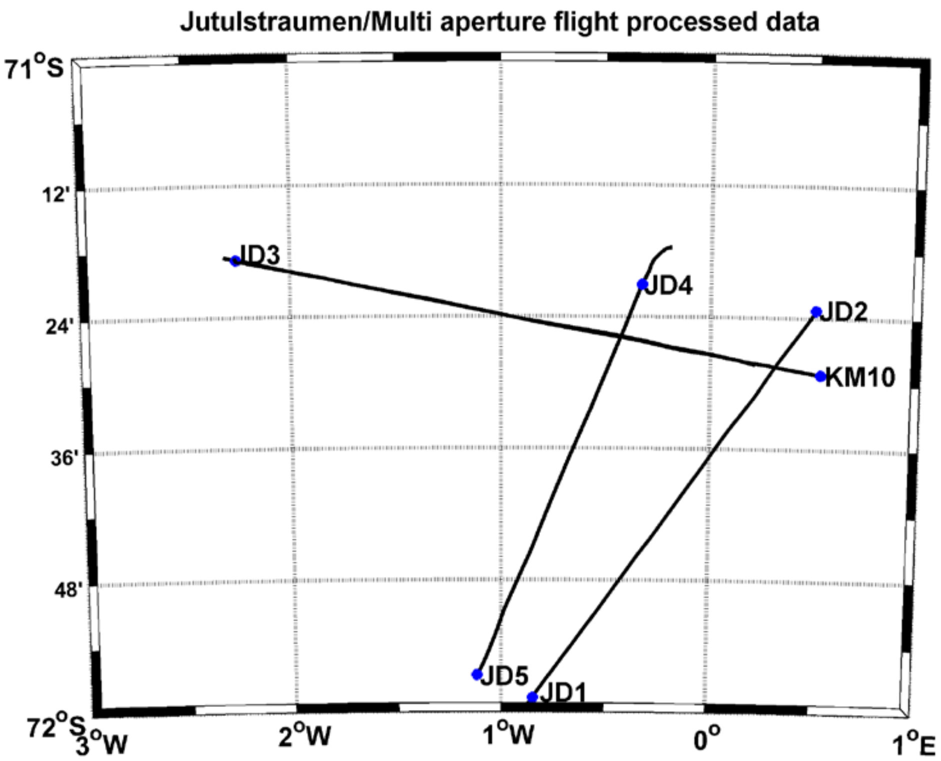

Figure 10 Processed lines (level 1c) for the Multi-aperture flight (large antenna) on Feb 19 level 1c. Four VV subapertures were collected. The antenna was erroneously configured with a transmit-null, see 7.5.

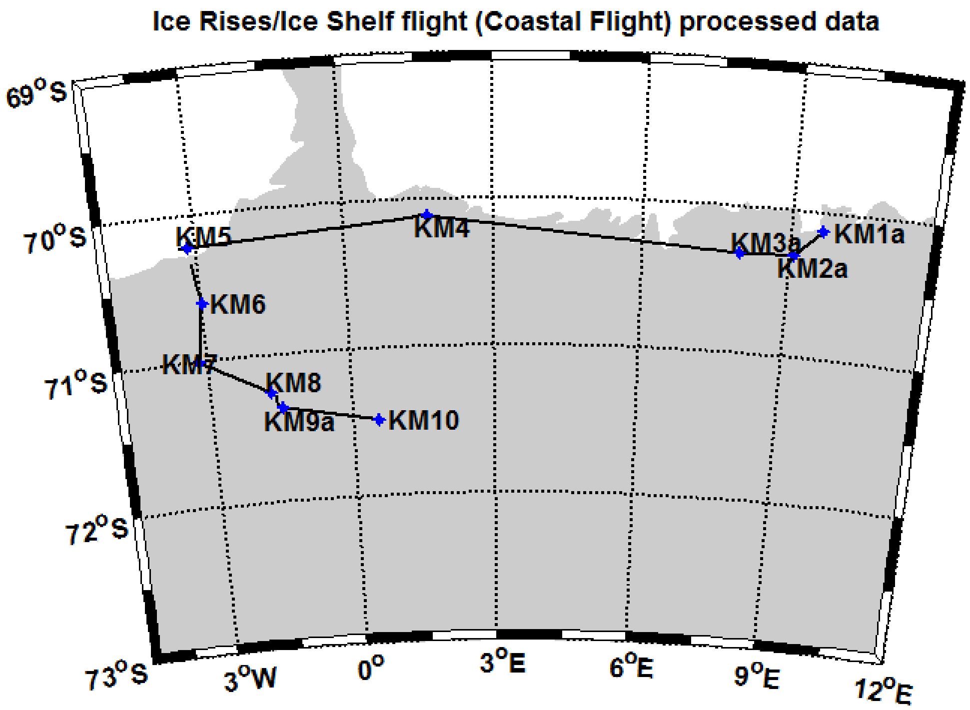

Figure 11 Processed lines (level 1c) for the coastal flight (large antenna) on Feb 19. Only VV-polarization is available due to the problems described in Section 7.4.

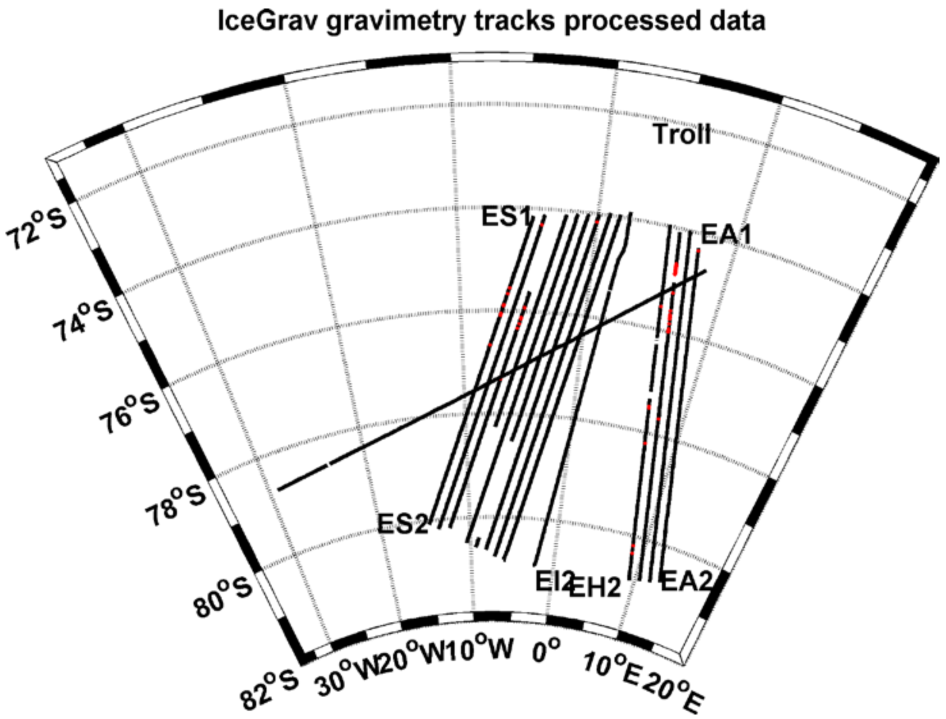

Figure 12 Processed lines (level 0c) for the IceGrav gravimetry tracks during Feb 14-24. Red dots indicate missing data where zeros have been inserted due to storage disk failure. For the two westernmost lines (ER and ES) and the crossing line, only VV-polarization exists (see Section 7.6).

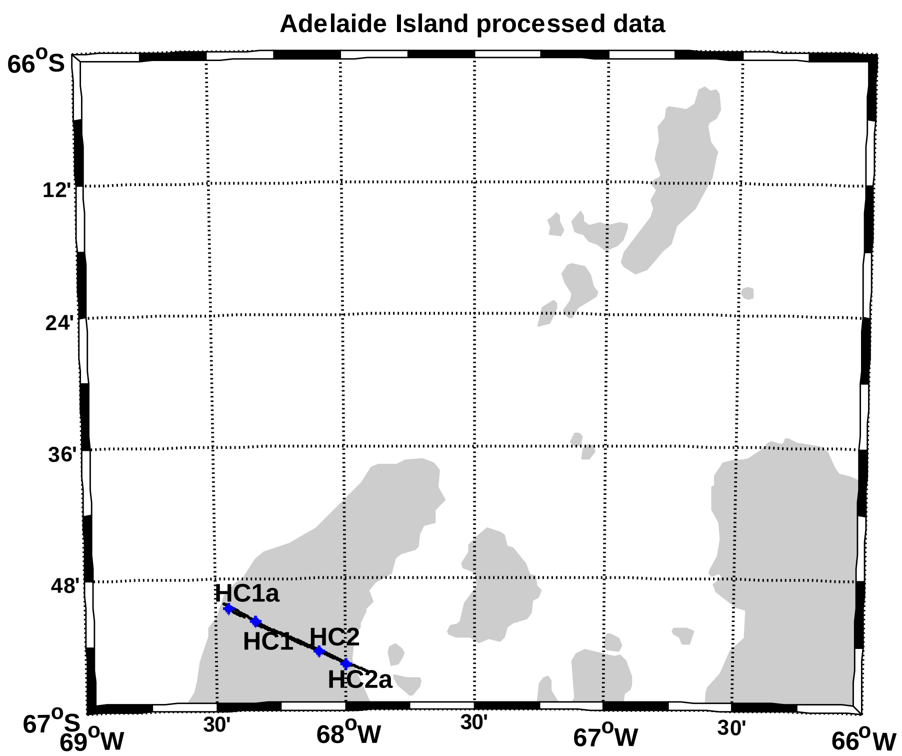

Figure 13 Processed lines (level 0c and 1c) for the Adelaide Island flight on Feb 26. Only VV is available due to the problems described in Section 7.6.

7 Data Quality Assessment

A number of issues affecting the quality of the acquired data have been identified and are treated in the following sections.

7.1 Storage problems

Throughout the campaign, the storage disks were a major problem, resulting in many small and large data drop outs. Disk failures occurred at flight altitudes significantly lower than those successfully used in Greenland during preceding POLARIS campaigns, and the most likely explanation is that new (larger) disks were used, though the aircraft environment and weather differences, might have an impact, too. This was mainly an issue on the long IceGrav gravimetry tracks, as shown on Figure 13, although a few isolated lines of missing data were also encountered on the coastal flight. In potential future campaigns, the storage system should be upgraded to use disks, which are expected to perform better at high altitude and in presence of aircraft vibrations, e.g. solid state disks.

7.2 Time stamping of radar data

On the first flights a datation problem resulted from a bad connection. After a thorough analysis, a work around has been implemented, and an accuracy of approximately 1 ms has been verified. The Digital Front End (DFE) did not receive the Pulse Per Second (PPS) signal from the Embedded GPS/INS (EGI), whereas it did receive the second of day (SOD) information from the EGI throughout the campaign. When the PPS is received, the time tag counter is sampled, and when the SOD is received, both are recorded. In the absence of the PPS signal, the PPS time tag has been estimated using the time tags from other data. This procedure has been verified by applying it to flights where the DFE did receive the PPS signal.

7.3 Radio Frequency Interference

Although RFI had barely been seen in the real-time processed imagery, the HiCARS radar was switched off shortly before passing EPICA on the gravimetry track taken on February 18, and switched on again shortly after. Processed level 0c data covering the passage of EPICA are shown on Figure 14. Clearly, HiCARS generates RFI in the VV and VH channels (vertical receive polarization), which disappears when HiCARS is turned off. The RFI in the HH channel does not seem to be related to whether HiCARS is on or off, and may be originating from the aircraft instrumentation or some of the other instruments in the aircraft - it has not been seen when flying POLARIS on the Twin Otter. Figure 15 is a plot of range-integrated power as HiCARS is turned off. The integration was carried out only on the trailing samples (i.e. the noise floor) of the radargram in which no echo signal is present. Clearly the H-pol RFI is unaffected by turning off HiCARS, whereas the V-pol RFI disappears completely. The HH RFI affects only 5% of the lines (with the PRF and presum factor used here), and it is possible to reduce this RFI by interpolating lines with RFI from the surrounding echo lines. During HiCARS operation, the VV RFI affects 33 % of the lines (with the PRF and presum factor used here) and is not easy to remove, as the affected lines are adjacent. The HiCARS radar was switched off when most of the ESA-funded data were acquired, i.e. during the Ice Rises flight and the Jutulstraumen multi-aperture flight, and the VV data available there are thus not affected by RFI.

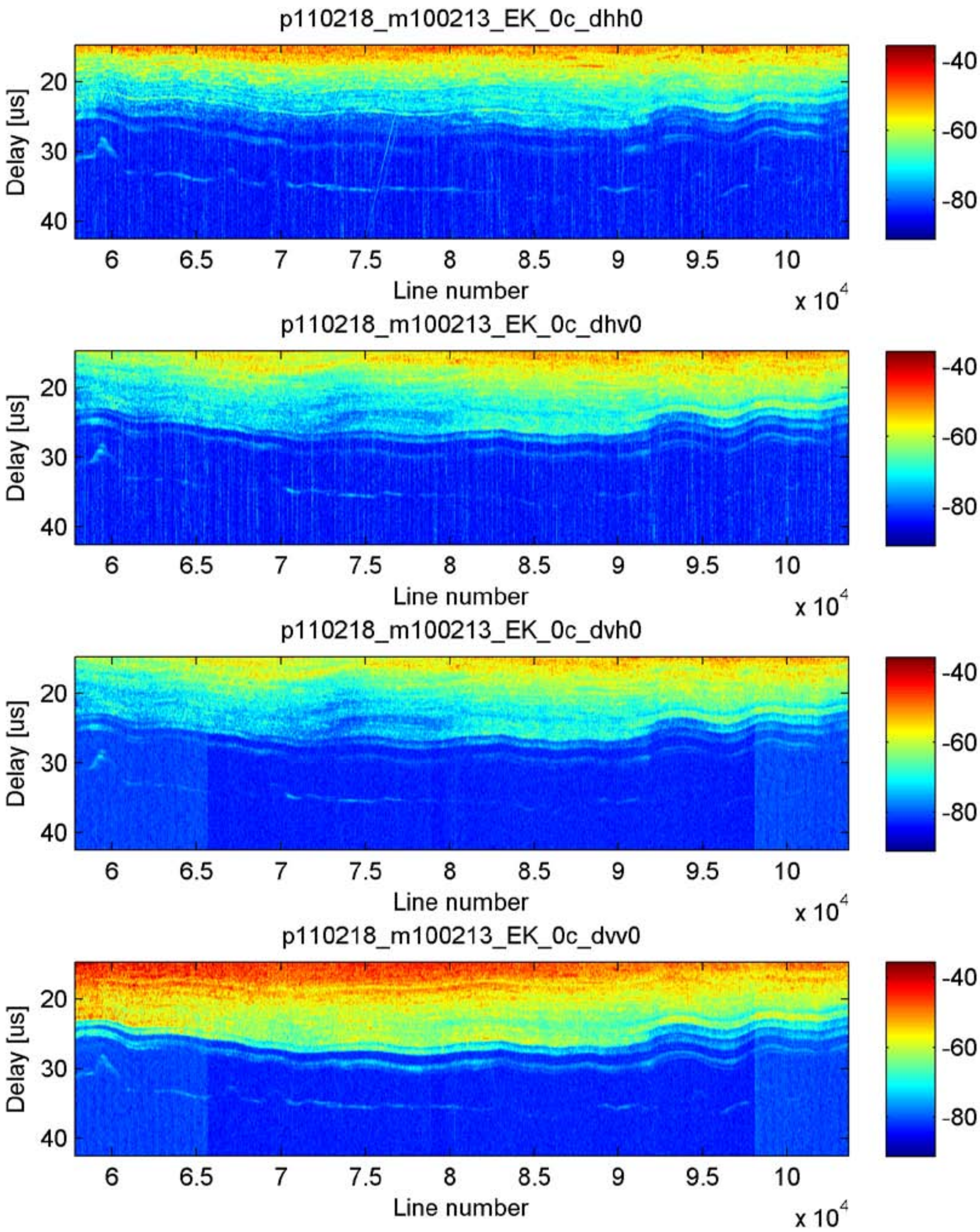

Figure 14 Deep channel echoes during passage of EPICA displaying RFI characteristics with HiCARS on (beginning and end of image) and off (middle of image).

.

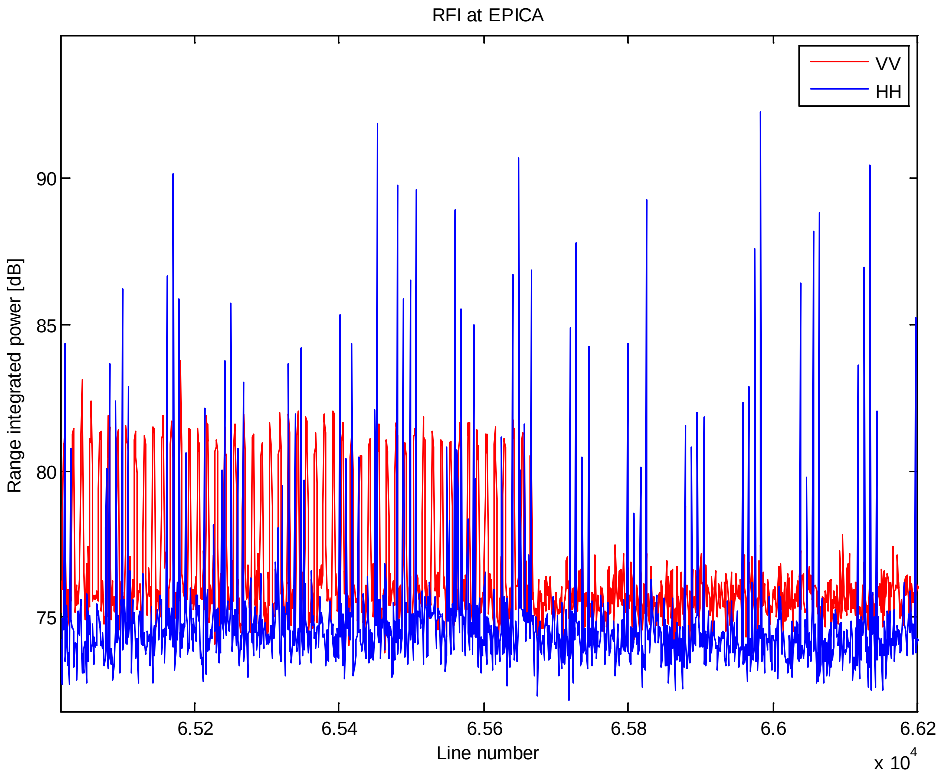

Figure 15 Range-integrated power during HiCARS turn-off.

A simple algorithm to reduce the H-pol RFI in the deep channel was developed. For each block of 1024 echo lines, the noise floor is calculated by taking the median of the mean power in the trailing part of the lines where no echo signal is present. Lines with an integrated power at some threshold (3dB was found to work well) above this noise level are flagged as RFI and replaced by an average of the two surrounding lines. Lines surrounded by one or more RFI-flagged lines, or surrounded by one or more zero-filled lines are not interpolated. This algorithm was applied to the HH and HV deep channel data of the gravimetry tracks. Both the original and the corrected data are delivered. The VV and VH RFI has not been reduced. An example of applying the HH deep channel RFI removal is shown in Figure 16.

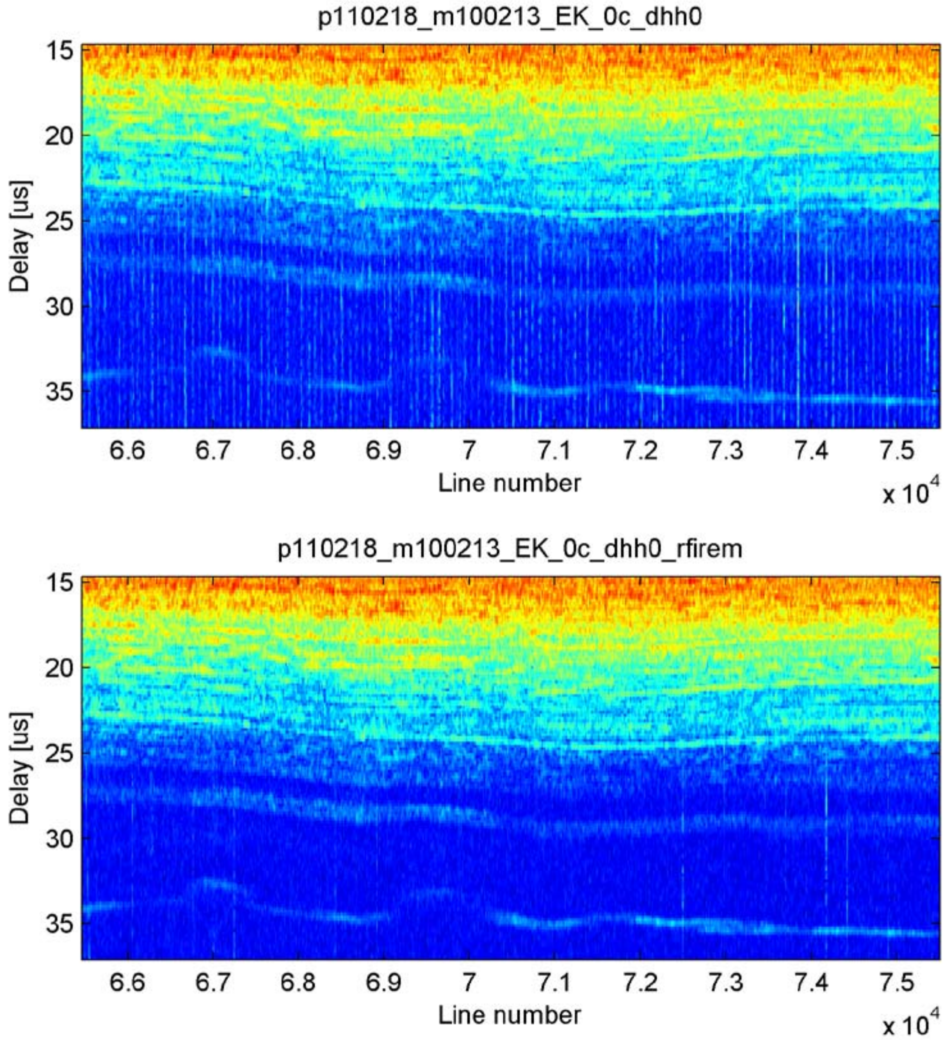

Figure 16 Effect of RFI removal at H-pol in deep channel, near EPICA.

7.4 Large antenna polarimetric configuration error

As indicated in Table 4, only VV polarized data are available from the flight with the large antenna over the ice rises. Actually, quad pol data were acquired as planned, but subsequently it turned out that two of the eight cables connecting the antenna to the electronics should have been interchanged. Without this interchange, the antenna pattern at H-polarization had a null in the nadir direction, as the signals from sub-aperture A and B got out of phase due to the fact that the large antenna was symmetric about its center *line*, whereas the small antenna is symmetric about its center *point*. The internal feed network has now been modified such as to compensate for the line symmetry and has been tested in Greenland in April 2011. The erroneous and the correct configuration are shown on Figure 17.

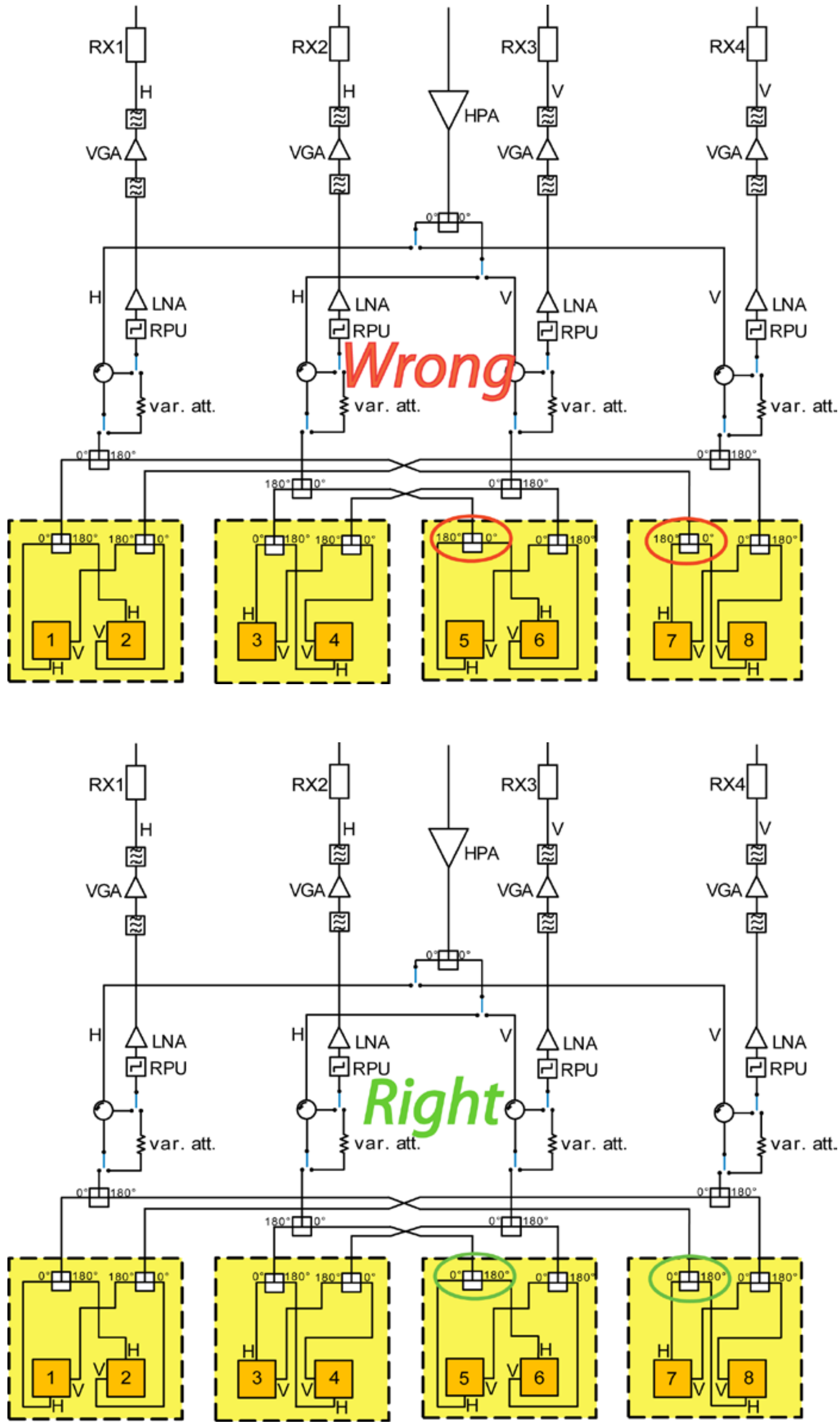

Figure 17 Quad-pol configuration of POLARIS using the large antenna. Top: The erroneous configuration used during the ice rises/coastal flight. The two sub-apertures A and B are 180º out of phase on transmit, causing a nadir null, and although each aperture was received in individual analog channels, these were combined in the digital front end before storage, causing a nadir null on receive also. Bottom: The configuration that should have been used.

7.5 Large antenna multi-aperture configuration error

The multi-aperture data were erroneously acquired with the polarization switches replaced by ordinary power dividers, not the correct power dividers shifting one output by 180°, as illustrated in Figure 18. Consequently, the resulting transmit antenna pattern attenuates the nadir signals and enhances the off-

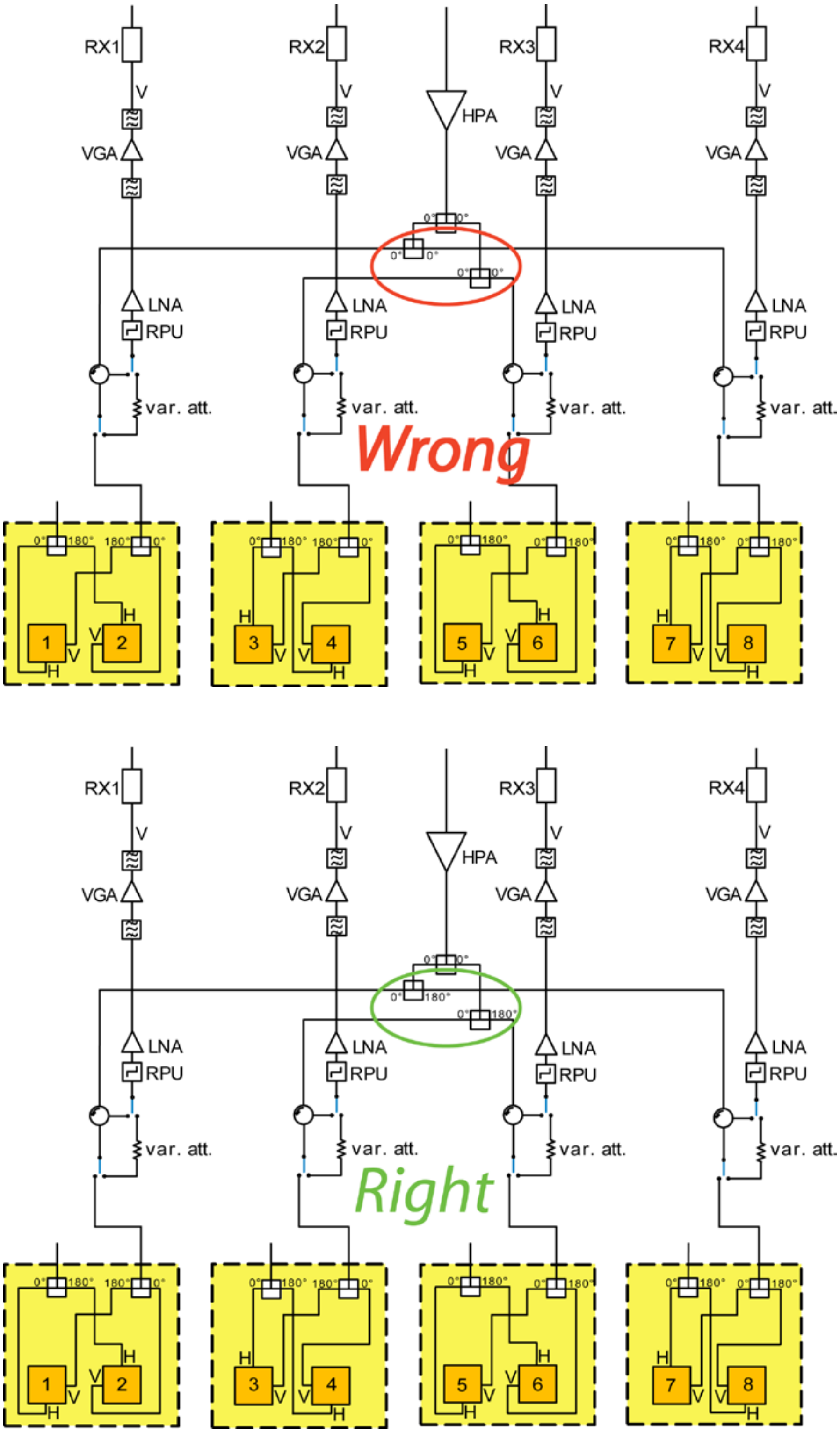

Figure 18 Multi-aperture configuration of POLARIS using the large antenna. Top: The configuration erroneously used during the Jutulstraumen/Multi-aperture flight. Bottom: The correct configuration that should have been used.

nadir signals. The sub-apertures were received individually and could thus be phase corrected during the processing, preserving the proper receive antenna pattern. Initial investigations indicate that the data are usable for clutter suppression studies, see 9.5.1.

7.6 Small antenna connector failure

From February 23, 24 and 25 only VV polarized data are available. February 23, immediately before take-off, it was discovered that the H-connector on element 3 of the small antenna was broken, and the system had to be operated in VV mode that day. No problem had been seen the day before. The next two days, two different workarounds were attempted, but none of them were successful.

February 26, the ice cap of Adelaide Island was passed twice, the first time in VV mode (in order to maximize the sensitivity), the second time in quad pol mode, but with a H-pol antenna aperture constituted by just a single element.

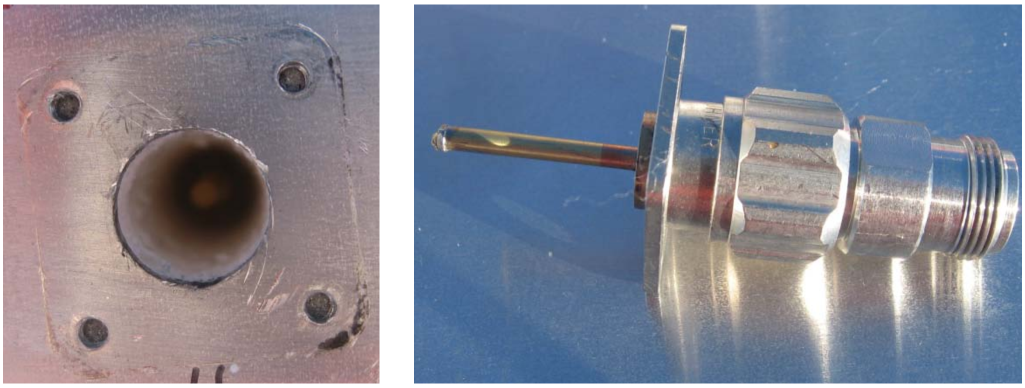

Figure 19 Small antenna connector failure. Left: The hole left in antenna element 3 H-pol. Right: The broken off connector.

8 Data processing

8.1 Processing Algorithms

The POLARIS processing chain currently operates with four levels of data

<u>Raw Data</u>

> Raw sounding data are stored online on a storage PC, in a single stream interleaved with a.o. calibration data, status data and time synchronization information. Thus the data from each flight consist of a number of large consecutive files, each file containing all radar data from a given time period. Typically, one file contains several maps. Navigation are stored in a single file for the entire flight, on a dedicated PC, and radar setups/parameters are stored on the control laptop.

<u>Level 0a</u>

> Level 0a processing extracts the individual maps in a raw data file into separate files. Two files for each channel acquired are always output, a binary file containing the echo data in 32-bit floating point format, and a time stamp file containing the UTC timestamp of each echo. As described in Section 7.2, there were on some initial flights problems with the radar not receiving the Pulse Per Second (PPS) signal from the Embedded GPS/INS (EGI). Fortunately, this can be corrected using other data, as the Seconds-of-day information was still received

and time stamped by the radar. This correction is carried out as part of level 0a processing. Also, as described in Section 7.1, there was an issue with the hard disks used in the storage PC failing, causing a loss of data. The level 0a processor detects missing data and inserts zeros in the affected lines in the echo data file, and for any file with missing data outputs an additional file with the positions of the inserted zeros.

Level 0c

Level 0c starts processing consists of scene splitting, equalization, internal calibration corrections, saturation detection and range pulse compression. Also navigation data are resampled to the echo times.

Each map may be split into several scenes, depending on how the data were acquired. For example on the ice rises flight and the clutter suppression flights (Figure 10 and Figure 11), only a few long, uninterrupted maps were acquired, and were split into several scenes in the level 0c processing, based on waypoints.

For each flight, a number of reference calibrations are carried out, using a long (30us) high bandwidth (100MHz) pulse, allowing an estimate of the transfer function of the system. Also prior to and after each map, calibrations are carried out using the same radar parameters (pulse length, bandwidth, gain) as in the sounding. The calibration data are equalized using the reference calibration transfer function, and are then pulse compressed. From the resulting impulse response, the gain, delay and phase differences between the different channels are estimated and used to correct the sounding data during the pulse compression. In case of missing data lines in the level 0a data, zero-filled lines are output.

An issue which had to be addressed for the long IceGrav tracks flown at varying altitude above the ice surface is that of saturation of the A/D-converters in the digital front end. In the deep channel, where a high receiver gain is used, the surface echo tends to saturate the A/D-converters, which can seriously impact the sidelobe levels after pulse compression if not suppressed. Flying at constant altitude above the ice, the trailing edge of the surface echo can be calculated from the sounding parameters, and the receive window can be set to start after the trailing edge of the surface echo. With a varying altitude above the ice, the saturated parts of the echo can be estimated if the altitude over the ice is known from laser altimeter data or from the shallow channel, but this will also discard data where there may be no saturation, e.g. where flying at a high altitude above the ice. Instead, a statistical method was used: For a block of 1024 lines, a 10-bin amplitude histogram of each range bin is calculated, with the 10 histogram bins spaced evenly over the full ADC output range multiplied by the pre-sum factor (the pre-summing is carried out online prior to data storage). Thus a 10-bin amplitude histogram is calculated for each range bin. Range bins where the largest histogram bin contains more than the average in the other histogram bins are zeroed prior to and after the pulse compression, and a file with the position of the first valid sample in each line is output.

Level 1c

Level 1c processing is an along-track focusing using a time-domain back-projection algorithm. During the back-projection, the data are also geocoded to a track following the actual track, but with constant along-track spacing. In the range direction a constant spatial sampling in a WGS-84 ellipsoidal height grid is used, enabling the elevation of e.g. bedrock to be seen directly from the level 1c radargrams. Knowledge of the surface position is required to perform this focusing, and since laser altimeter data collected by Univeristy of Texas were not available as of November 2011, the surface has been tracked using the POLARIS shallow channel data. VV-polarisation was used, as this contains the smallest amount of RFI. Due to time constraints, and per agreement with ESA, level 1c processing has not yet been carried out for the long gravimetry tracks.

9 Data Analysis

In this chapter, examples of the processed data are presented and used to assess the fulfillment of the objectives for the campaign as stated in [5], and listed here in Section 2 for reference.

9.1 Detection and mapping of deep ice layers and bedrock in cold ice

The capability of POLARIS observe internal layers and bedrock in the Antarctic cold ice has been examined using the IceGrav gravimetry tracks flown with the small antenna south of Troll, see also Figure 12. These were flown in shallow/deep quad-pol mode (Quad_SDS), with an 85 MHz, 2 µs pulse in the shallow channel, and a 6 MHz, 10 µs pulse in the deep channel. Example data are shown on Figure 20, Figure 21, and Figure 22.

In the shallow channel, internal layering is consistently observed down to around 1.5 km depth, whereas in the deep channel, layering is consistently observed down to below 2 km depth. Also in the deep channel, bedrock echoes were detectable down to about 3 km, but not consistently, and in large parts of the flown lines, bedrock was not detectable, at least by an initial visual inspection. The University of Texas 60 MHz radar also had gaps in bedrock observability, as indicated by Figure 23. A comparison has not yet been made, as software for automatically detecting/tracking the bedrock from POLARIS data is still in development. From a preliminary inspection, no bedrock was observed below 3 km. The impact of RFI from HiCARS can be seen in Figure 20, by noting the absence of RFI around EPICA from line 70000-100000. It is conceivable that the sensitivity is deteriorated by the RFI, and future campaigns involving several ice sounders should address this issue.

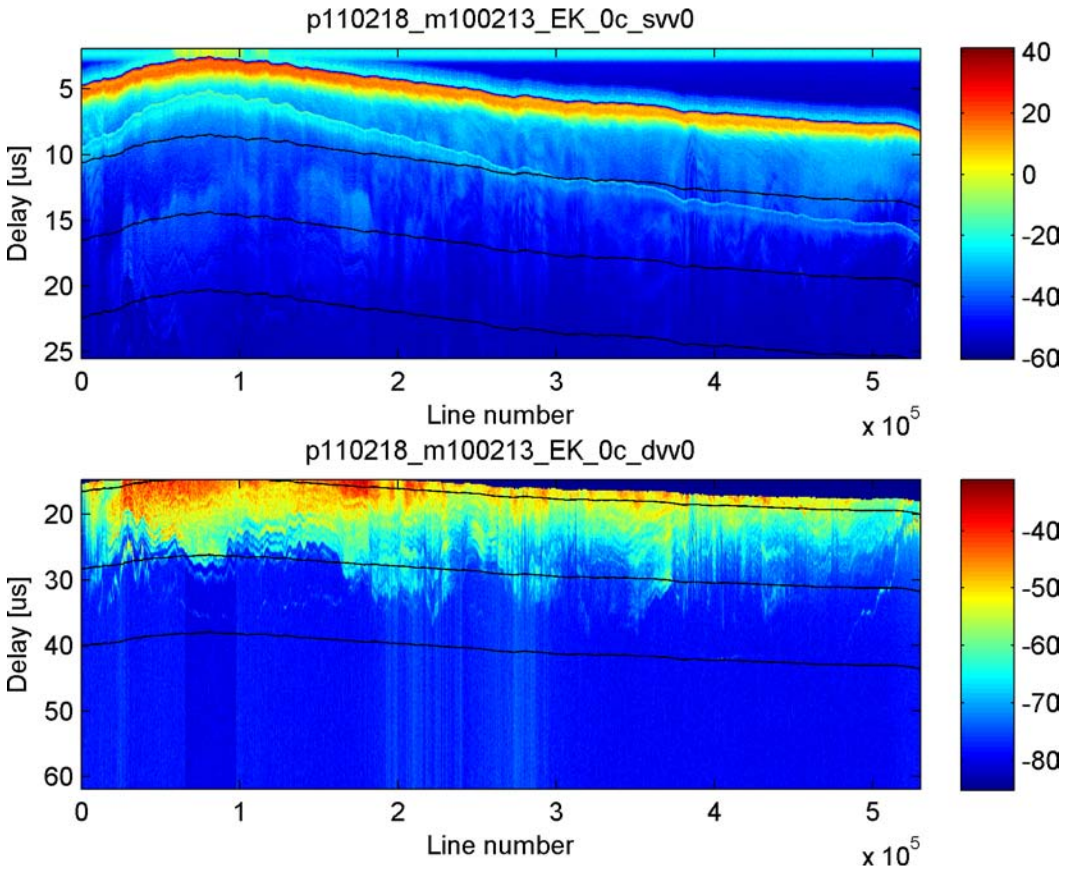

Figure 20 VV shallow (top) and deep (bottom) channel from the EK flight line, approximately 800 km. In the shallow channel, the three black lines represent a depth of 500, 1000, and 1500 m. The double bounce is clearly seen. In the deep channel, the three black lines correspond to 1000, 2000 and 3000 m depth. EPICA/Kohnen is around line 80000.

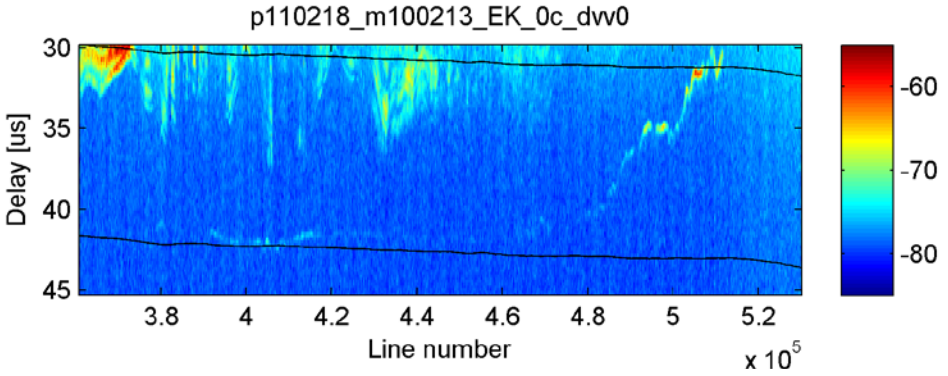

Figure 21 Zoom-in on deep channel of Figure 20 (220 km length), with adjusted intensity range. Bedrock is seen at 3 km depth.

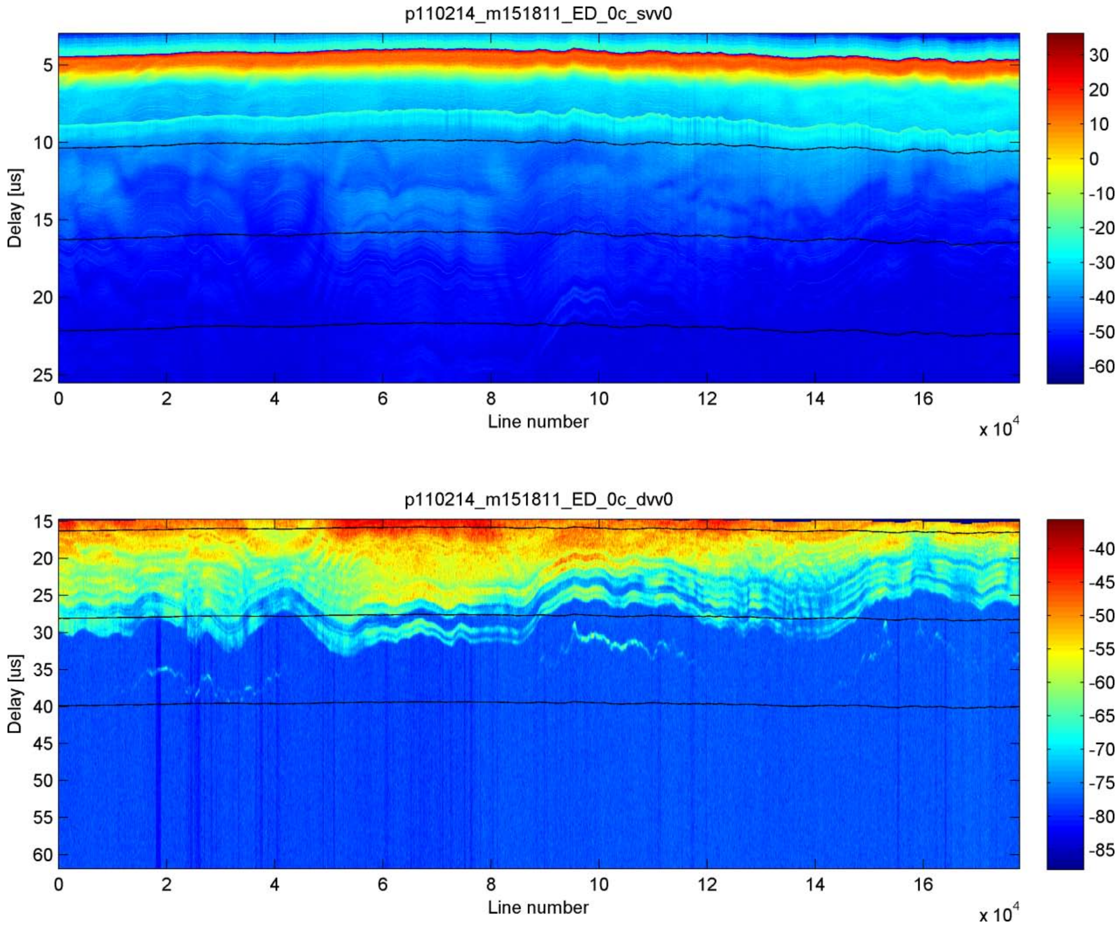

Figure 22 VV shallow (top) and deep (bottom) channel from part of the ED flight line (approximately 250 km). In the shallow channel, the three black lines represent a depth of 500, 1000, and 1500 m, and the double-bounce surface echo is seen at 8μs delay. In the deep channel, the three black lines correspond to 1000, 2000 and 3000 m depth.

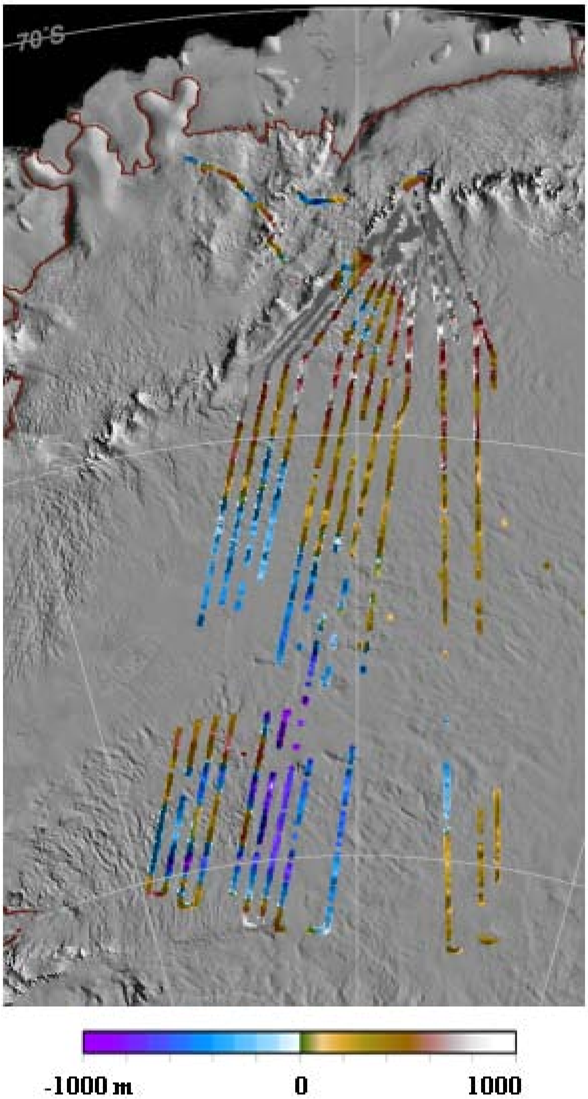

Figure 23 IceGrav preliminary bedrock elevation map from the HiCARS 60 MHz system, courtesy of Jamin S. Greenbaum, University of Texas.

9.2 Sensitivity limit (depth) in warm ice

According to Section 2, the penetration capabilities of POLARIS in warm ice should be examined using two test sites:

1. The ice shelf Fimbulisen, which was covered on the ice rises/coastal flight (Figure 11).
2. Adelaide Island (Figure 13).

The KM1a-KM2 radargram, flown across an ice rise in the coastal flight is shown on Figure 24. The basal interface is discernible almost all the way, down to a depth of 700 m (at 25 km along track), at which point the basal echo becomes very strong again after crossing the grounding line.

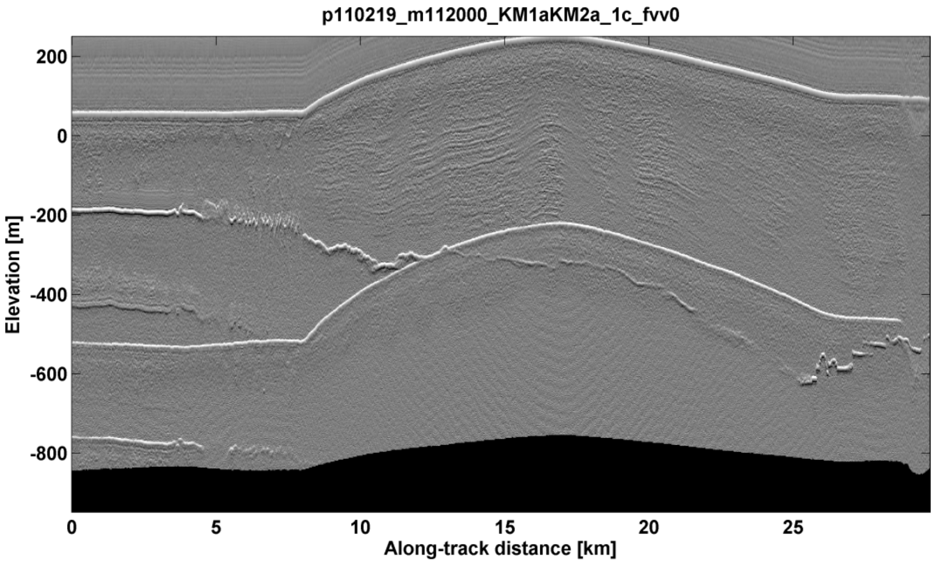

Figure 24 KM1a-KM2 The data have been level 1c processed, and the image shown is the range derivative of the logarithm of the amplitude.

The KM3a-KM4 radargram is shown on Figure 25. The basal interface is in general very bright, but the basal interface beneath the thin ice to the left is less bright than that beneath the thicker ice to the right. This suggests changes in the basal interface, ice-column properties (temperature, fabric, chemistry), or both. The strong double bounce echo (i.e. surface-aircraft-surface) is due to a smooth surface (and a high flight altitude).

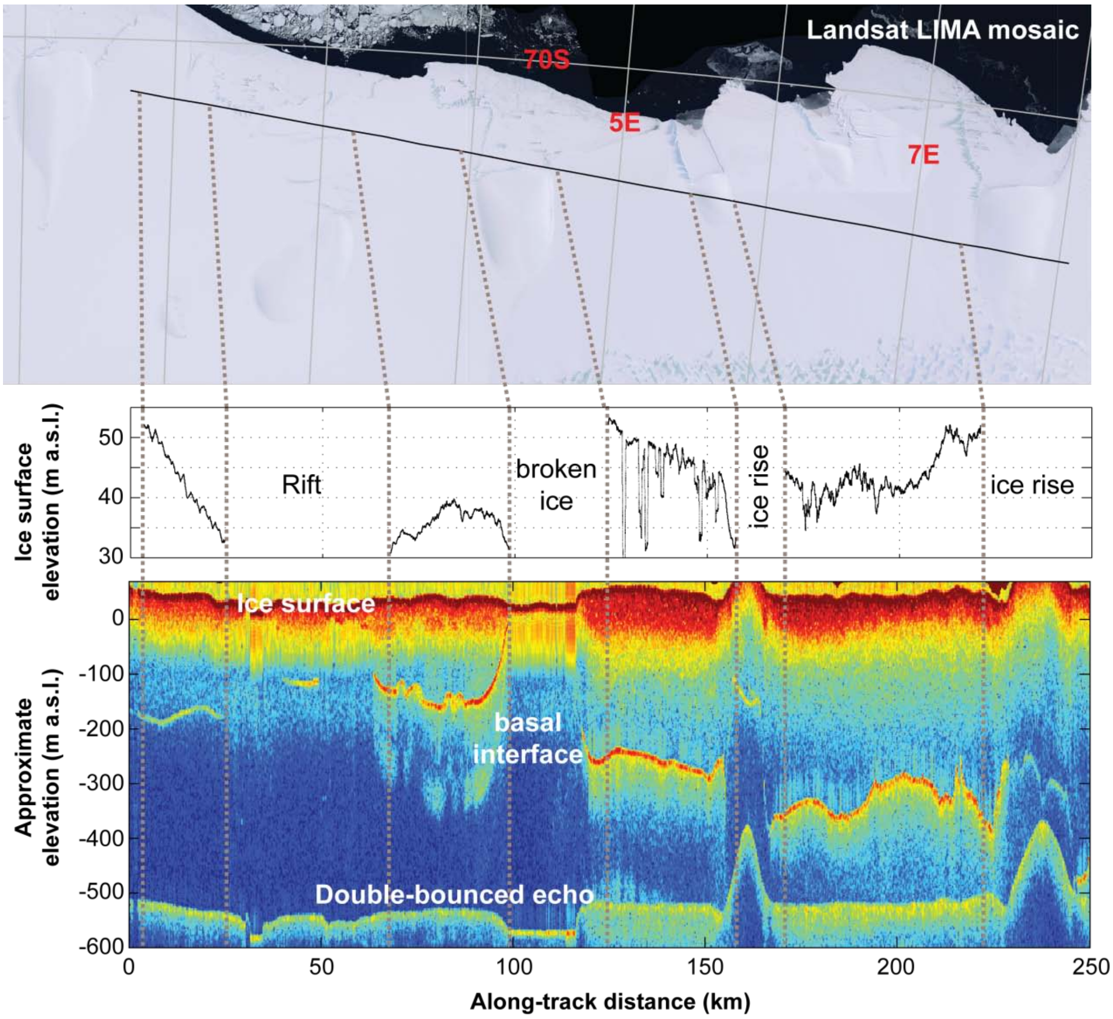

Figure 25 KM3a-KM4 Level 1c processed flight line from the coastal flight, with a corresponding Landsat mosaic and an interpretation of the image, courtesy of K. Matsuoka, Norwegian Polar Institute. Acquired with a 2 µs, 30 MHz pulse.

The level 1c processed VV data acquired with the small antenna while crossing the Adelaide Island ice cap are shown in Figure 26. The HH data acquired with one patch were also processed to level 1c, but no layers or basal reflections could be seen in these data. In the VV data, the basal reflection is detectable under most of the ice cap, down to a depth of around 500 m. Internal layers are observed at a maximum depth of 400 m.

It is observed that the internal layers disappear in the level 1c processed data when there is a large slope. This is probably due to the fact that the level 1c processing focuses a bandwidth around zero Doppler. It could be changed to modify the Doppler centroid dynamically, but this would require a means of determining the Doppler centroid of the data.

In summary, it seems POLARIS was able to penetrate the major part of the warm ice test sites. At Adelaide Island the penetration limit seems to be around the actual thickness of the ice cap, i.e. 500 m, and on the coastal flight, the maximum observed penetration depth was 700 m, also the maximum thickness of the ice cap.

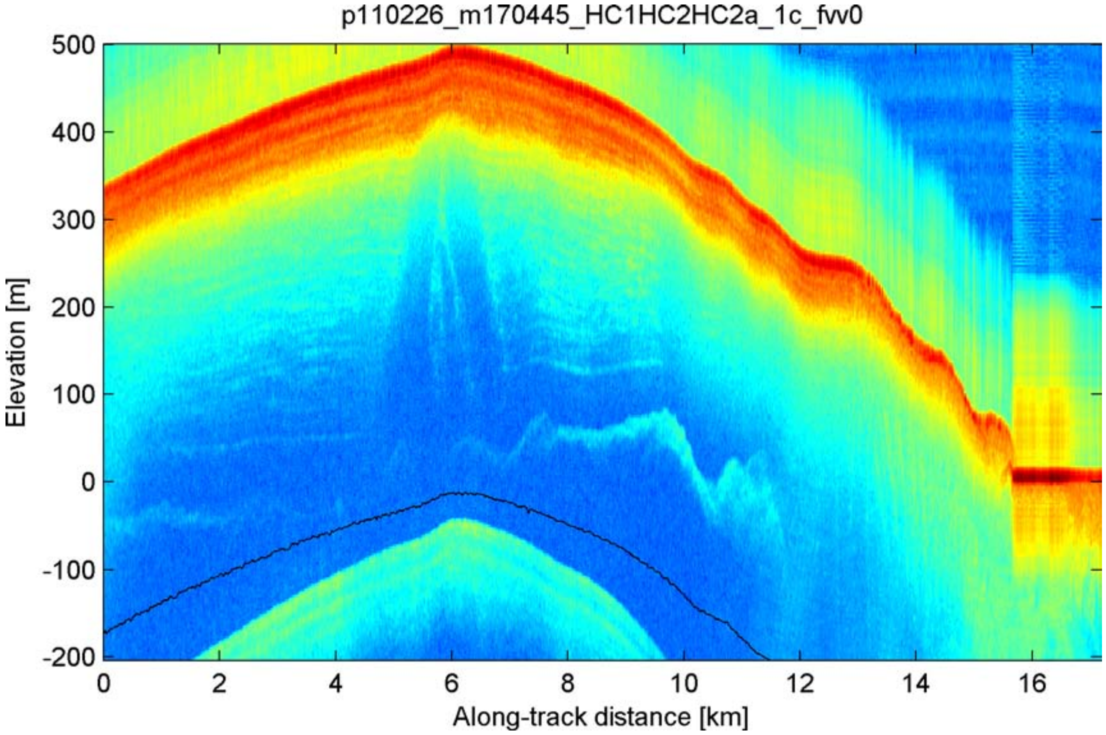

Figure 26 Adelaide Island level 1c processed VV data, acquired with a 2 µs, 30 MHz pulse. The black line corresponds to a depth of 500m.

9.3 Observability of radar reflection horizons

As mentioned in Section 2, the observability of radar reflection horizons were to be examined for three types of ice, cold ice, warm ice, and dynamical ice, covered in the following sections.

9.3.1 Cold ice

This objective has been dealt with in Sections 9.1 and 9.4, where it is seen that in the shallow channel, reflecting layers are consistently observed down to around 1.5 km depth with a 2 µs, 85 MHz pulse. In the deep channel, layering is consistently observed down to below 2 km depth with a 6 µs, 30 MHz pulse.

9.3.2 Warm ice

This objective has been dealt with in Section 9.2. The maximum depth where reflection horizons are observed in the warm ice data, is around 400 m, as can be seen from Figure 24 and Figure 26. In both cases, the reflection horizons are observed at a minimum elevation of 100 m above the basal interface.

9.3.3 Dynamical ice

This objective should be examined using data from the crossing of the floating tongue of the Jutulstraumen glacier. This line was flown both on the coastal flight and the multi-aperture flight. Data from the coastal flight have been used here, as they do not suffer from the antenna transmit null that was present on the multi-aperture flight (see 7.5), and since they were acquired from a much lower altitude above the ice (600 m vs 3km). The processed data are shown in Figure 27 The basal interface is readily observable at a depth below 700 m, but no reflection horizons can be seen whatsoever. A photo of the glacier is shown on Figure 28.

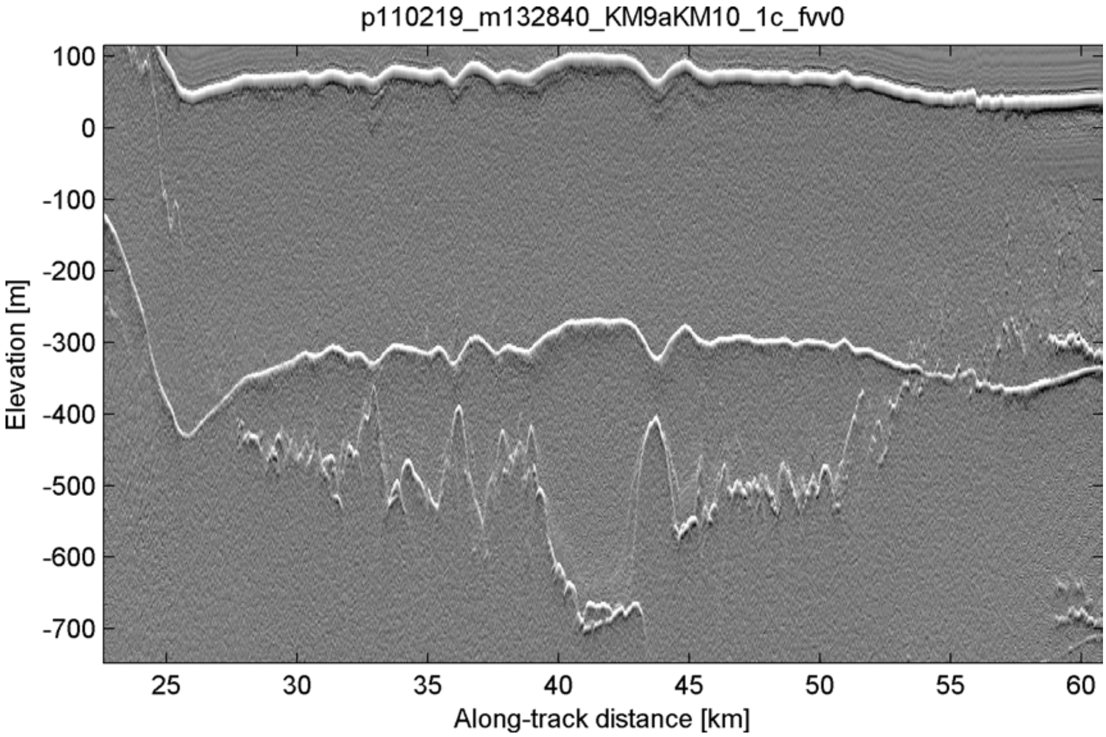

Figure 27 Part of KM9a-KM10 crossing Jutulstraumen glacier (located around 42 km along-track). The data have been level 1c processed, and the image shown is the range derivative of the logarithm of the amplitude. Acquired with 2 µs, 30 MHz pulse. Surface, double bounce and basal reflections are clearly visible.

Figure 28 Upstream view of the Jutulstraumen Glacier from 11000 feet (orthogonal to the track on Figure 27).

9.4 Potential of polarimetry for observing ice anisotropy (COF) in flowing ice over ice divides and dynamical regions

According to Section 2, this objective should be examined using three test sites:

1. The track crossing Jutulstraumen glacier on the ice rises/ice shelf coastal flight
2. The track crossing the ice shelf also on the coastal flight
3. Adelaide Island
4. The EPICA drilling site

Unfortunately, due to the problems described in Section 7.4, no polarimetry is available for the first two. Also, no useful polarimetric data are available for Adelaide Island, due to the problems described in Section 7.6. This leaves the EPICA/Kohnen drilling site (located on a ridge from which the ice flows away), for which full polarimetry data are available, see Figure 29. The bedrock is observed at around 100 m elevation (WGS-84 ellipsoid height), and the ice depth is approximately 2780 m. In the shallow channel, differences are observed between the HH and VV polarizations, with generally more pronounced layers in the HH channel. The shallow channel layers are observed down to a depth of around 1.6 km. In the deep channel, clear differences between HH and VV are observed, with the layers observable down to a depth of 2.2 km. Note that there is an overlap between the upper part of the deep window and the lower part of the shallow window, and the brighter layering at HH-polarization is also seen in the deep channels, albeit at a much reduced resolution, due to the 6 MHz bandwidth in the deep channel. These observations indicate that P-band polarimetry could be used to study ice anisotropy in Antarctica, at least in cold ice conditions. This is consistent with the observations with POLARIS in Greenland at the NEEM and NGRIP drilling sites.

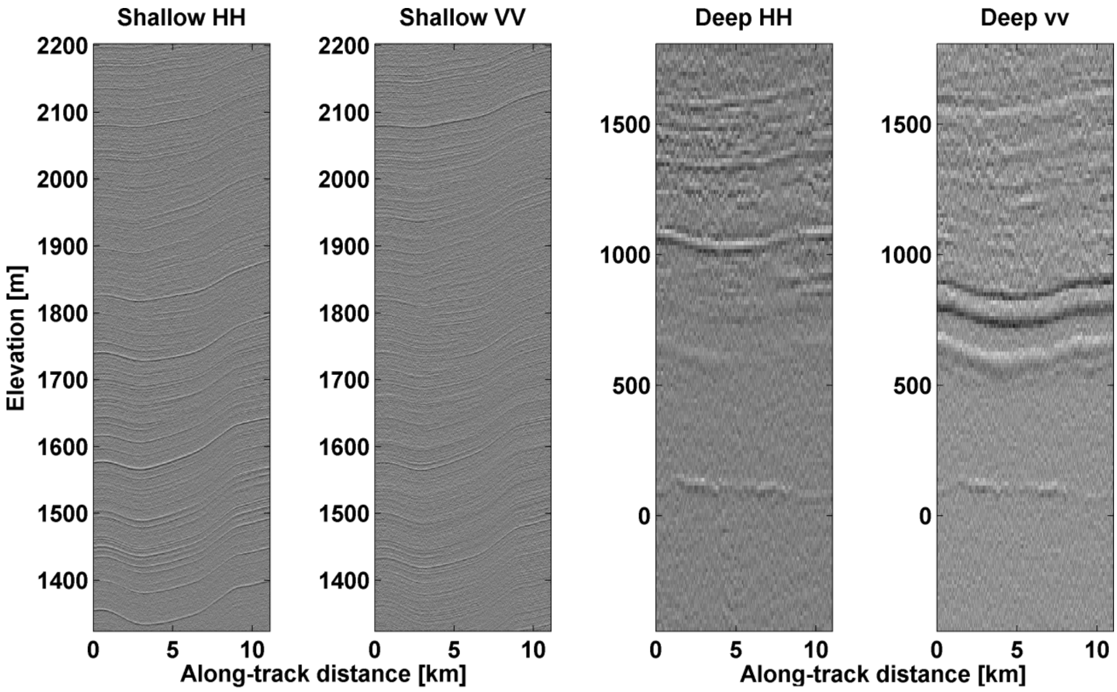

Figure 29 Polarimetric data from EPICA drilling site. The data have been level 1c processed, and the images show the range derivative of the logarithm of the amplitude.

9.5 Multiple phase-centre data acquisition

Multi-aperture data were collected along several tracks, one crossing Jutulstraumen, and two parallel to the glacier, see Figure 10.

When acquiring the multi-aperture data at Jutulstraumen the radar setting was alternating on a pulse by pulse bases. Like in the SDS mode, the pulse length, the bandwidth, and the receiver gain were alternating, whereas the range window was fixed. The objective was to increase the chances of receiving a basal return in spite of the strong attenuation expected for the crevassed glacier, while at the same time detecting the surface with a better resolution and shorter range sidelobes and not risking saturation. As it turns out, despite the high altitude and problems with the antenna pattern described in Section 7.5 (the used antenna patterns are shown on Figure 30), the basal return is clearly visible even with the short 2 µs, 85 MHz pulse, as can be seen from Figure 31.

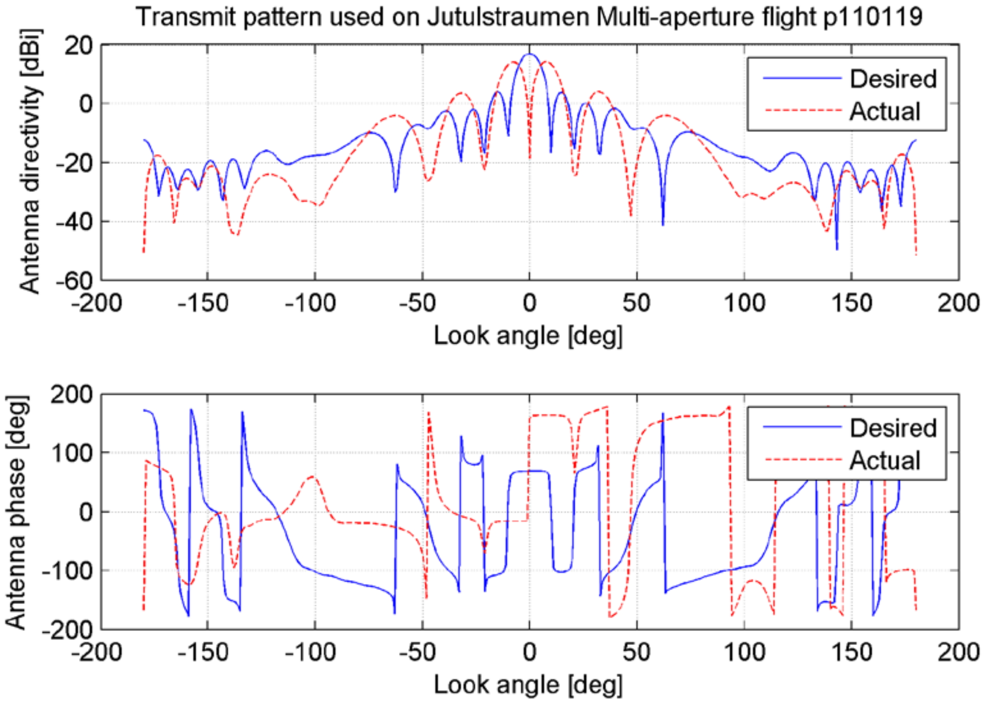

Figure 30 Transmit Antenna pattern used for the multi-aperture data acquisition, based on radio anechoic chamber measurements of the POLARIS 8-element antenna. The actual (erroneous) Transmit pattern has been synthesized from the measured patterns of the individual subapertures.

9.5.1 Preliminary analysis of multi-aperture data

The multi-phase-centre data supports across-track surface clutter suppression by means of array signal processing techniques. One promising technique is based on synthesizing range-varying antenna patterns with nulls in the direction of arrival (DOA) of the received clutter. The clutter DOA can be calculated from an existing digital elevation model, but it can also be estimated from the multi-phase-centre data. This technique has been applied to parts of the data. Figure 32 shows the maximum likelihood (ML) DOA estimate from a part of the data, where the surface is relatively flat and smooth. This scenario results in two surface clutter components – a left hand signal, and a right hand signal. The two signals will be symmetrical around nadir for a perfect flat surface in the ideal case, as illustrated by the red dashed line in the figure. It is seen how the estimate is in agreement with the model. The deviation around 125 m is due to a null in the transmission pattern and spatial undersampling caused by an excessive antenna element spacing. The undersampling is also the reason for the bend in the curves at 140 m. This depth corresponds to the spatial Nyquist frequency, which results in DOA aliasing and wrapping for larger depths. The peaks at 330 m represent the bedrock echoes, which are the two dominating signal components at this depth.

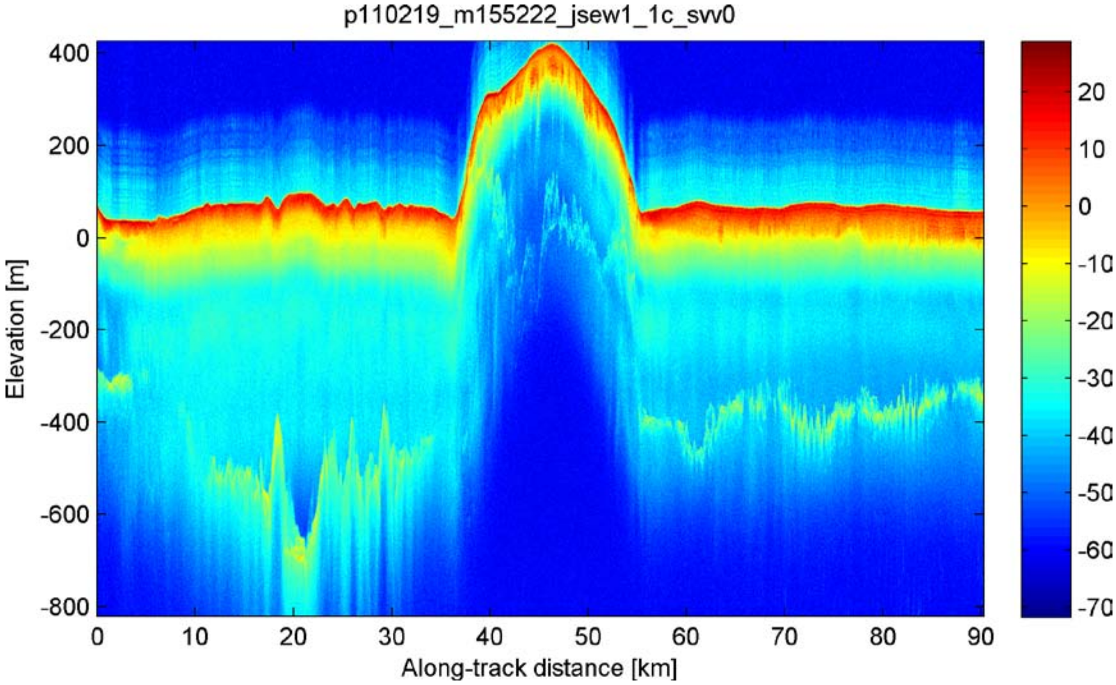

Figure 31 Data from multi-aperture flight crossing Jutulstraumen glacier (JD3-KM10). These shallow channel data were acquired from an altitude of 3 km above the ice with a 2 µs, 85 MHz pulse. The four sub-aperture channels have been level 1c processed individually and subsequently coherently summed for this image.

The DOA estimate has been used for clutter suppression. The result is shown in Figure 33, which is an intensity profile in range at a given azimuth position. The dashed red curve, denoted beam steering, corresponds to ordinary single channel reception with the full aperture, and with the main beam directed towards nadir. The black solid curve is the result of the synthesized pattern technique, which is given by the maximum likelihood estimator. It is seen how clutter is suppressed in the near-surface depths from 0 to 25 m (antenna mainlobe) and again around 250 m (first sidelobe). This preliminary analysis suggests that the data can indeed be used for investigating clutter suppression techniques.

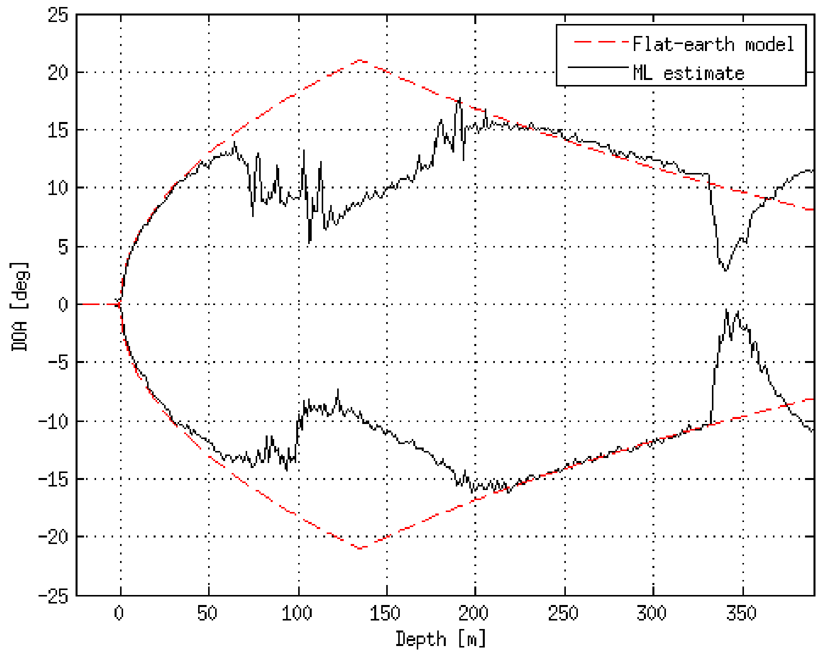

Figure 32 DOA estimate of the surface clutter signals.

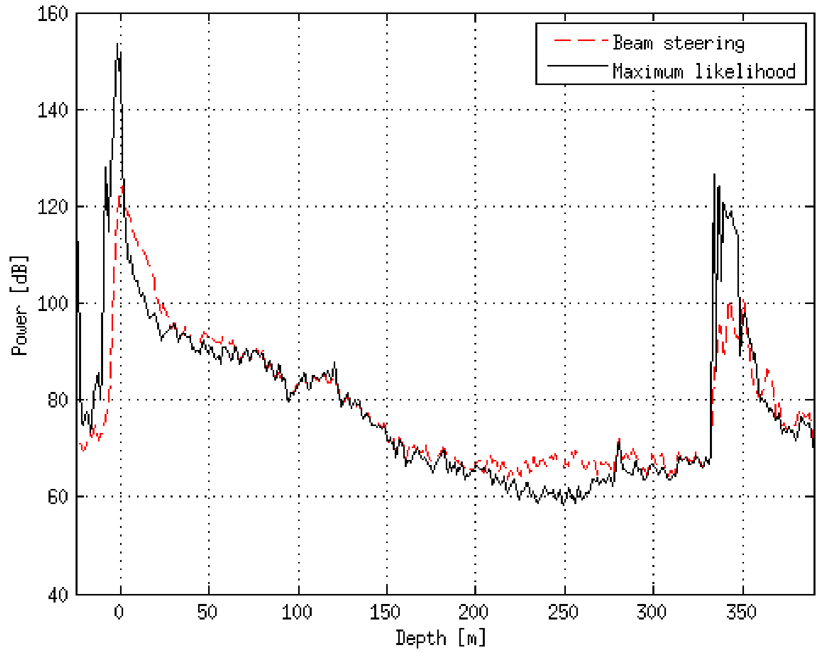

Figure 33 Intensity profiles with and without clutter suppression.

10 Conclusions

The acquisition of POLARIS data during the IceGrav campaign has been successful in the sense that all the data needed to address the objectives listed in Section 2 have been acquired. The two missing gravimetry flights, the data gaps south of Troll, and the H-polarizations missing in some cases are not crucial. Likewise, the HiCARS radar caused RFI, but it was switched off during most of the ESA-funded data takes (including the fully polarimetric EPICA scene).

The campaign demonstrated that POLARIS could detect bedrock at 3 km depth in the cold ice regions covered by the IceGrav tracks, although not consistently. A quantitative analysis awaits the development of software for bedrock detection/tracking. Internal layers were consistently observed below 2 km depth.

The sensitivity limit in warm ice was also investigated, and POLARIS was able to penetrate the major part of the warm ice test sites. At Adelaide Island the penetration limit seems to be around the actual thickness of the ice cap, i.e. 500 m, whereas on the coastal flight along the ice shelf and ice rises, the maximum observed penetration depth was 700 m. Internal layers in the warm ice regions were observed down to 400 m depth.

Use of POLARIS for sounding dynamic ice was also investigated. The basal return from the 700 m thick Jutulstraumen glacier was easily detectable, even with a short pulse at high altitude, but no internal layers could be observed.

Polarimetry for studying crystal orientation fabrics was also addressed with fully polarimetric data acquired over the EPICA/Kohnen drilling site. Differences between HH and VV reflection horizons were clearly observed down to below 2 km depth.

Finally, multi-aperture data for studying clutter suppression algorithms were acquired, and a preliminary analysis indicates they can indeed be used for investigating clutter suppression, despite a problem with the large antenna transmit pattern.

11 References

[1] J. Dall, S.S. Kristensen, V. Krozer, C.C. Hernández, J. Vidkjær, A. Kusk, J. Balling, N. Skou, S.S. Søbjærg, E.L. Christensen, "ESA's polarimetric airborne radar ice sounder (POLARIS): Design and first results", *IET Radar, Sonar & Navigation*, Vol. 4, No. 3, pp. 488-496, June 2010.

[2] "Statement of work; P-Band Ice Sounding Radar Demonstrator Development", *ESTEC*, TEC-ETP/2004.31, version 2, ESTEC, November 2004.

[3] A, Kusk, J. Dall, S.S. Kristensen, "P-Band Ice Sounding Radar Demonstrator Development; Campaign Data Inventory", (ESA Contract No 19307/05/NL/JA), *DTU Space, Technical University of Denmark,* April 2009.

[4] A. Kusk, J. Dall, "POLARIS Additional Test Campaign; Campaign report and Data Inventory", (ESA Contract No 19307/05/NL/JA), *DTU Space, Technical University of Denmark,* Sep. 2009.

[5] T. Casal, M. Davidson, "Technical Assistance for POLARIS during the 2010/2011 ICEGRAV validation experiment", *ESTEC*, SOW, EOP-SM/2155/MWJD-mwjd, ESTEC, September 2010.

[6] K. Matsuoka, Norwegian Polar Institute, *Personal Communication*, October, 2011.

[7] "Annex 2 to P-Band Ice Sounding Radar Demonstrator Development, A simplified scattering model", *ESTEC*, TEC-ETP/2004.31, version 2, November 2004.

Appendix A Supplemental Type Certificates

Transport Canada Transports Canada

Department of Transport

Supplemental Type Certificate

This approval is issued to:

Kenn Borek Air Ltd.
290 McTavish Road, N.E.
Calgary, Alberta
Canada T2E 7G5

Number: C-LSA10-215/D
Issue No.: 1
Approval Date: November 23, 2010
Issue Date: November 23, 2010

Responsible Office:	Prairie and Northern
Aircraft/Engine Type or Model:	DOUGLAS DC3C, DC3C-S1C3G
Registration/Serial No.:	C-GJKB/13383, C-FMKB/19950
Canadian Type Certificate or Equivalent:	A669
Description of Type Design Change:	Installation of P-Band Radar Antenna Under Fuselage

**Installation/Operating Data,
Required Equipment and Limitations:**

Installation of P-Band Radar Antenna to be done in accordance with Transport Canada Civil Aviation (TCCA) approved Infinion Certification Engineering Installation Instructions EO-1433-02, Issue 1 dated October 12, 2010, or later TCCA approved issue.

Operation to be in accordance with TCCA approved Infinion Flight Manual Supplement FMS-1433-02, Issue 1 dated October 20, 2010 or later TCCA approved issue.

Limitation: Lower Fuselage Hard Points installation approved under STC C-LSA10-214/D is a pre-requisite.

Basis of Certification: As per Basler Turbo Conversion basis of certification defined in STC SA00-9 (CAR 4b plus FAR 25 requirements as listed).

– End –

DEPARTMENT OF TRANSPORT CANADA MINISTÈRE DES TRANSPORTS

Conditions: This approval is only applicable to the type/model of aeronautical product specified therein. Prior to incorporating this modification, the installer shall establish that the interrelationship between this change and any other modification(s) incorporated **will not** adversely affect the airworthiness of the modified product.

T.C. Clark, DAR 326
For Minister of Transport

Canada

Transport Canada   Transports Canada

Department of Transport

Supplemental Type Certificate

This approval is issued to:	***Number:*** C-LSA10-216/D
Kenn Borek Air Ltd.	**Issue No.:** 1
290 McTavish Road, N.E.	**Approval Date:** November 23, 2010
Calgary, Alberta	**Issue Date:** November 23, 2010
Canada T2E 7G5	

Responsible Office:	Prairie and Northern
Aircraft/Engine Type or Model:	DOUGLAS DC3C
Registration/Serial No.:	C-GJKB/13383
Canadian Type Certificate or Equivalent:	A669
Description of Type Design Change:	Installation of DTU - U of Texas 2010 Antarctic Survey Equipment

Installation/Operating Data,
Required Equipment and Limitations:

Installation of Antarctic Science Equipment is to be done in accordance with TCCA approved Infinion Certification Engineering Installation Instruction EO-1433-01, Issue 1 dated October 12, 2010, or later TCCA approved issue.

Operation in accordance with TCCA approved Infinion Flight Manual Supplement FMS-1433-01, Issue 1 dated October 20, 2010, or later TCCA approved issue. The Instructions for Continued Airworthiness for the aircraft are not affected by this modification.

Limitations: With the survey equipment installed, the aircraft is only eligible for the issue of a Special C of A – Restricted. Refer to Flight Manual Supplement for additional limitations.

Basis of Certification: As per Basler Turbo Conversion basis of certification defined in STC SA00-9 (CAR 4b plus FAR 25 requirements as listed).

– End –

DEPARTMENT OF TRANSPORT · CANADA · MINISTÈRE DES TRANSPORTS

Conditions: This approval is only applicable to the type/model of aeronautical product specified therein. Prior to incorporating this modification, the installer shall establish that the interrelationship between this change and any other modification(s) incorporated **will not** adversely affect the airworthiness of the modified product.

T.C. Clark, DAR 326
For Minister of Transport

Canada

Appendix B Test sites overview

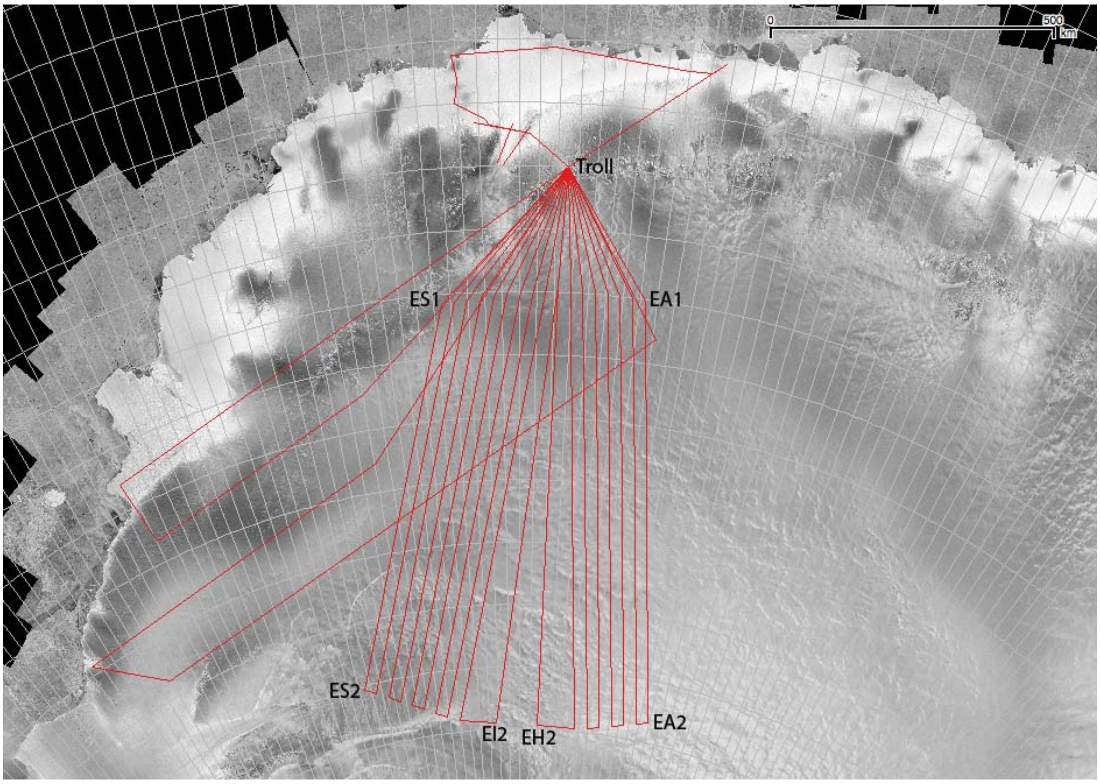

Figure 34 South site (dictated by gravimetry) tracks.

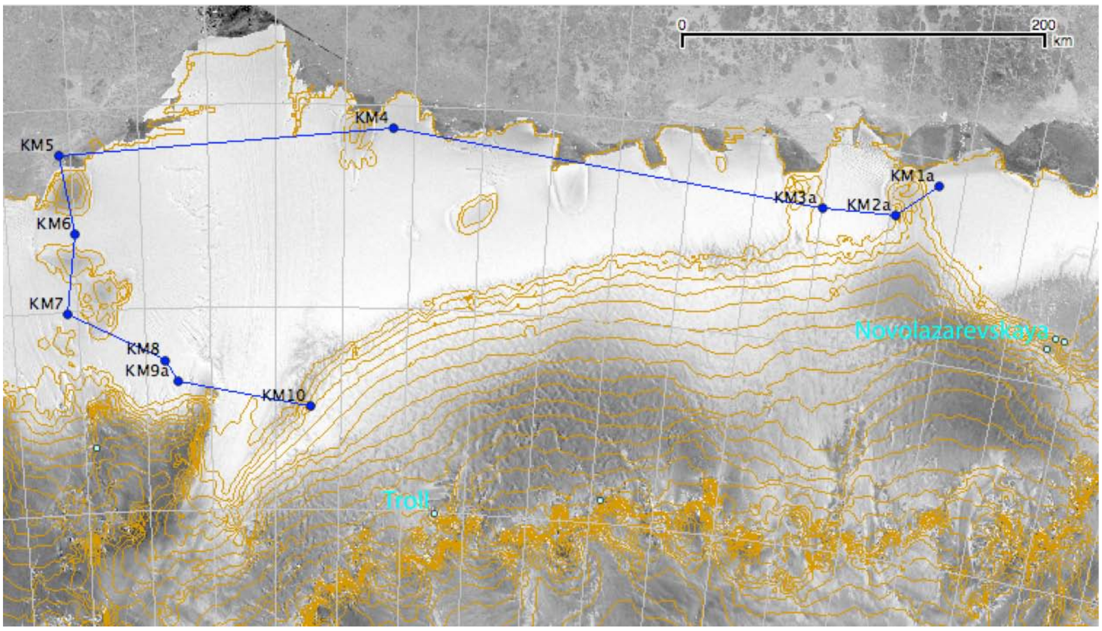

Figure 35 Ice rises, and Jutulstraumen ⊥ (obj. 3-4: KM9a-KM10, KM4-KM5).

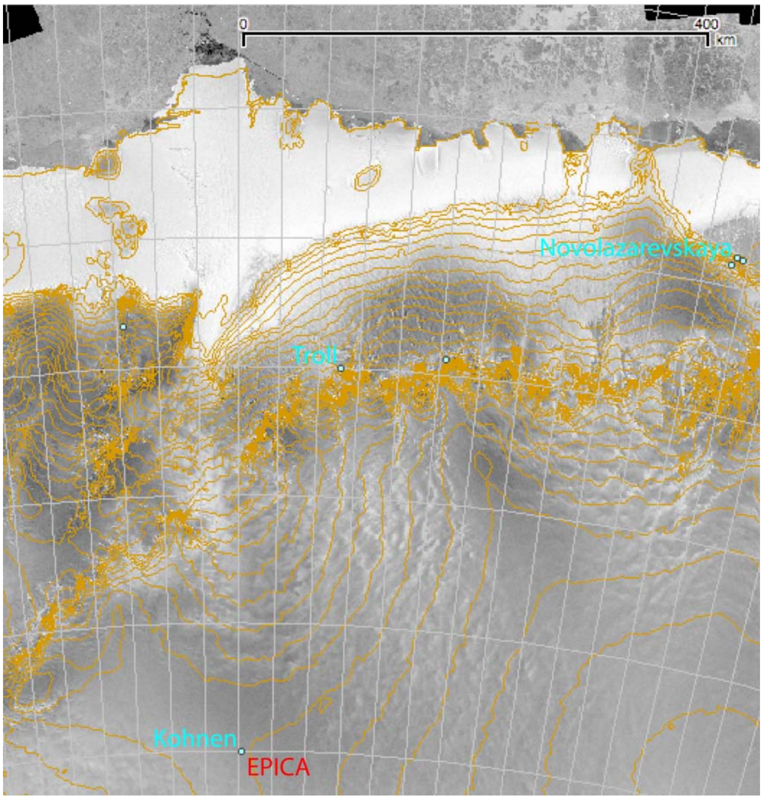

Figure 36 EPICA site.

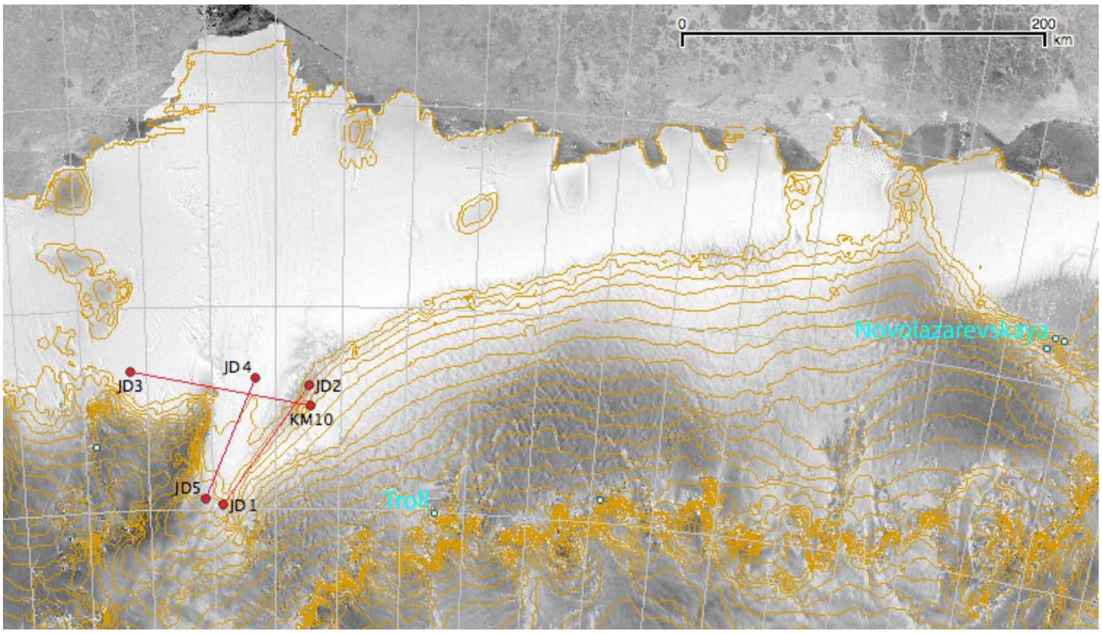

Figure 37 Ice shelf, Jutulstraumen || and Jutulstraumen ⊥ (obj. 5: JD3-KM10).

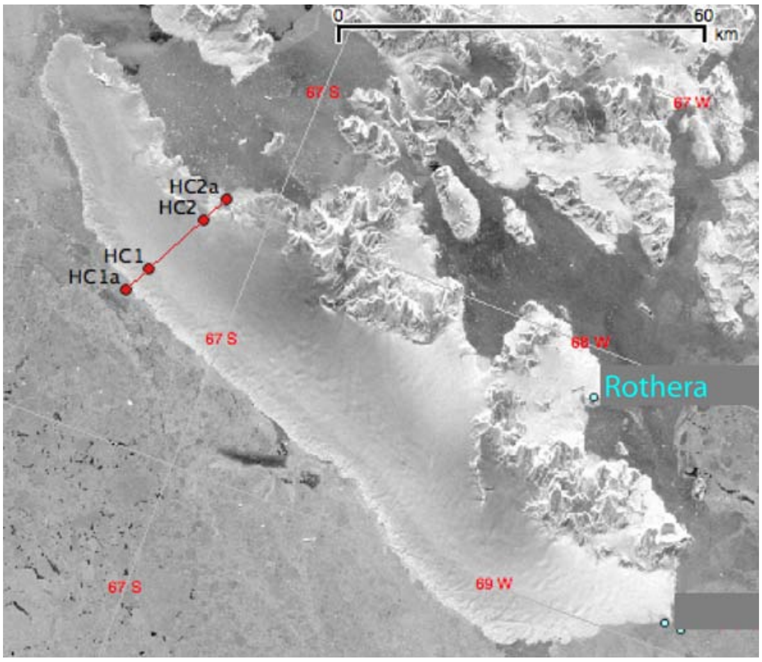

Figure 38 Adelaide Island.

Appendix C Test site coordinates

Table 5 Waypoint coordinates (WGS84, negative lon = W, negative lat = S).

Flight	Waypoint	Longitude	Latitude	Est. max surf. elev.
Ice rises etc.	KM1a	9.63864°	-70.13311°	400 m
	KM2a	9.07542°	-70.30764°	400 m
	KM3a	7.99890°	-70.32575°	400 m
	KM4	1.68582°	-70.11446°	400 m
	KM5	-3.16312°	-70.22736°	400 m
	KM6	-2.98192°	-70.61434°	400 m
	KM7	-3.15548°	-71.00744°	400 m
	KM8	-1.71858°	-71.25542°	400 m
	KM9a	-1.50524°	-71.36430°	400 m
	KM10	0.52773°	-71.48625°	400 m
Jutulstraumen	JD1	-0.84584°	-71.97914°	400 m
	JD2	0.50093°	-71.38814°	400 m
	KM10	0.52773°	-71.48625°	400 m
	JD3	-2.25548°	-71.31300°	400 m
	KM10	0.52773°	-71.48625°	400 m
	JD3	-2.25548°	-71.31300°	400 m
	KM10	0.52773°	-71.48625°	400 m
	JD4	-0.32812°	-71.35119°	400 m
	JD5	-1.11579°	-71.94434°	400 m
EPICA/South Site	EPICA	0.06783°	-75.00166°	2900 m
Adelaide Island	HC1a	-68.44701°	-66.84424°	500 m
	HC1	-68.34587°	-66.86370°	500 m
	HC2	-68.10092°	-66.91035°	500 m
	HC2a	-67.99783°	-66.92979°	500 m

www.space.dtu.dk

National Space Institute

Technical University of Denmark

Ørsteds Plads

Building 348

DK-2800 Kgs. Lyngby

Denmark

Tel: (+45) 45 25 38 00

Fax: (+45) 45 93 16 34

E-mail: info@space.dtu.dk